

Review

The Peter Day Series of Magnetic (Super)Conductors †

 Samia Benmansour * and Carlos J. Gómez-García *

ICMol, Departamento de Química Inorgánica, Universidad de Valencia, C/Catedrático José Beltrán 2, 46980 Paterna, Spain

* Correspondence: sam.ben@uv.es (S.B.); carlos.gomez@uv.es (C.J.G.-G.);

Tel.: +34-963544423 (S.B.); +34-963544423 (C.J.G.-G.); Fax: +34-963543273 (S.B.); +34-963543273 (C.J.G.-G.)

† In memory of Peter Day, an enthusiastic and clever chemist and a good friend.

Abstract: Here, we review the different series of (super)conducting and magnetic radical salts prepared with organic donors of the tetrathiafulvalene (TTF) family and oxalato-based metal complexes (ox = oxalate = $C_2O_4^{2-}$). Although most of these radical salts have been prepared with the donor bis(ethylenedithio)tetrathiafulvalene (BEDT-TTF = ET), we also include all the salts prepared with other TTF-type donors such as tetrathiafulvalene (TTF), tetramethyl-tetrathiafulvalene (TM-TTF), bis(ethylenediseleno)tetrathiafulvalene (BEST), bis(ethylenedithio)tetraselenafulvalene (BETS) and 4,5-bis((2S)-2-hydroxypropylthio)-4',5'-(ethylenedithio)tetrathiafulvalene (DMPET). Most of the oxalato-based complexes are monomers of the type $[M^{III}(C_2O_4)_3]^{3-}$, $[Ge(C_2O_4)_3]^{2-}$ or $[Cu(C_2O_4)_2]^{2-}$, but we also include the reported salts with $[Fe_2(C_2O_4)_5]^{4-}$ dimers, $[M^{II}(H_2O)_2[M^{III}(C_2O_4)_3]_2]^{4-}$ trimers and homo- or heterometallic extended 2D layers such as $[M^{II}M^{III}(C_2O_4)_3]^-$ and $[M^{II}_2(C_2O_4)_3]^{2-}$. We will present the different structural families and their magnetic properties (such as diamagnetism, paramagnetism, antiferromagnetism, ferromagnetism and even long-range magnetic ordering) that coexist with interesting electrical properties (such as semiconductivity, metallic conductivity and even superconductivity). We will focus on the electrical and magnetic properties of the so-called Day series formulated as $\beta''-(BEDT-TTF)_4[A^+M^{III}(C_2O_4)_3]\cdot G$, which represents the largest family of paramagnetic metals and superconductors reported to date, with more than fifty reported examples.

Keywords: oxalato; tris(oxalato) complexes; TTF; BEDT-TTF; radical salts; conducting; superconducting; metallic; conductivity; paramagnetism; ferromagnetism



Citation: Benmansour, S.; Gómez-García, C.J. The Peter Day Series of Magnetic (Super)Conductors. *Magnetochemistry* **2021**, *7*, 93. <https://doi.org/10.3390/magnetochemistry7070093>

Academic Editor: Marius Andruh

Received: 31 May 2021
 Accepted: 23 June 2021
 Published: 26 June 2021

Publisher's Note: MDPI stays neutral with regard to jurisdictional claims in published maps and institutional affiliations.

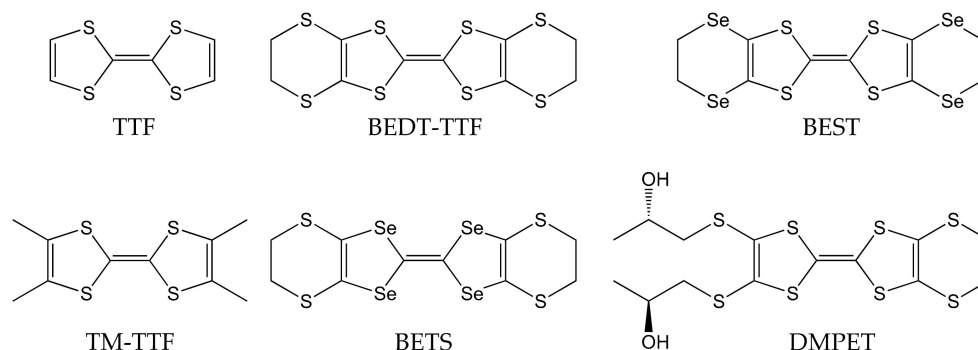


Copyright: © 2021 by the authors. Licensee MDPI, Basel, Switzerland. This article is an open access article distributed under the terms and conditions of the Creative Commons Attribution (CC BY) license (<https://creativecommons.org/licenses/by/4.0/>).

1. Introduction

Among the many legacies of Peter Day's work, besides the Robin and Day classification for mixed-valence compounds [1], one of the best known is the discovery of the superconducting paramagnetic radical salts prepared with bis(ethylenedithio)tetrathiafulvalene BEDT-TTF (ET, Scheme 1) and $[M(ox)_3]^{3-}$ anions (M = Fe, Cr, Ga, etc.) [2,3] The discovery of the first paramagnetic molecular superconductors boosted the research in the field and led to the preparation of around twenty-five molecular superconductors in the so-called Peter Day series. The first member of this series, initially formulated with a water molecule as $\beta''-(BEDT-TTF)_4[(H_2O)Fe^{III}(C_2O_4)_3]\cdot PhCN$ [2,3], and later with a H_3O^+ cation as $\beta''-(BEDT-TTF)_4[(H_3O)Fe^{III}(C_2O_4)_3]\cdot PhCN$ [4], showed a superconducting transition at 8.5(3) K, one of the highest T_c observed in any molecular superconductor to date. As Peter Day noticed in his first report, this discovery paved the way to a synthetic strategy for obtaining further magnetic molecular superconductors [3]. Only two months later, P. Day's group published a deeper characterization of this compound and a second phase (*pseudo-κ* or κ') obtained with the same donor (BEDT-TTF) and the same anion ($[Fe(C_2O_4)_3]^{3-}$), but with different A^+ cations: $\kappa'-(BEDT-TTF)_4[AFe^{III}(C_2O_4)_3]\cdot PhCN$ (A = K^+ and NH_4^+). This orthorhombic (*Pbcn*) pseudo-kappa or κ' phase was also paramagnetic, but it was a semiconductor (as we will see below, all the known members of this κ' phase are semiconductors) [2]. These two initial reports in 1995 initiated the search for novel molecular conductors and superconductors with interesting magnetic properties. Besides the more than one hundred metals,

semiconductors and superconductors that will be presented in this review, this search also led to the synthesis of the first molecular superconducting antiferromagnets [5,6], metallic ferromagnets [7,8] or field-induced magnetic superconductors [9].



Scheme 1. Donors of the TTF family that have been combined with metal-oxalato complexes or lattices: tetrathiafulvalene (TTF), tetramethyl-tetrathiafulvalene (TMTTF), bis(ethylenedithio)tetrathiafulvalene (BEDT-TTF = ET), bis(ethylenediseleno)tetrathiafulvalene (BEDS-TTF = BEST), bis(ethylenedithio)tetraselenafulvalene (BEDT-TSF = BETS) and 4,5-bis((2S)-2-hydroxypropylthio)-4',5'-(ethylenedithio)tetrathiafulvalene (DMPET).

The synthesis of these radical salts was performed in H-shaped or U-shaped electrochemical cells containing two compartments separated by a glass frit. The anode compartment is filled with a solution of the TTF-type donor (Scheme 1) in solvents such as CH_2Cl_2 and $\text{CHCl}_2\text{-CH}_2\text{Cl}$. The cathode compartment is filled with a solution containing the desired oxalate-based magnetic anion dissolved in different solvents or mixtures of solvents. As we will see below, the choice of the solvents is crucial in many cases to determine the structure and properties of the radical salt obtained. Very often, a few drops of water were added to furnish the needed H_3O^+ cations. As we will see in Section 4.1, in some cases, a crown ether such as 18-crown-6 was added to the cathode to increase the solubility of the K^+ or NH_4^+ salts of the anions. Application of a very low constant DC current (in the 0.1–1 μA range) through platinum electrodes (usually with a diameter of 1 mm) results in a slow oxidation of the TTF-type donors in the presence of the magnetic oxalate-based anions that yields, after a few days or weeks, high-quality single crystals in most cases. The co-crystallization of neutral donor molecules together with the oxidized ones leads, in most cases, to lattices with a mixed-valence state in the donors and, therefore, to a combination of electrical and magnetic properties [2,4].

As it will be shown here, the continuous efforts of P. Day's group (and others) led to the synthesis and characterization of more than one hundred radical salts prepared with different TTF-type donors (Scheme 1) and metal-oxalato complexes (Figure 1). Although a revision with a part of the work conducted in this area was published by P. Day in 2004 [10], since then, the number of published salts has multiplied by a factor of four, passing from less than thirty to more than one hundred and twenty. Therefore, as a late homage to the legacy of Peter Day and his group in the area of molecular conductors, here, we will revise the work conducted in this field since the first report of a molecular paramagnetic superconductor by P. Day's group in 1995 [3].

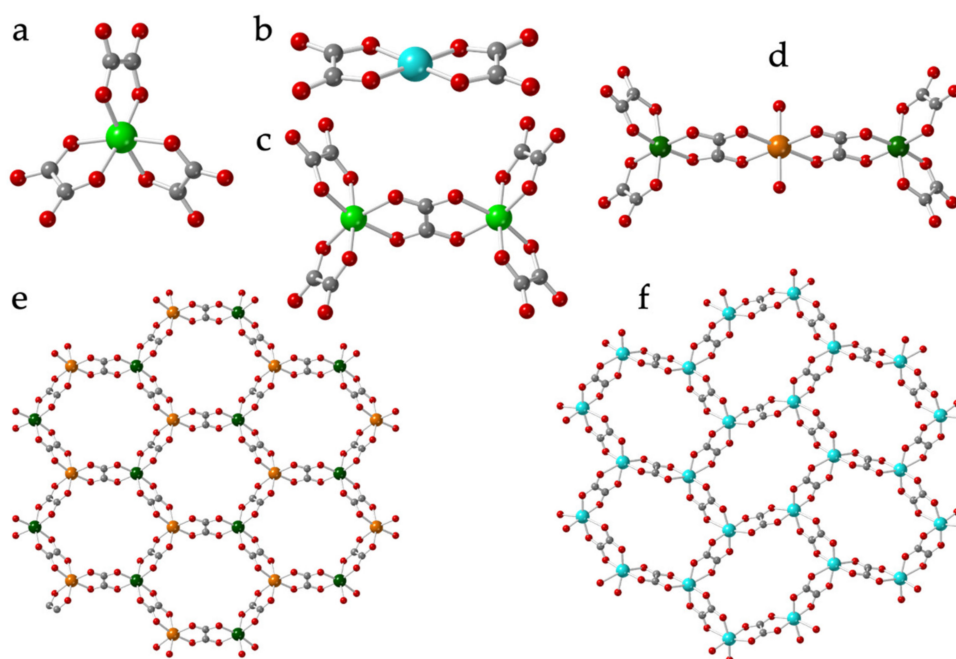


Figure 1. Metal-oxalato anions combined with TTF-type donors: **(a)** monomers $[M^{III}(C_2O_4)_3]^{3-}$ ($M^{III} = Fe, Cr, Mn, Co, Al, Ga, Rh, Ru$ and Ge) and $[Ge(C_2O_4)_3]^{2-}$, **(b)** the monomer $[Cu(C_2O_4)_2]^{2-}$, **(c)** dimers $[M^{III}_2(C_2O_4)_5]^{4-}$ ($M^{III} = Fe$ and Cr), **(d)** trimers $\{Mn(H_2O)_2[M^{III}(C_2O_4)_3]_2\}^{4-}$, **(e)** heterometallic layers $[Mn^{II}M^{III}(C_2O_4)_3]^{-}$ ($M^{III} = Cr$ and Rh) and **(f)** homometallic layers $[Cu^{II}_2(C_2O_4)_3]^{2-}$. Color code: Fe = light green, Cr = dark green, Mn = orange, Cu = blue, C = gray and O = red.

In this review, we present all the reported structures of radical salts with TTF-type donors and metal-oxalato complexes, divided into five different sections. In the first section, we present Peter Day's series with more than fifty reported monoclinic conductors and superconductors formulated as β'' -(BEDT-TTF) $_4$ [AM^{III}(C₂O₄)₃]-G with $A^+ = H_3O^+, NH_4^+$ and K^+ ; $M^{III} = Fe, Cr, Ga, Rh$ and Ru ; and $G = C_6H_5N$ (py), $PhNO_2$, $PhCN$, 1,2- $PhCl_2$, PhI , $PhBr$, $PhCl$, PhF , dimethylformamide (dmf), 2-Clpy, 2-Brpy, 3-Clpy, 3-Brpy and CH_2Cl_2 .

In the second section, we show all the reported BEDT-TTF radical salts with the orthorhombic *pseudo*- κ or κ' phase formulated as κ' -(BEDT-TTF) $_4$ [AM^{III}(C₂O₄)₃]-G, with $A^+ = H_3O^+, NH_4^+$ and K^+ ; $M^{III} = Fe, Cr, Co, Al, Mn, Rh$ and Ru ; and $G = PhCN$ and 1,2- $PhCl_2$.

In the third section, we present all the salts with BEDT-TTF and $[M(C_2O_4)_3]^{n-}$ anions with other crystallographic phases including those containing 18-crown-6, those with two different BEDT-TTF layers, those with 3:1 BEDT-TTF:[$M(C_2O_4)_3$]³⁻ stoichiometry, those with other different and unusual packings and those with the monomeric dianions $[Ge(C_2O_4)_3]^{2-}$ and $[Cu(C_2O_4)_2]^{2-}$.

The fourth section shows all the reported salts with metal-oxalato complexes other than the monomeric complexes. These complexes include dimers of the type $[Fe_2(C_2O_4)_5]^{4-}$, trimers such as $\{M^{II}(H_2O)_2[M^{III}(C_2O_4)_3]_2\}^{4-}$, heterometallic M(II)/M(III) layers such as $[Mn^{II}M^{III}(C_2O_4)_3]^{-}$ ($M^{III} = Cr$ and Rh) and homometallic M(II)/M(II) layers such as $[Cu^{II}_2(C_2O_4)_3]^{2-}$.

Finally, in the fifth section, we will include the radical salts prepared with metal-oxalate complexes and other TTF-type donors such as tetrathiafulvalene (TTF), tetramethyltetrathiafulvalene (TMTTF), bis(ethylenediseleno)tetrathiafulvalene (BEST), bis(ethylenedithio)tetrathiafulvalene (BETS) and 4,5-bis((2S)-2-hydroxypropylthio)-4',5'-(ethylenedithio)tetrathiafulvalene (DMPET) (Scheme 1).

2. The Superconducting Monoclinic β'' Phase

2.1. β'' -BEDT-TTF Salts with the $[\text{Fe}(\text{C}_2\text{O}_4)_3]^{3-}$ Anion

As it can be seen in Table 1 (and 2), there are a total of 54 reported radical salts with BEDT-TTF and $[\text{M}(\text{C}_2\text{O}_4)_3]^{3-}$ anions showing the β'' packing mode. Among them, there are 35 salts with the $[\text{Fe}(\text{C}_2\text{O}_4)_3]^{3-}$ anion, formulated as β'' -(BEDT-TTF)₄[AFe(C₂O₄)₃]-G with $\text{A}^+ = \text{H}_3\text{O}^+$ or NH_4^+ and $\text{G} = \text{pyridine (py), PhNO}_2, \text{PhCN, 1,2-PhCl}_2, \text{PhI, PhBr, PhCl, PhF, dmf, 2-Clpy, 2-Brpy, 3-Clpy}$ and 3-Brpy (Table 1). All these isostructural salts crystallize in the monoclinic space group $\text{C2}/c$ and show alternating layers of BEDT-TTF donors and anionic layers in the ab plane (Figure 2).

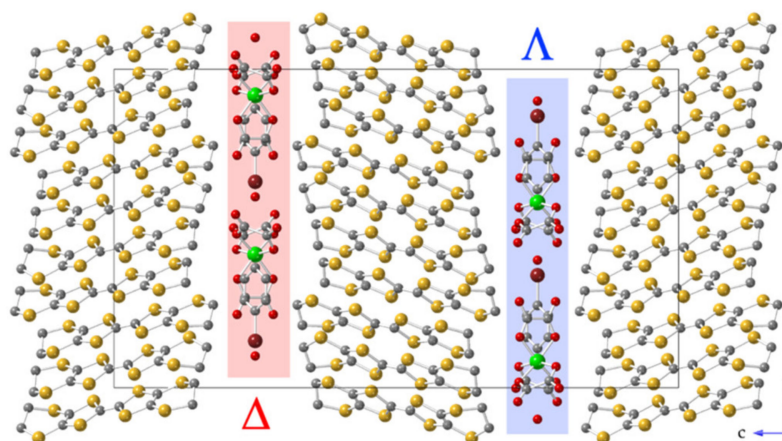


Figure 2. View of the alternating cationic/anionic layers at 292 K in compound β'' -(BEDT-TTF)₄(H₃O)Fe(C₂O₄)₃-PhBr (15). Color code: Fe = light green, C = gray, O = red, S = yellow and Br = brown. H atoms are omitted for clarity.

The BEDT-TTF layer presents the so-called β'' packing motif where the donor molecules form parallel chains with the BEDT-TTF molecules tilted with respect to the chain direction (Figure 3a) [11]. The chains contain two independent BEDT-TTF molecules (A and B) following the sequence ... AABB ... Along the chain, the A-type molecules (in red in Figure 3b) show an eclipsed packing with their neighboring A-type molecule but are displaced half-rings along the long molecular axis with respect to the neighboring B-type molecules. In contrast, B-type molecules (in blue in Figure 3b) are displaced half-rings with both neighboring molecules (A and B). There are numerous S...S contacts between BEDT-TTF molecules of consecutive stacks that favor electron delocalization. The anionic layer contains the $[\text{Fe}(\text{C}_2\text{O}_4)_3]^{3-}$ anions, the A^+ cations and the solvent molecule (G). The $[\text{Fe}(\text{C}_2\text{O}_4)_3]^{3-}$ anions and the A^+ cations form a hexagonal honeycomb layer with the Fe ions and A cations located in the vertices of the hexagons and the solvent molecules in the center of the hexagonal cavities (Figure 3b).

There are two different anionic layers in the unit cell. Each layer contains a single enantiomer, resulting in an achiral salt with the layers following the sequence ... \otimes - Λ - \otimes - Λ ... (Figure 2). The Fe-O bond distances are, as expected, very similar in all the structures.

In all these salts, the charge of the anionic $[\text{AFe}(\text{C}_2\text{O}_4)_3]^{2-}$ layers is balanced by four ET molecules. The charge estimated for each BEDT-TTF molecule from the bond distances in the BEDT-TTF molecules [12] (and from Raman spectroscopy) is +0.5, leading to a mixed-valence state with a typical $3/4$ filling of the four BEDT-TTF HOMO bands, resulting in a high electrical conductivity, as we will see below.

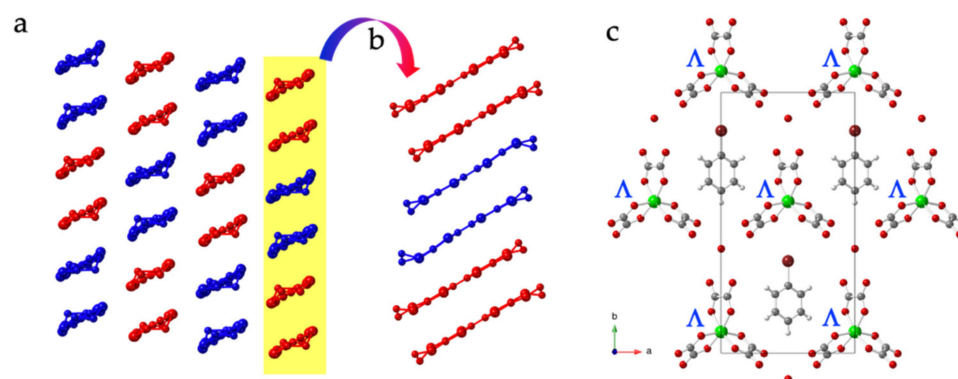


Figure 3. Structure of β'' -(BEDT-TTF)₄[(H₃O)Fe(C₂O₄)₃]·PhBr (**15**): (a) View of the BEDT-TTF layer with the β'' packing mode. A and B molecules are represented in red and blue, respectively. (b) Side view of a BEDT-TTF chain. (c) View of one hexagonal anionic layer (with the Δ enantiomers) with the PhBr molecules in the hexagonal cavity. Color code: Fe = light green, C = gray, O = red, S = yellow, Br = brown and H = white.

Despite the large number of reported structures in the series β'' -(BEDT-TTF)₄[AFe(C₂O₄)₃]·G (Table 1), there is only one reported example [13] with NH₄⁺ (and one where the exact composition could not be determined from X-ray data) [14]. All the other solved structures contain the H₃O⁺ cation. In contrast, there are many different solvents that can be found in the hexagonal cavities of the anionic layers. Thus, as it can be seen in Table 1, besides the PhCN molecule used in the first example (**35**) [3], there are also reported salts with PhNO₂ (**3**, **4**), pyridine (py) (**1**, **2**), PhF (**19**, **20**), PhCl (**17**, **18**), PhBr (**15**, **16**), PhI (**14**), 1,2-PhCl₂ (**13**), 2-Clpy (**29**, **30**), 3-Clpy (**33**), 2-Brpy (**31**, **32**), 3-Brpy (**34**) and mixtures of PhCN and py (**5–12**) or PhCN with halobenzenes (**21–27**) and even with dimethylformamide (dmf) (**28**), the only non-aromatic solvent used in the β'' series with Fe(III) [13].

The key role of the solvent on the physical properties was soon noticed by P. Day's group after the synthesis of the py (**1**, **2**) and PhNO₂ (**4**) derivatives with the same anion and the same structure [14,15]. Thus, the pyridine derivative showed a metal–insulator transition at T_{M-I} = 116 K, whereas the PhNO₂ derivative became a superconductor at T_c = 6.2 K, slightly below the PhCN derivative that showed a T_c of 8.5 K [3]. Further studies showed that the solvent molecules interact with the ethylene groups of the BEDT-TTF molecules of consecutive layers and play a key role in the order/disorder observed in these ethylene groups. The stronger the solvent–BEDT-TTF interaction, the better, since it facilitates the ordering of the ethylene groups and, therefore, favors the superconducting state. The lack of superconductivity in the salts with pyridine and the study by P. Day's group [16] showing a modulation of T_c with the PhCN/py ratio in the series of salts (ET)₄[(H₃O)Fe(C₂O₄)₃]·(PhCN)_x(py)_{1-x} (**5–12**) further supported this conclusion. Detailed studies by E. B. Yagubskii et al. confirmed this effect with other different solvents and mixtures of them [17–19]. A final proof of this key role of the solvent is provided by the series of salts (ET)₄[(H₃O)Fe(C₂O₄)₃]·PhX with X = F, Cl, Br and I (**14–20**) [20]. In this series with halobenzene derivatives, the polarity and size of the halobenzene molecules determine the presence of superconducting transitions at 1.0 and 4.0 K for X = F and Br, respectively, but no superconducting transition is observed for X = Cl above 0.4 K, and a semiconducting behavior is observed for X = I. In this series, the differences were attributed to the combined effect of the size and the electronegativity of X. For X = F, the solvent–BEDT-TTF interaction is quite strong, despite a longer distance, given the high inductive effect of F. For X = Br, the larger size of X reduces the solvent–BEDT-TTF distance, increasing the interaction. For X = Cl, we are in an intermediate situation that does not favor the interaction (too far and not enough electronegativity). Finally, for X = I, the PhI molecule is too large and cannot fit in the hexagonal cavity and appears slightly out of the hexagonal cavity, with a tilted orientation that displaces the BEDT-TTF molecules, resulting

in a loss of the metallic behavior. In fact, this compound is the only semiconducting salt reported in P. Day's series with Fe(III) (Table 1) [20].

A final interesting aspect of this series is the presence of a structural transition from the high-temperature monoclinic $C2/c$ space group to a triclinic $P-1$ one below ca. 200 K, only observed in the salts with $G = \text{PhF}$ (19, 20), PhCl (17, 18), PhBr (15, 16), 2-Clpy (29, 30) and 2-Brpy (31, 32). The first preliminary observation of this transition was reported in compound $(\text{ET})_4[(\text{H}_3\text{O})\text{Fe}(\text{C}_2\text{O}_4)_3]\cdot\text{PhBr}$ (15, 16), where a change in the unit cell parameters to a lower symmetry phase was observed at ca. 180–200 K by single-crystal X-ray data and heat capacity measurements [21]. This result was later confirmed and studied in more detail in the series $(\text{ET})_4[(\text{H}_3\text{O})\text{Fe}(\text{C}_2\text{O}_4)_3]\cdot\text{PhX}$ (15–20) and $(\text{ET})_4[(\text{H}_3\text{O})\text{Fe}(\text{C}_2\text{O}_4)_3]\cdot(\text{PhCN})_x(\text{PhX})_{1-x}$, with $X = \text{F}$ (21, 22), Cl (24, 25) and Br (26, 27) [18,20], and in compounds $(\text{ET})_4[(\text{H}_3\text{O})\text{Fe}(\text{C}_2\text{O}_4)_3]\cdot 2\text{-Clpy}$ (29, 30) and $(\text{ET})_4[(\text{H}_3\text{O})\text{Fe}(\text{C}_2\text{O}_4)_3]\cdot 2\text{-Brpy}$ (31, 32) [19]. The symmetry loss that appears due to the change in the space group from the monoclinic $C2/c$ space group to the triclinic $P-1$ one leads to the appearance of two independent BEDT-TTF layers in the unit cell (layers I and II, Figure 4), both keeping the β'' packing motif (Figure 4a,c). The number of independent BEDT-TTF molecules increases from two in the monoclinic $C2/c$ phase (A and B) to four in the triclinic $P-1$ phase (A-B in layer I and C-D in layer II).

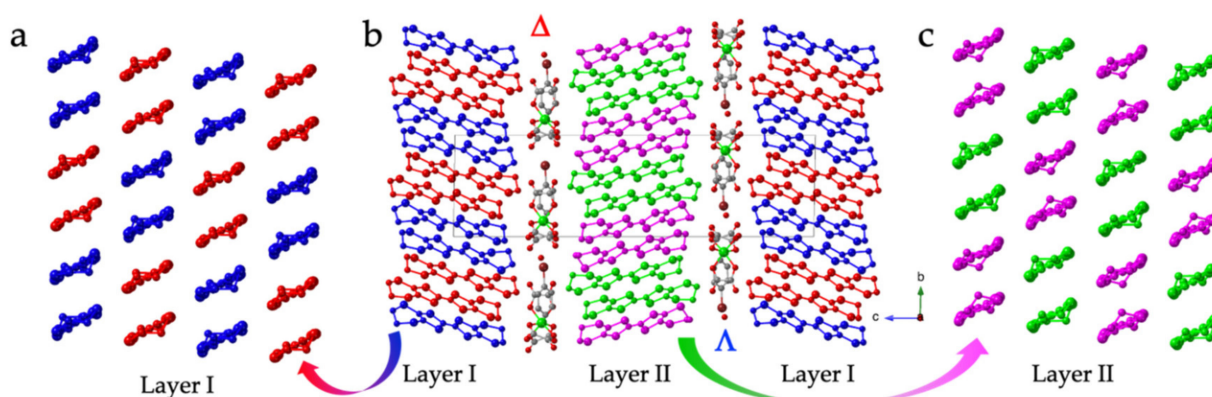


Figure 4. (a) View of layer I formed by A (red) and B (blue) BEDT-TTF molecules. (b) View of the structure of the triclinic $P-1$ phase of $\beta''\text{-(ET)}_4[(\text{H}_3\text{O})\text{Fe}(\text{C}_2\text{O}_4)_3]\cdot\text{PhBr}$ (16) at 120 K showing the two independent BEDT-TTF layers (I and II). (c) View of layer II formed by C (green) and D (pink) BEDT-TTF molecules.

As in the monoclinic phase, the chains are also formed following the sequence ... AABBB... or ... CCDD..., and the overlap between neighboring molecules follows the same scheme in both layers: A-A is eclipsed but A-B and B-B are shifted in layer I, and C-C is eclipsed but C-D and D-D are shifted in layer II.

Nevertheless, the most important changes in the triclinic $P-1$ phase are observed in the anionic layer, where the change in symmetry implies a decrease in four of the six sides of the hexagons that forces a change in the location and orientation of the solvent molecules. Thus, in the monoclinic $C2/c$ phase, the hexagons are planar, and the solvent molecule is located with the C-X bond in the hexagon plane pointing towards one Fe atom (Figure 5a). In contrast, in the triclinic $P-1$ phase, there is a reduction in the sides of the hexagons, the hexagons are not planar and the C-X bond is slightly out of the average plane and does not point to one Fe atom (Figure 5b).

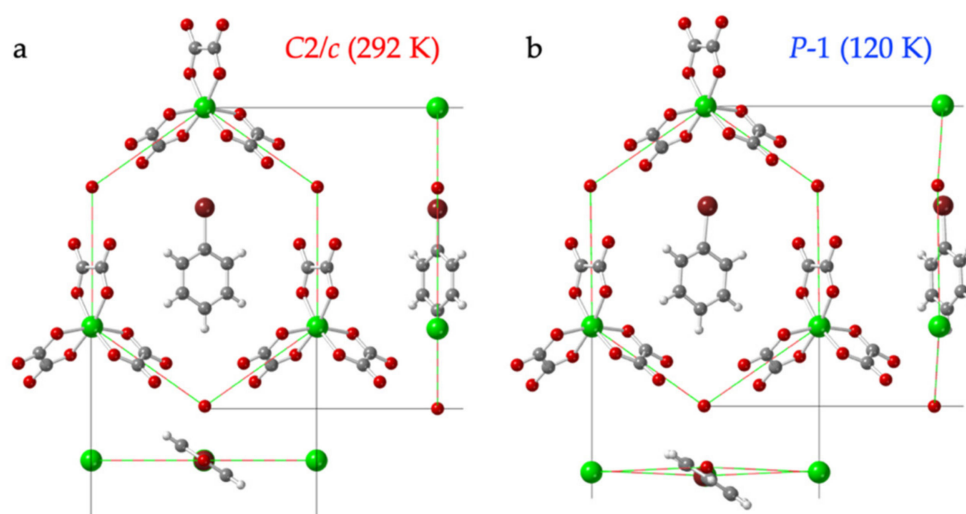


Figure 5. Front and side views of one hexagonal cavity in (a) the monoclinic $C2/c$ phase at 292 K and (b) the triclinic $P-1$ phase at 120 K in the radical salt $\beta''\text{-(BEDT-TTF)}_4[(\text{H}_3\text{O})\text{Fe}(\text{C}_2\text{O}_4)_3]\cdot\text{PhBr}$ (**15**, **16**). Color code: Fe = light green, C = gray, O = red, Br = brown and H = white.

The most interesting aspect of the series $\beta''\text{-(ET)}_4[\text{AFe}(\text{C}_2\text{O}_4)_3]\cdot\text{G}$ (**1-35**) is their electrical properties. As mentioned above, compound $(\text{ET})_4[(\text{H}_3\text{O})\text{Fe}(\text{C}_2\text{O}_4)_3]\cdot\text{PhCN}$ (**35**) is the first molecular paramagnetic superconductor and shows an ordering temperature of 6.5–8.5 K (depending on the quality of the single crystals and on the exact synthetic conditions) [2–4,17]. There is a total of seventeen superconductors reported to date in the $\beta''\text{-(ET)}_4[\text{AFe}(\text{C}_2\text{O}_4)_3]\cdot\text{G}$ series, with T_c ranging from 1.0 to 8.5 K (Table 1). These superconductors include the derivatives with G = PhNO₂ (**4**) with T_c = 6.2 K [14]; G = (PhCN)_x(py)_{1-x} (**5**, **7–12**) with T_c = 3.9–7.3 K [16]; G = PhBr (**15**) with T_c = 4.0 K [21] (Figure 6); G = PhF (**19**) with an onset of T_c = 1.0 K [20] (Figure 6); G = (PhCN)_{0.4}(PhF)_{0.6} (**21**) with T_c = 6.0 K [17]; G = (PhCN)_{0.86}(PhCl)_{0.14} (**23**) with T_c = 7.2 K [17]; G = (PhCN)_{0.35}(PhCl)_{0.65} (**24**) with T_c = 6.0 K [17]; G = (PhCN)_{0.17}(PhBr)_{0.83} (**26**) with T_c = 4.2 K [17]; G = 2-ClPy (**29**) with T_c = 2.4–4.0 K [19]; G = 2-BrPy (**31**) with T_c = 4.3 K [19]; and G = PhCN (**35**) with T_c = 8.5 K [2–4]. Except for the salt with G = PhI (**14**) [20] (Figure 6), and for a salt with H₂O and G = PhNO₂ (**3**) [22], all the other reported salts in the $\beta''\text{-(ET)}_4[(\text{H}_3\text{O})\text{Fe}(\text{C}_2\text{O}_4)_3]\cdot\text{G}$ series are metallic at room temperature and show metal–semiconductor or metal–insulator transitions at lower temperatures (Table 1).

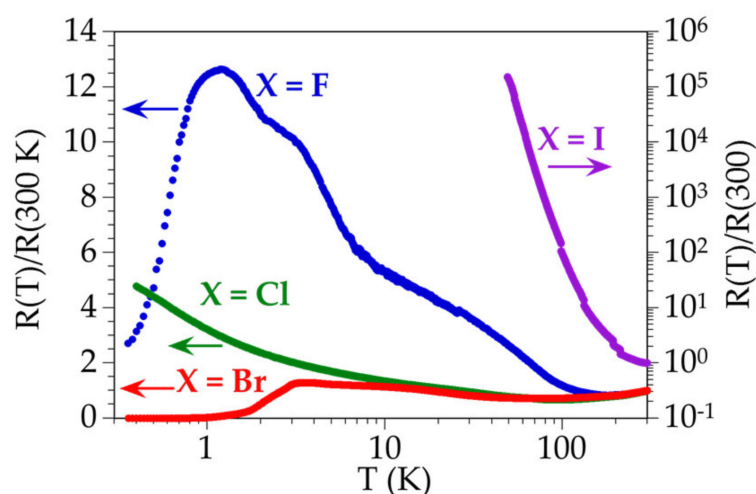


Figure 6. Electrical conductivity of the series $\beta''\text{-(BEDT-TTF)}_4[(\text{H}_3\text{O})\text{Fe}(\text{C}_2\text{O}_4)_3]\cdot\text{PhX}$ with X = F (**19**), Cl (**17**), Br (**15**) and I (**14**).

All the superconductors in the β'' -(ET)₄[(H₃O)Fe(C₂O₄)₃] \cdot G series show abrupt transitions with a sharp decrease in the resistivity values. Most of the salts reach zero resistance around one kelvin below the onset of the superconducting transition (Figures 6 and 7). The band structure calculations show that the monoclinic β'' phase is a 2D metal with stronger inter-chain than intra-chain interactions. These calculations also show the formation of $3/4$ filled bands with the Fermi level intersecting the two upper bands, leading to the observed metallic behavior [13].

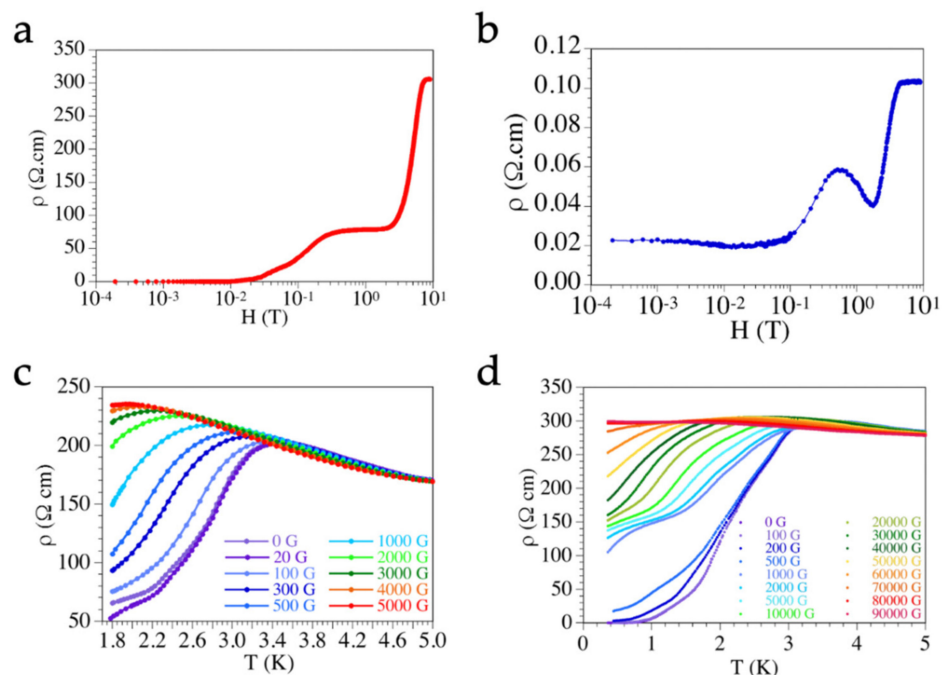


Figure 7. (a) Field dependence of the resistivity of compounds β'' -(ET)₄[(H₃O)Fe(C₂O₄)₃] \cdot PhBr (15) with the magnetic field applied perpendicular to the conducting layers. (b) Field dependence of the resistivity of compound β'' -(ET)₄[(H₃O)Fe(C₂O₄)₃] \cdot PhF (19) with the magnetic field applied parallel to the conducting layers. (c,d) Temperature dependence of the resistivity of compound β'' -(ET)₄[(H₃O)Fe(C₂O₄)₃] \cdot PhBr (15) with different applied DC fields parallel (c) and perpendicular (d) to the conducting layer.

Magnetoconductance measurements show that these salts are type II superconductors with low first critical fields of a few mT (H_{c1} , beginning of the penetration of the magnetic field) and very high second critical fields of several tesla (H_{c2} , complete suppression of the superconductivity) (Figure 7a,b). Furthermore, as expected for these quasi-2D superconductors, the effect of the magnetic field and the values of the critical fields are anisotropic and strongly depend on the direction of the applied DC field (Figure 7c,d).

The magnetic properties of these paramagnetic superconductors are those expected for isolated high-spin $S = 5/2$ [Fe(C₂O₄)₃]³⁻ anions plus a temperature-independent paramagnetism arising from the conducting sublattice (Pauli paramagnetism, Figure 8a). At very low temperatures, there is a sharp decrease in the magnetic moment due to the presence of a zero-field splitting (ZFS) in the $S = 5/2$ ground spin state.

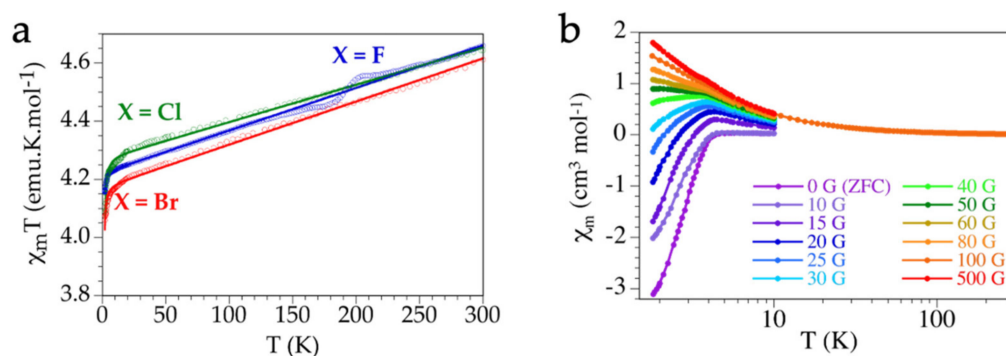


Figure 8. (a) Temperature dependence of the $\chi_m T$ product for the series β'' -(BEDT-TTF)₄[(H₃O)Fe(C₂O₄)₃]·PhX with X = F (19), Cl (17) and Br (15). (b) Temperature dependence of the zero field and field-cooled susceptibility with different applied fields for compound β'' -(BEDT-TTF)₄[(H₃O)Fe(C₂O₄)₃]·PhBr (15).

Additionally, when the samples are cooled under zero magnetic field (zero field cooling, ZFC), the superconducting transitions can be detected by the appearance of negative magnetization values (Meissner effect, Figure 8b) below the transition temperature. Heating the samples with increasing magnetic fields shows the progressive cancellation of the Meissner effect and an increase in the susceptibility values, typical of type II superconductivity (Figure 8b). For magnetic fields above a certain value, the susceptibility becomes positive at any temperature since the paramagnetic contribution of the [Fe(C₂O₄)₃]^{3−} anion dominates the magnetic response of the sample (Figure 8b).

Magnetic measurements in the presence of an alternating magnetic field (AC susceptibility) further confirm the superconducting transitions in these radical salts and allow a precise estimation of T_c and of the critical fields. Thus, AC measurements show the presence of a negative in-phase signal (χ'_m) below T_c , very similar to the ZFC susceptibility. This in-phase signal also reduces its absolute value when a DC field is applied and becomes positive at any temperature above a critical DC field when the paramagnetic contribution of the [Fe(C₂O₄)₃]^{3−} anion becomes dominant (Figure 9a). AC measurements also show an out-of-phase signal (χ''_m) that becomes non-zero at T_c (Figure 9b). The application of a DC field also reduces the χ''_m signal, which eventually cancels above the critical field (Figure 9b).

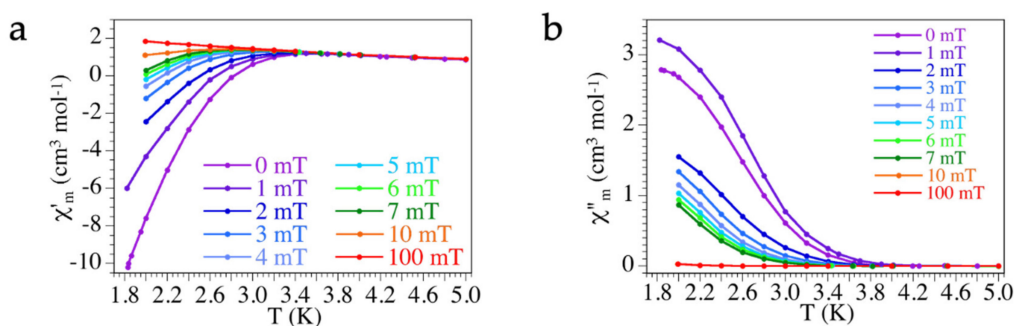


Figure 9. AC measurements of compound β'' -(BEDT-TTF)₄[(H₃O)Fe(C₂O₄)₃]·PhBr (15): temperature dependence of (a) the in-phase (χ'_m) and (b) the out-of-phase (χ''_m) AC susceptibility with different applied DC fields.

Table 1. Fe-containing radical salts of P. Day's series: β'' -(ET)₄[AFe(C₂O₄)₃]-G (1–35).

#	CCDC	Formula ^a	SG ^b	Elect. Prop	A ⁺	G	Ref.
1	BEMPEO	(ET) ₄ [(H ₃ O)Fe(ox) ₃]·0.5 py	C2/c	M > 116 K	H ₃ O ⁺	Py	[15]
2	BEMQAL	(ET) ₄ [(H ₃ O)Fe(ox) ₃]·py	C2/c	-	H ₃ O ⁺	py	[15]
3	COQNEB	(ET) ₄ [(H ₂ O)Fe(ox) ₃]·PhNO ₂	C2/c	σ = 10 S/cm Semi	-	PhNO ₂	[22]
4	ECOPIV	(ET) ₄ [(H ₃ O/NH ₄)Fe(ox) ₃]·PhNO ₂	C2/c	T _c = 6.2 K	H ₃ O ⁺ /NH ₄ ⁺	PhNO ₂	[14]
5	KILFOB	(ET) ₄ [(H ₃ O)Fe(ox) ₃]·(PhCN) _{0.78} (py) _{0.22}	C2/c	T _c = 3.9 K	H ₃ O ⁺	PhCN/py	[16]
6	KILFOB01	(ET) ₄ [(H ₃ O)Fe(ox) ₃]·(PhCN) _{0.77} (py) _{0.23}	C2/c	-	H ₃ O ⁺	PhCN/py	[16]
7	KILFOB02	(ET) ₄ [(H ₃ O)Fe(ox) ₃]·(PhCN) _{0.66} (py) _{0.34}	C2/c	T _c = 5.8 K	H ₃ O ⁺	PhCN/py	[16]
8	KILFOB03	(ET) ₄ [(H ₃ O)Fe(ox) ₃]·(PhCN) _{0.62} (py) _{0.38}	C2/c	T _c = 6.9 K	H ₃ O ⁺	PhCN/py	[16]
9	KILFOB04	(ET) ₄ [(H ₃ O)Fe(ox) ₃]·(PhCN) _{0.57} (py) _{0.43}	C2/c	T _c = 6.7 K	H ₃ O ⁺	PhCN/py	[16]
10	KILGOC	(ET) ₄ [(H ₃ O)Fe(ox) ₃]·(PhCN) _{0.46} (py) _{0.54}	C2/c	T _c = 5.9 K	H ₃ O ⁺	PhCN/py	[16]
11	KILGUI	(ET) ₄ [(H ₃ O)Fe(ox) ₃]·(PhCN) _{0.39} (py) _{0.61}	C2/c	T _c = 4.2 K	H ₃ O ⁺	PhCN/py	[16]
12	KILHAP	(ET) ₄ [(H ₃ O)Fe(ox) ₃]·(PhCN) _{0.10} (py) _{0.90}	C2/c	T _c = 7.3 K	H ₃ O ⁺	PhCN/py	[16]
13	PONMEL	(ET) ₄ [(H ₃ O)Fe(ox) ₃]·1,2-PhCl ₂	C2/c	M > 0.5 K	H ₃ O ⁺	1,2-PhCl ₂	[23]
14	QAXSIT	(ET) ₄ [(H ₃ O)Fe(ox) ₃]·PhI	C2/c	σ = 3.4 S/cm E _a = 64 meV	H ₃ O ⁺	PhI	[20]
15	SAPWEM	(ET) ₄ [(H ₃ O)Fe(ox) ₃]·PhBr	C2/c	T _c = 4.0 K	H ₃ O ⁺	PhBr	[21]
16	SAPWEM02	(ET) ₄ [(H ₃ O)Fe(ox) ₃]·PhBr	P-1	T _c = 4.0 K	H ₃ O ⁺	PhBr	[20]
17	UJOXAT	(ET) ₄ [(H ₃ O)Fe(ox) ₃]·PhCl	C2/c	M > 0.4 K	H ₃ O ⁺	PhCl	[17,20]
18	UJOXAT01	(ET) ₄ [(H ₃ O)Fe(ox) ₃]·PhCl	P-1	M > 4.2 K	H ₃ O ⁺	PhCl	[18,20]
19	UJOXEX	(ET) ₄ [(H ₃ O)Fe(ox) ₃]·PhF	C2/c	T _c = 1.0 K	H ₃ O ⁺	PhF	[17,20]
20	UJOXEX01	(ET) ₄ [(H ₃ O)Fe(ox) ₃]·PhF	P-1	T _c = 1.0 K	H ₃ O ⁺	PhF	[18,20]
21	UJOXIB	(ET) ₄ [(H ₃ O)Fe(ox) ₃]·(PhCN) _{0.4} (PhF) _{0.6}	C2/c	T _c = 6.0 K	H ₃ O ⁺	PhCN/PhF	[17]
22	UJOXIB01	(ET) ₄ [(H ₃ O)Fe(ox) ₃]·(PhCN) _{0.4} (PhF) _{0.6}	P-1	T _c = 6.0 K	H ₃ O ⁺	PhCN/PhF	[18]
23	UJOXOH	(ET) ₄ [(H ₃ O)Fe(ox) ₃]·(PhCN) _{0.86} (PhCl ₂) _{0.14}	C2/c	T _c = 7.2 K	H ₃ O ⁺	PhCN/PhCl ₂	[17]

Table 1. Cont.

#	CCDC	Formula ^a	SG ^b	Elect. Prop	A ⁺	G	Ref.
24	UJOYAU	(ET) ₄ [(H ₃ O)Fe(ox) ₃]·(PhCN) _{0.35} (PhCl) _{0.65}	C2/c	T _c = 6.0 K	H ₃ O ⁺	PhCN/PhCl	[17]
25	UJOYAU02	(ET) ₄ [(H ₃ O)Fe(ox) ₃]·(PhCN) _{0.35} (PhCl) _{0.65}	P-1	T _c = 6.0 K	H ₃ O ⁺	PhCN/PhCl	[18]
26	UJOYEY	(ET) ₄ [(H ₃ O)Fe(ox) ₃]·(PhCN) _{0.17} (PhBr) _{0.83}	C2/c	T _c = 4.2 K	H ₃ O ⁺	PhCN/PhBr	[17]
27	UJOYEY01	(ET) ₄ [(H ₃ O)Fe(ox) ₃]·(PhCN) _{0.17} (PhBr) _{0.83}	P-1	T _c = 4.2 K	H ₃ O ⁺	PhCN/PhBr	[18]
28	UMACEQ	(ET) ₄ [(NH ₄)Fe(ox) ₃]·dmf	C2/c	M > 4.2 K	NH ₄ ⁺	dmf	[13]
29	YUYTUJ	(ET) ₄ [(H ₃ O)Fe(ox) ₃]·2-Clpy	C2/c	T _c = 2.4–4.0 K	H ₃ O ⁺	2-Clpy	[19]
30	YUYTUJ01	(ET) ₄ [(H ₃ O)Fe(ox) ₃]·2-Clpy	P-1	T _c = 2.4–4.0 K	H ₃ O ⁺	2-Clpy	[19]
31	YUYVEV	(ET) ₄ [(H ₃ O)Fe(ox) ₃]·2-Brpy	C2/c	T _c = 4.3 K	H ₃ O ⁺	2-Brpy	[19]
32	YUYVEV01	(ET) ₄ [(H ₃ O)Fe(ox) ₃]·2-Brpy	P-1	T _c = 4.3 K	H ₃ O ⁺	2-Brpy	[19]
33	YUYVOF	(ET) ₄ [(H ₃ O)Fe(ox) ₃]·3-Clpy	C2/c	M > 0.5 K	H ₃ O ⁺	3-Clpy	[19]
34	YUYVUL	(ET) ₄ [(H ₃ O)Fe(ox) ₃]·3-Brpy	C2/c	M > 0.5 K	H ₃ O ⁺	3-Brpy	[19]
35	ZIGYET	(ET) ₄ [(H ₃ O)Fe(ox) ₃]·PhCN	C2/c	T _c = 6.5–8.5 K	H ₃ O ⁺	PhCN	[2–4,17]

^a ox = oxalate = C₂O₄²⁻; py = pyridine; dmf = dimethylformamide. ^b SG = space group.

2.2. β'' -BEDT-TTF Salts with Other $[M(C_2O_4)_3]^{3-}$ Anions ($M \neq Fe$)

Soon after the discovery of superconductivity in compound β'' -(ET)₄[(H₃O)Fe(C₂O₄)₃]·PhCN, P. Day's group explored the $[Cr(C_2O_4)_3]^{3-}$ anion and prepared the salts β'' -(ET)₄[(H₃O)Cr(C₂O₄)₃]·G with G = PhCN (**47**) [24,25] and PhNO₂ (**40**) [14], which also present superconducting transitions at T_c = 6.0 and 5.8 K, respectively. As it can be seen in Table 2, the $[Cr(C_2O_4)_3]^{3-}$ anion has also been combined in BEDT-TTF salts with other solvents such as PhBr, PhCl, CH₂Cl₂, dmf, 2-Clpy and 2-Brpy with A⁺ cations such as H₃O⁺, K⁺, NH₄⁺ and mixtures of them, giving rise to a superconducting salt with T_c = 1.7 K for A⁺/G = H₃O⁺/PhBr (**53**) [21], two metallic salts that remain metallic down to low temperatures for A⁺/G = (K⁺/NH₄⁺)/dmf (**50**) and K⁺/dmf (**51**) [13] and three metallic salts that show metal-insulator transitions at low temperature for A⁺/G = (K⁺/H₃O⁺)/2-Clpy (**36**), (K⁺/H₃O⁺)/2-Brpy (**37**) and H₃O⁺/PhCl (**54**) [26,27]. In one case, with A⁺/G = H₃O⁺/CH₂Cl₂ (**48**), the obtained salt is a semiconductor (although not a classical one), most probably due to the lack of interactions between the BEDT-TTF and solvent molecules [28].

Parallel to the Cr-containing $[Cr(C_2O_4)_3]^{3-}$ anion, P. Day's group also checked the diamagnetic $[Ga(C_2O_4)_3]^{3-}$ anion and obtained one superconductor formulated as (ET)₄[(H₃O)Ga(C₂O₄)₃]·PhNO₂ (**46**) [29] with T_c = 7.5 K, and also the pyridine derivative (ET)₄[(H₃O)Ga(C₂O₄)₃]·py (**45**), which might be a superconductor below 2 K, although no clear evidence was observed [29]. E. B. Yagubskii et al. also used the $[Ga(C_2O_4)_3]^{3-}$ anion to prepare the semiconducting salt (ET)₄[K_{0.33}(H₃O)_{0.67}Ga(C₂O₄)₃]·PhBr (**44**) [30], and the metallic salts (ET)₄[K_{0.8}(H₃O)_{0.2}Ga(C₂O₄)₃]·G with G = 2-Clpy (**38**) and 2-Brpy (**39**) [27]. Yagubskii's group also prepared the first example in this series with a 4d metal: (ET)₄[K_{0.7}(H₃O)_{0.3}Ru(C₂O₄)₃]·PhBr (**49**). This compound is a superconductor with T_c ranging from 2.8 to 6.3 K, depending on the measured sample [31].

There is also a preliminary account of a salt with the anion $[Mn(C_2O_4)_3]^{3-}$ formulated as (ET)₄[(H₃O)Mn(C₂O₄)₃]·PhBr (**52**) that is also a superconductor with T_c = 2.0 K [20].

Finally, L. Martin et al. prepared the only known examples in this series with the $[Rh(C_2O_4)_3]^{3-}$ anion: (BEDT-TTF)₄[ARh(C₂O₄)₃]·PhX with A/X = NH₄⁺/Br (**41**), H₃O⁺/F (**42**) and NH₄⁺/Cl (**43**) [32]. The PhBr derivative is a superconductor with T_c = 2.5 K, but the PhF and PhCl derivatives are metallic with metal-insulator transitions at 180 and 10 K, respectively (Table 2). As observed for the $[Fe(C_2O_4)_3]^{3-}$ anion, the adequate size of PhBr seems to be at the origin of the superconducting transition in the salt with $[Rh(C_2O_4)_3]^{3-}$.

A detailed revision of Tables 1 and 2 shows that among the β'' -(ET)₄[AM(C₂O₄)₃]·G salts with pure solvents, the one that has produced more superconductors is bromobenzene. This solvent has originated, to date, five superconductors, with A⁺/M^{III} = H₃O⁺/Fe (**15**), NH₄⁺/Rh (**41**), (H₃O⁺/K⁺)/Ru (**49**), H₃O⁺/Mn (**52**) and H₃O⁺/Cr (**53**). The other solvents that have given rise to more superconductors are PhNO₂, which has produced three superconductors, with A⁺/M^{III} = (H₃O⁺/NH₄⁺)/Fe (**4**), (H₃O⁺/NH₄⁺)/Cr (**40**) and H₃O⁺/Ga (**46**), and PhCN, with two superconductors, with A⁺/M^{III} = H₃O⁺/Fe (**35**) and H₃O⁺/Cr (**47**). It is interesting to note that the size of the PhBr, PhCN and PhNO₂ molecules seems to fit very well in the hexagonal cavity, and their large size allows a close contact with the ethylene groups of the BEDT-TTF molecules. This size effect of the PhBr solvent is clearly seen in the halobenzenes, where PhCl is too small and does not give superconductivity and PhI is too big and does not fit in the hexagonal cavities [20].

Table 2. Radical salts of the series β'' -(ET)₄[AM(C₂O₄)₃]·G with M ≠ Fe (36–54).

#	CCDC	Formula ^a	SG ^b	Elect. Prop.	A ⁺	M	G	Ref.
36	CIWMED	(ET) ₄ [K _{0.8} (H ₃ O) _{0.2} Cr(ox) ₃]·2-Clpy	C2/c	T _{MI} ≈ 10 K	K ⁺ /H ₃ O ⁺	Cr	2-Clpy	[27]
37	CIWMIH	(ET) ₄ [K _{0.8} (H ₃ O) _{0.2} Cr(ox) ₃]·2-Brpy	C2/c	T _{MI} ≈ 10 K	K ⁺ /H ₃ O ⁺	Cr	2-Brpy	[27]
38	CIWMON	(ET) ₄ [K _{0.8} (H ₃ O) _{0.2} Ga(ox) ₃]·2-Clpy	C2/c	T _{MI} ≈ 10 K	K ⁺ /H ₃ O ⁺	Ga	2-Clpy	[27]
39	CIWMUT	(ET) ₄ [K _{0.8} (H ₃ O) _{0.2} Ga(ox) ₃]·2-Brpy	C2/c	T _{MI} ≈ 10 K	K ⁺ /H ₃ O ⁺	Ga	2-Brpy	[27]
40	ECOPUH	(ET) ₄ [(H ₃ O/NH ₄)Cr(ox) ₃]·PhNO ₂	C2/c	T _c = 5.8 K	H ₃ O ⁺ /NH ₄ ⁺	Cr	PhNO ₂	[14]
41	FEBLIK	(ET) ₄ [(NH ₄)Rh(ox) ₃]·PhBr	C2/c	T _c = 2.5 K	NH ₄ ⁺	Rh	PhBr	[32]
42	FECDAV	(ET) ₄ [(H ₃ O)Rh(ox) ₃]·PhF	C2/c	T _{MI} ≈ 180 K	H ₃ O ⁺	Rh	PhF	[32]
43	FECDID	(ET) ₄ [(NH ₄)Rh(ox) ₃]·PhCl	C2/c	T _{MI} ≈ 10 K	NH ₄ ⁺	Rh	PhCl	[32]
44	HOBROH	(ET) ₄ [K _{0.33} (H ₃ O) _{0.67} Ga(ox) ₃]·PhBr	C2/c	Semi	K ⁺ /H ₃ O ⁺	Ga	PhBr	[30]
45	HUNQIQ	(ET) ₄ [(H ₃ O)Ga(ox) ₃]·py	C2/c	T _c ≈ 2 K ??	H ₃ O ⁺	Ga	py	[29]
46	HUNQUC	(ET) ₄ [(H ₃ O)Ga(ox) ₃]·PhNO ₂	C2/c	T _c = 7.5 K	H ₃ O ⁺	Ga	PhNO ₂	[29]
47	JUPGUW01	(ET) ₄ [(H ₃ O)Cr(ox) ₃]·PhCN	C2/c	T _c = 6.0 K	H ₃ O ⁺	Cr	PhCN	[4,24,25]
48	MEQZIR	(ET) ₄ [(H ₃ O)Cr(ox) ₃]·CH ₂ Cl ₂	C2/c	Semi	H ₃ O ⁺	Cr	CH ₂ Cl ₂	[28]
49	UDETUU	(ET) ₄ [K _{0.7} (H ₃ O) _{0.3} Ru(ox) ₃]·PhBr	C2/c	T _c = 2.8–6.3 K	K ⁺ /H ₃ O ⁺	Ru	PhBr	[31]
50	UMACAM	(ET) ₄ [(K/NH ₄)Cr(ox) ₃]·dmf	C2/c	M > 4.2	K ⁺ /NH ₄ ⁺	Cr	dmf	[13]
51	UMACIU	(ET) ₄ [KCr(ox) ₃]·dmf	C2/c	M > 4.2	K ⁺	Cr	dmf	[13]
52	-	(ET) ₄ [(H ₃ O)Mn(ox) ₃]·PhBr	C2/c	T _c = 2.0 K	H ₃ O ⁺	Mn	PhBr	[20]
53	-	(ET) ₄ [(H ₃ O)Cr(ox) ₃]·PhBr	C2/c	T _c = 1.7 K	H ₃ O ⁺	Cr	PhBr	[21,26]
54	-	(ET) ₄ [(H ₃ O)Cr(ox) ₃]·PhCl	C2/c	M > 130 K σ ₃₀₀ = 3 × 10 ⁻³ S/cm	H ₃ O ⁺	Cr	PhCl	[26]

^a ox = oxalate = C₂O₄²⁻; py = pyridine; dmf = dimethylformamide. ^b SG = space group.

3. The Semiconducting *pseudo-κ* or *κ'* Phase

κ'-BEDT-TTF Radical Salts with $[M(C_2O_4)_3]^{3-}$ Anions

Besides the monoclinic $C2/c$ β'' salts described in the previous section, P. Day's group also obtained an orthorhombic $Pbcn$ phase with the same $[Fe(C_2O_4)_3]^{3-}$ anion and the same PhCN solvent, but with $A^+ = NH_4^+$ and K^+ [2]. These orthorhombic salts show an original packing, called *pseudo-κ* or *κ'* phase, and present the same general formula as the β'' phase: κ' -(BEDT-TTF) $_4$ [AM(C₂O₄)₃] \cdot G (Table 3). The structure of the *κ'* phase also consists of alternating cationic layers containing the BEDT-TTF molecules and anionic layers containing the A^+ cations, the $[M(C_2O_4)_3]^{3-}$ anions and the solvent molecules (Figure 10).

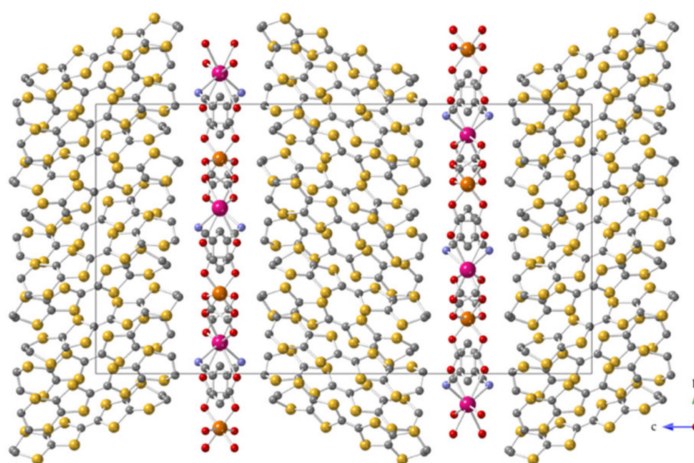


Figure 10. View of the alternating cationic/anionic layers in compound κ' -(BEDT-TTF) $_4$ [(H₃O)Mn(C₂O₄)₃] \cdot PhCN (55). Color code: Mn = orange, K = pink, C = gray, O = red, N = blue and S = yellow. H atoms are omitted for clarity.

The BEDT-TTF layer is also formed by two independent BEDT-TTF molecules noted as A and B. A-type molecules bear a charge of +1, whereas B-type molecules are neutral. The BEDT-TTF layer presents the so-called *pseudo-κ* or *κ'* packing motif formed by eclipsed A-A dimers surrounded by six B-type monomers in a distorted hexagonal arrangement (Figure 11a). As in the monoclinic β'' phase, the anionic layer contains the $[M(C_2O_4)_3]^{3-}$ anions and the A^+ cations forming a hexagonal lattice with the solvent molecules (G) inside the hexagonal cavities. The main difference is that now the anionic layers are equivalent since they contain both enantiomers in a 1:1 ratio arranged in alternating rows (Figure 11b). In both phases, the anionic layers are related by a C_2 axis. This different disposition of the \otimes and Λ enantiomers in the anionic layers is at the origin of the different packing motifs of the BEDT-TTF molecules in both phases [4].

As already noted by Peter Day's group [4], a close look at the cation–anion interlayer interactions shows that the relative orientation of the BEDT-TTF molecules depends on the chirality of the closest $[M(C_2O_4)_3]^{3-}$ anions. Thus, in the monoclinic β'' phase, when the ethylene groups of the BEDT-TTF molecules interact with the terminal O atoms of \otimes - $[M(C_2O_4)_3]^{3-}$ anions, the BEDT-TTF chains run from bottom right to top left (Figure 12a), whereas, when they interact with Λ - $[M(C_2O_4)_3]^{3-}$ anions, the BEDT-TTF chains run from bottom left to top right (Figure 12b). In the orthorhombic *κ'* phase, the anionic layers contain both enantiomers arranged in rows located close to the BEDT-TTF dimers, and, accordingly, the orientation of these dimers follows the same trend: they run from bottom right to top left when they interact with \otimes - $[M(C_2O_4)_3]^{3-}$ anions (in green in Figure 12c) and from bottom left to top right when they interact with Λ - $[M(C_2O_4)_3]^{3-}$ anions (in orange in Figure 12c). The monomers in the *κ'* phase (in pink in Figure 12c) do not interact with the $[M(C_2O_4)_3]^{3-}$ anions and are packed following the BEDT-TTF dimers that they enclose.

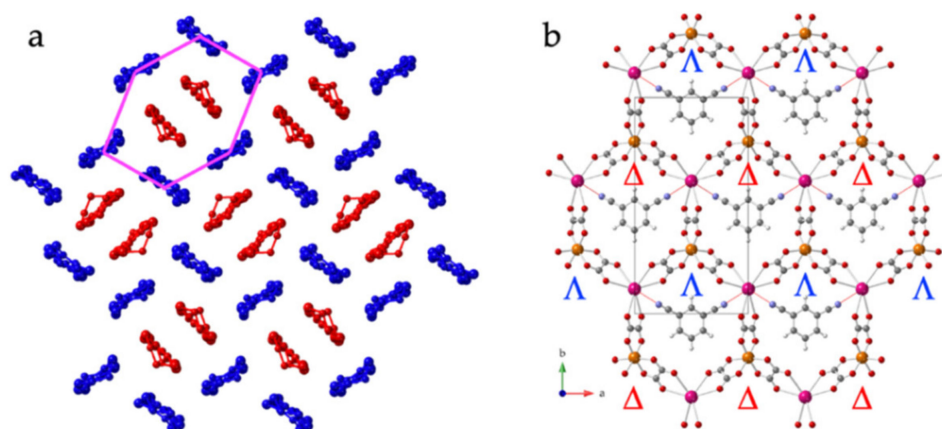


Figure 11. Structure of κ' -(BEDT-TTF)₄[KMn(C₂O₄)₃]·PhCN (55): (a) View of the BEDT-TTF layer with the κ' packing mode (A and B molecules are drawn in red and blue, respectively). (b) View of one hexagonal anionic layer showing the Λ and \otimes enantiomers arranged in rows and the PhCN molecules in the hexagonal cavities (the CN groups are disordered over two positions). Color code in (b): Mn = orange, K = pink, C = gray, O = red, N = blue and H = white.

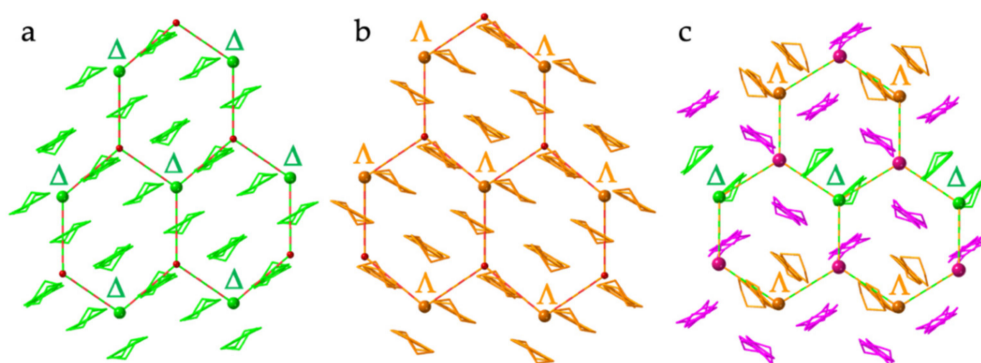


Figure 12. View of the relative orientation of the BEDT-TTF molecules with the chirality of the $[M(C_2O_4)_3]^{3-}$ anions closest to them (only the metal centers and the A^+ cations are shown): (a) \otimes -type layer in β'' -(ET)₄[(H₃O)Fe(C₂O₄)₃]·PhBr (15). (b) Λ -type layer in β'' -(ET)₄[(H₃O)Fe(C₂O₄)₃]·PhBr (15). (c) Alternating \otimes - Λ layer in κ' -(ET)₄[KMn(C₂O₄)₃]·PhCN (55) showing the two different orientations of the BEDT-TTF dimers depending on the chirality (\otimes = green, Λ = orange) of the closest $[M(C_2O_4)_3]^{3-}$ anion.

The orthorhombic *pseudo*- κ phase has been observed in a total of nine salts to date (Table 3). Interestingly, in all these salts, the solvent is always PhCN (in one case with a small fraction of PhCl₂) [17]. Despite the low number of reported salts, this series presents a large variability in the anionic layer with three different A^+ cations (K^+ , NH_4^+ or H_3O^+) and seven different metal ions ($M = Mn, Rh, Cr, Co, Al, Ru$ and Fe).

Analysis of the bond distances in the BEDT-TTF molecules indicates that the molecules forming the dimers (A-type) are completely ionized, whereas the isolated BEDT-TTF molecules (B-type) are neutral. The presence of totally ionized (BEDT-TTF)₂²⁺ dimers surrounded by neutral BEDT-TTF molecules precludes the electron delocalization in the BEDT-TTF layers, and, accordingly, all the reported κ' salts are semiconductors (Table 3) with activation energies in the range 140 to 245 meV in all cases (Figure 13).

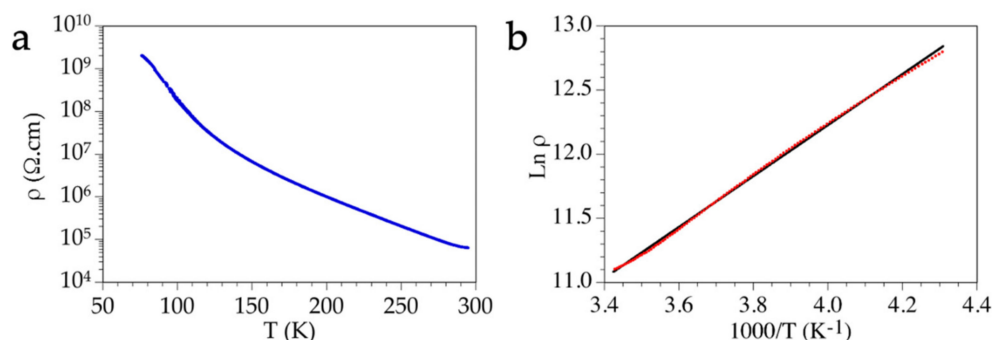


Figure 13. (a) Thermal dependence of the resistivity and (b) Arrhenius plot ($\ln \rho$ vs. $1/T$) for the salt $\kappa'-(\text{ET})_4[\text{KMn}(\text{C}_2\text{O}_4)_3]\cdot\text{PhCN}$ (**55**) (red line is the fit to the Arrhenius equation for a classical semiconductor).

Band structure calculations indicate that there is a very strong intradimer (A-A) interaction corresponding to the overlap of the BEDT-TTF⁺ molecules of the almost eclipsed face-to-face dimers. The transfer integrals are around ten times larger than those between the neutral isolated molecules and the dimers (A-B). The transfer integrals between the isolated neutral molecules (B-B) are very small except for one case [2]. The presence of (BEDT-TTF)₂²⁺ dimers leads to the formation of a full band and an empty band, separated by a band gap, resulting in the observed semiconducting behavior in all these orthorhombic salts [4].

Table 3. Radical salts of the orthorhombic P. Day series $\kappa'-(\text{ET})_4[\text{AM}(\text{C}_2\text{O}_4)_3]\cdot\text{G}$ (**55–63**).

#	CCDC	Formula ^a	SG ^b	Elect. Prop.	A ⁺	M	G	Ref.
55	CISMEZ	$\kappa'-(\text{ET})_4[\text{KMn}(\text{ox})_3]\cdot\text{PhCN}$	<i>Pbcn</i>	$\sigma = 2 \times 10^{-5} \text{ S/cm}$ $E_a = 180 \text{ meV}$	K ⁺	Mn	PhCN	[33]
56	FECDEZ	$\kappa'-(\text{ET})_4[(\text{NH}_4)\text{Rh}(\text{ox})_3]\cdot\text{PhCN}$	<i>Pbcn</i>	$E_a = 245 \text{ meV}$	NH ₄ ⁺	Rh	PhCN	[32]
57	JUPGUW	$\kappa'-(\text{ET})_4[(\text{H}_3\text{O})\text{Cr}(\text{ox})_3]\cdot\text{PhCN}$	<i>Pbcn</i>	$E_a = 153 \text{ meV}$	H ₃ O ⁺	Cr	PhCN	[4,25]
58	QIWMOY	$\kappa'-(\text{ET})_4[(\text{NH}_4)\text{Co}(\text{ox})_3]\cdot\text{PhCN}$	<i>Pbcn</i>	$E_a = 225 \text{ meV}$	NH ₄ ⁺	Co	PhCN	[4]
59	QIWMUE	$\kappa'-(\text{ET})_4[(\text{NH}_4)\text{Al}(\text{ox})_3]\cdot\text{PhCN}$	<i>Pbcn</i>	$E_a = 222 \text{ meV}$	NH ₄ ⁺	Al	PhCN	[4]
60	UDET00	$\kappa'-(\text{ET})_4[\text{K}_{0.8}(\text{H}_3\text{O})_{0.2}\text{Ru}(\text{ox})_3]\cdot\text{PhCN}$	<i>Pbcn</i>	Semi	K ⁺ /H ₃ O ⁺	Ru	PhCN	[31]
61	UJOXUN	$\kappa'-(\text{ET})_4[(\text{H}_3\text{O})\text{Fe}(\text{ox})_3]\cdot(\text{PhCN})_{0.88}(\text{PhCl}_2)_{0.12}$	<i>Pbcn</i>	Semi	H ₃ O ⁺	Fe	PhCl ₂ /PhCN	[17]
62	ZIWNEY	$\kappa'-(\text{ET})_4[(\text{NH}_4)\text{Fe}(\text{ox})_3]\cdot\text{PhCN}$	<i>Pbcn</i>	$\sigma = 10^{-4} \text{ S/cm}$ $E_a = 140 \text{ meV}$	NH ₄ ⁺	Fe	PhCN	[2,4]
63	ZIWNIC	$\kappa'-(\text{ET})_4[\text{KFe}(\text{ox})_3]\cdot\text{PhCN}$	<i>Pbcn</i>	$\sigma = 10^{-4} \text{ S/cm}$ $E_a = 140 \text{ meV}$	K ⁺	Fe	PhCN	[2]

^a ox = oxalate = C₂O₄²⁻; ^b SG = space group.

4. Other Phases with BEDT-TTF and Oxalato Complexes

Besides the β'' and κ' phases, the intense research in the field has led to the synthesis of several other crystallographic phases with BEDT-TTF, different [M(C₂O₄)₃]³⁻ anions (or the dianions [Ge(C₂O₄)₃]²⁻ and [Cu(C₂O₄)₂]²⁻), different solvents (including chiral ones) and even the inclusion of 18-crown-6 molecules. In this section, we will revise all these salts and classify them according to their composition and crystallographic phase.

4.1. BEDT-TTF Salts with [M(C₂O₄)₃]³⁻ Anions and 18-Crown-6

The use of the crown ether 18-crown-6 in order to solubilize the precursor NH₄⁺ salts of different [M(C₂O₄)₃]³⁻ anions has led to the inclusion of the 18-crown-6 molecules into the crystal structure in a total of eight salts (Table 4). The first of these 18-crown-6-containing salts was also reported by P. Day's group in compound β''-(BEDT-TTF)₄[(H₃O)Cr(C₂O₄)₃]₂-

$[(\text{H}_3\text{O})_2(18\text{-crown-6})]\cdot 5\text{H}_2\text{O}$ (**64**) [34]. The structure shows alternating cationic and anionic layers (Figure 14a). The anionic layers are formed by two layers of $[\text{M}(\text{C}_2\text{O}_4)_3]^{3-}$ anions separated by a layer with the 18-crown-6 molecules and the crystallization water molecules (Figure 14a). Each of the two $[\text{M}(\text{C}_2\text{O}_4)_3]^{3-}$ layers contains only one enantiomer (Figure 14b). The cationic layers are formed by two independent BEDT-TTF molecules with the β'' packing mode (Figure 14c) with chains of BEDT-TTF molecules following the sequence ... AABB ... with the same overlap mode (Figure 14d) as the superconducting monoclinic phase. This salt presents proton channels formed by the 18-crown-6 molecules containing H_3O^+ cations (Figure 14e) and presents a proton conductivity above 10^{-3} S/cm at room temperature. There is a Ga/ NH_4^+ derivative with the same structure: $\beta''\text{-(ET)}_4[(\text{NH}_4)\text{Ga}(\text{C}_2\text{O}_4)_3]_2[(\text{NH}_4)_2(18\text{-crown-6})]\cdot 5\text{H}_2\text{O}$ (**68**), also reported by P. Day's group [35]. Interestingly, both salts are metallic at room temperature but show metal-insulator transitions at 190 and 240 K, respectively.

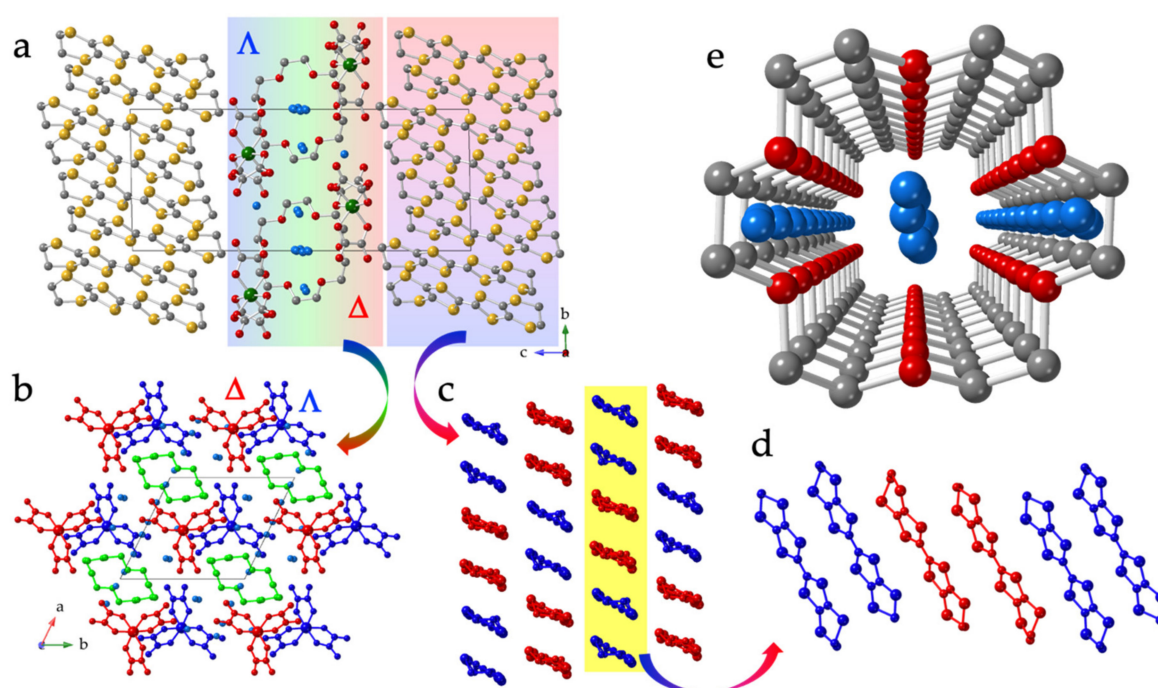


Figure 14. Structure of $\beta''\text{-(ET)}_4[(\text{H}_3\text{O})\text{Cr}(\text{C}_2\text{O}_4)_3]_2[(\text{H}_3\text{O})_2(18\text{-crown-6})]\cdot 5\text{H}_2\text{O}$ (**64**). (a) View of the alternating cationic and anionic layers parallel to the ab plane. (b) Top view of the anionic triple layer containing the $\otimes\text{-}[\text{Cr}(\text{C}_2\text{O}_4)_3]^{3-}$ anions (in red), the 18-crown-6 ether (in green) and the $\Lambda\text{-}[\text{Cr}(\text{C}_2\text{O}_4)_3]^{3-}$ anions (in blue). (c) View of the BEDT-TTF layers showing the β'' packing (A- and B-type molecules are drawn in red and blue, respectively). (d) Side view of one BEDT-TTF stack. (e) View of the proton channels formed by the 18-crown-6 molecules. Color code in (a,e): Cr = dark green, C = gray, O = red, O_{water} = blue and S = yellow. H atoms are omitted for clarity.

A second phase obtained with 18-crown-6 is the series of salts formulated as $\beta''\text{-(ET)}_2[(\text{H}_2\text{O})(\text{NH}_4)_2\text{M}(\text{C}_2\text{O}_4)_3]\cdot 18\text{-crown-6}$, with $\text{M} = \text{Ir}$ (**65**) [36], Ru (**66**) [36], Cr (**67**) [37] and Rh (**69**) [38] (Table 3). The structure resembles that of the previously described compounds $\beta''\text{-(ET)}_4[(\text{A})\text{M}(\text{C}_2\text{O}_4)_3]_2[(\text{A})_2(18\text{-crown-6})]\cdot 5\text{H}_2\text{O}$ with $\text{A}^+/\text{M} = \text{H}_3\text{O}^+/\text{Cr}$ (**64**) and NH_4^+/Ga (**68**). It also consists of alternating layers of BEDT-TTF molecules with the β'' packing motif and double anionic layers separated by the 18-crown-6 molecules, although, now, the 18-crown-6 molecules are inserted in the hexagonal cavities formed by the $[\text{M}(\text{C}_2\text{O}_4)_3]^{3-}$ anions.

The Cr and Rh salts are superconductors with $T_c = 4.0\text{--}4.9$ K and 2.7 K, respectively [37,38]. This phase is the second one with a $[\text{M}(\text{C}_2\text{O}_4)_3]^{3-}$ complex to show superconductivity and is the phase with single-donor packing with the widest gap between conducting layers. The Ir and Ru salts are not superconductors due to the shorter inter-

layer M–M distance (worse 2D systems). The M–I transition in these salts may originate from changes in the anionic layer which induce changes in the BEDT-TTF layer, although Berezinski–Kosterlitz–Thouless (BKT) effects are not discarded [36]. The Ir salt is the first radical salt with a 5d tris(oxalato)metalate anion [36].

There are two additional radical salts with $[M(C_2O_4)_3]^{3-}$ anions containing 18-crown-6: α -(ET)₁₀(18-crown-6)₆K₆[Fe(C₂O₄)₃]₄·24H₂O (70) [39] and (ET)₄[Ga(C₂O₄)₃](18-crown-6)(H₂O)₆ (71). In compound 70, the packing is original and consists of three types of alternating layers: BEDT-TTF layers (A-layers), layers containing $[Fe(C_2O_4)_3]^{3-}$ anions, water, 18-crown-6 and K⁺ cations (B-layers) and layers with water, 18-crown-6 and K⁺ cations (C-layers). These three layers alternate following the sequence . . . ABCBABCBA . . . This salt behaves as a classical semiconductor with an activation energy of 15 meV [39]. The last salt with 18-crown-6: (ET)₄[Ga(C₂O₄)₃](18-crown-6)(H₂O)₆ (71), has been deposited in the CCDC database but has not been published yet.

Table 4. Radical salts of BEDT-TTF with $[M(C_2O_4)_3]^{3-}$ anions containing 18-crown-6 (64–71).

#	CCDC	Formula ^a	SG ^b	Elect. Prop.	A ⁺	M	G	Ref.
64	ACAGUG	β'' -(ET) ₄ [(H ₃ O)Cr(ox) ₃] ₂ [(H ₃ O) ₂ (18-c-6)]·5H ₂ O	P-1	$\sigma = 300$ S/cm $T_{MI} = 190$ K	H ₃ O ⁺	Cr	H ₂ O/18-c-6	[34,35]
65	COLWUY	β'' -(ET) ₂ [(H ₂ O)(NH ₄) ₂ Ir(ox) ₃]·18-c-6	P-1	$T_{MI} \approx 100$ K	NH ₄ ⁺	Ir	H ₂ O/18-c-6	[36]
66	COLYOU	β'' -(ET) ₂ [(H ₂ O)(NH ₄) ₂ Ru(ox) ₃]·18-c-6	P-1	$T_{MI} \approx 155$ K	NH ₄ ⁺	Ru	H ₂ O/18-c-6	[36]
67	FENHEO	β'' -(ET) ₂ [(H ₂ O)(NH ₄) ₂ Cr(ox) ₃]·18-c-6	P-1	$T_c = 4.0$ – 4.9 K	NH ₄ ⁺	Cr	H ₂ O/18-c-6	[37]
68	FEQQUAU	β'' -(ET) ₄ [(NH ₄) ₂ Ga(ox) ₃] ₂ [(NH ₄) ₂ (18-c-6)]·5H ₂ O	P-1	$\sigma = 200$ S/cm $T_{MI} = 240$ K	NH ₄ ⁺	Ga	H ₂ O/18-c-6	[35]
69	KATLAV	β'' -(ET) ₂ [(H ₂ O)(NH ₄) ₂ Rh(ox) ₃]·18-c-6	P-1	$T_c = 2.7$ K	NH ₄ ⁺	Rh	H ₂ O/18-c-6	[38]
70	NIHPEA	α -(ET) ₁₀ (18-c-6) ₆ K ₆ [Fe(ox) ₃] ₄ ·24H ₂ O	$P2_1/c$	$E_a = 105$ meV	K ⁺	Fe	H ₂ O/18-c-6	[39]
71	UJEYIR	(ET) ₄ [Ga(ox) ₃](18-c-6)(H ₂ O) ₆	P-1	-	-	Ga	H ₂ O/18-c-6	^c

^a ox = oxalate = C₂O₄²⁻; 18-c-6 = 18-crown-6 = C₁₂H₂₄O₆; ^b SG = space group. ^c Unpublished results.

4.2. BEDT-TTF Salts with $[M(C_2O_4)_3]^{3-}$ Anions and Two Different Donor Layers

The use of larger non-planar solvent molecules and chiral ones has led to some nice examples of double-layered phases. These chiral and large non-planar solvent molecules do not fit in the hexagonal cavities of the anionic layers and are forced to cross the cavities, resulting in anionic layers with two different sides. This asymmetry of the two sides of the anionic layers induces two different packing modes in the BEDT-TTF molecules, resulting in salts with two different cationic layers. There are two different series of double-layered phases: the α, β'' , and the α, κ' .

The α, β'' phase has been observed in the series α, β'' -(ET)₄[(NH₄)M(C₂O₄)₃]·G with M/G = Ga/PhN(CH₃)CHO (72) [40], M/G = Ga/PhCH₂CN (73) [40], M/G = Fe/PhCOCH₃ (74) [40], M/G = Fe/(S)-PhC(OH)HCH₃ (75) [41] and M/G = Fe/(R/S)-PhC(OH)HCH₃ (77) [41] (Table 5). These salts are isostructural and crystallize in the triclinic P -1 space group, except the salt α, β'' -(ET)₄[(NH₄)Fe(C₂O₄)₃](S)-PhC(OH)HCH₃ (75) that contains a single enantiomer (S) of the chiral solvent PhC(OH)HCH₃ and crystallizes in the $P1$ space group. The α, β'' salts show alternating cationic and anionic layers following the sequence . . . / β'' /⊗/ α /Λ/ . . . (Figure 15a). The anionic layers are very similar to those of the monoclinic β'' phase: they contain the $[M(C_2O_4)_3]^{3-}$ anions and the NH₄⁺ cations forming

a hexagonal honeycomb lattice with the solvent molecules located in the hexagonal cavities. There are two homochiral layers that alternate along the c axis (Figure 15b,c), each with a different $[\text{M}(\text{C}_2\text{O}_4)_3]^{3-}$ enantiomer and a slightly different orientation of the polar group of the solvent molecule. The main difference with the monoclinic β'' phase is that, now, there are two different sides since the large solvent molecules cross the hexagonal cavities with the X groups pointing to one of the two sides to generate a corrugated side, next to the β'' layer, and a smoother face, next to the α layer (Figure 15a). The polar groups of the solvent molecules point to the β'' layer (purple circles in Figure 15a).

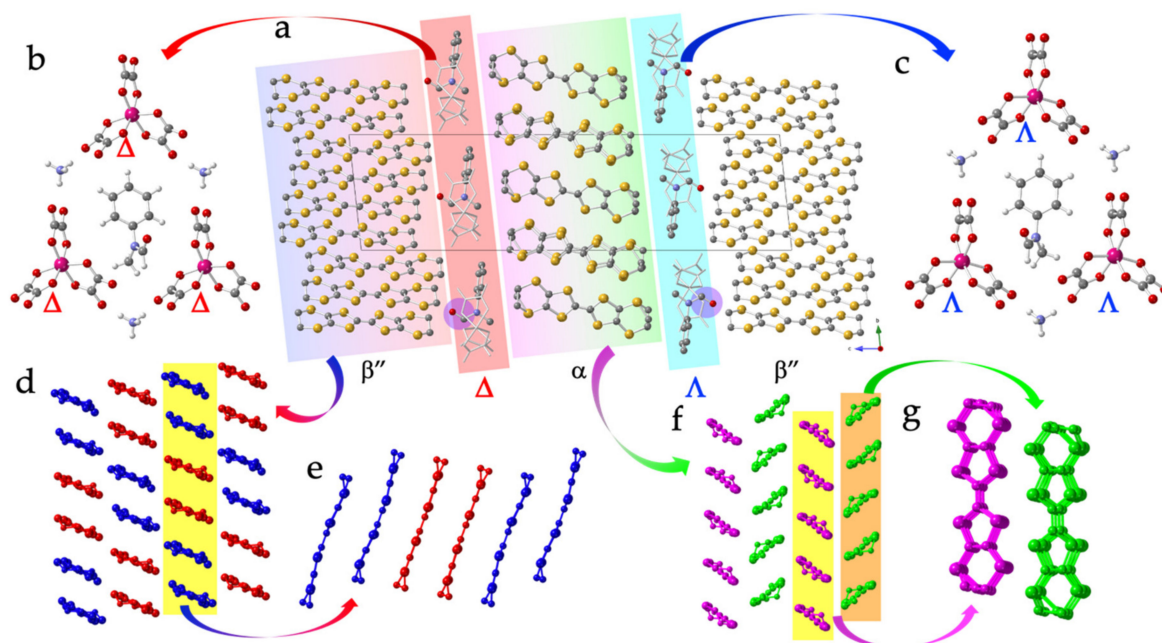


Figure 15. Structure of α, β'' -(ET)₄[(NH_4) $\text{Ga}(\text{C}_2\text{O}_4)_3$]· $\text{PhN}(\text{CH}_3)\text{CHO}$ (**72**): (a) View of the alternating cationic and anionic layers following the sequence $\dots \beta''$ - \otimes - α - Δ - β'' \dots . The purple circles mark the position of the CHO groups of the solvent molecules pointing to the β'' layer. (b) View of the \otimes layer. (c) View of the Δ layer. (d) View of the β'' layer showing the two independent BEDT-TTF molecules (A and B) in red and blue, respectively. (e) Side view of one BEDT-TTF chain. (f) View of the α layer showing the two independent BEDT-TTF molecules (C and D) in pink and green, respectively. (g) Frontal view of the C- and D-type chains. Color code in (a–c): Ga = pink, C = gray, O = red, N = blue, H = white and S = yellow. Except in (b,c), H atoms are omitted for clarity.

There are two different cationic layers, with β'' and α packing modes, alternating along the c axis. The β'' layer (Figure 15d) is formed by two independent BEDT-TTF molecules (A and B) packing in chains with the sequence $\dots \text{AABB} \dots$, as in the monoclinic β'' phase. The only difference is that, now, the overlap between the BEDT-TTF molecules in the chain is eclipsed for AA and AB but shifted for BB. This overlap mode generates groups of four eclipsed BEDT-TTF molecules (Figure 15e). In the α layer, the molecules of consecutive stacks are tilted in opposite directions (Figure 15f). There are also two independent molecules (C and D) that form two different stacks containing only C or only D molecules packed with an eclipsed overlap (Figure 15g).

Compounds **72–74**, also reported by P. Day's group [40], were the first examples of the α, β'' phase (which is the third phase found in the ET_4 series, after the β'' and κ' ones). All the reported α, β'' salts show relatively high room temperature conductivities but are semiconductors, although band structure calculations indicate that both BEDT-TTF layers should be metallic [40].

The other double-layer phase is the α, κ' one, reported in two isostructural compounds with the same solvent molecule (1,2-dibromobenzene): α, κ' -(ET)₄[$\text{K}_{0.45}(\text{H}_3\text{O})_{0.55}\text{Ga}(\text{C}_2\text{O}_4)_3$]·1,2- PhBr_2 (**76**) [30] and α, κ' -(ET)₄[(H_3O) $\text{Fe}(\text{C}_2\text{O}_4)_3$]·1,2- PhBr_2 (**78**) [42] (Table 5). The structure of these

salts also consists of alternating cationic and anionic layers (Figure 16a). There are also two alternating cationic layers with two different packing motifs: κ' and α (Figure 16b,c). The κ' layers are formed by four independent BEDT-TTF molecules (A–D) forming two different face-to-face dimers (AA and CC) surrounded by isolated BEDT-TTF molecules (B and D) (Figure 16b). The α layers also contain four independent BEDT-TTF molecules (E–H) forming three different stacks containing only E, only H and alternating F/G molecules (Figure 16c). The BEDT-TTF molecules are packed in an eclipsed way in the three stacks. The anionic layers present the same hexagonal disposition observed in the β'' and κ' phases and contain both enantiomers of the $[\text{M}(\text{C}_2\text{O}_4)_3]^{3-}$ anions (arranged in parallel rows, as observed in the κ' phase), together with A^+ cations (Figure 16d). The 1,2-PhBr₂ solvent molecules are located in the cavities with the two Br atoms pointing towards the α layer (Figure 16a). This asymmetry in both faces of the anionic layers induces the crystallization of two different layers, as observed in the α, β'' phase. Both salts are metallic down to low temperatures, although they do not show superconductivity. This metallic behavior is attributed to the α layers that show a homogeneous charge distribution in the BEDT-TTF molecules, in contrast to the κ' layers that present the same charge localization observed in the other κ' phases: $(\text{BEDT-TTF})_2^{2+}$ dimers surrounded by neutral BEDT-TTF molecules.

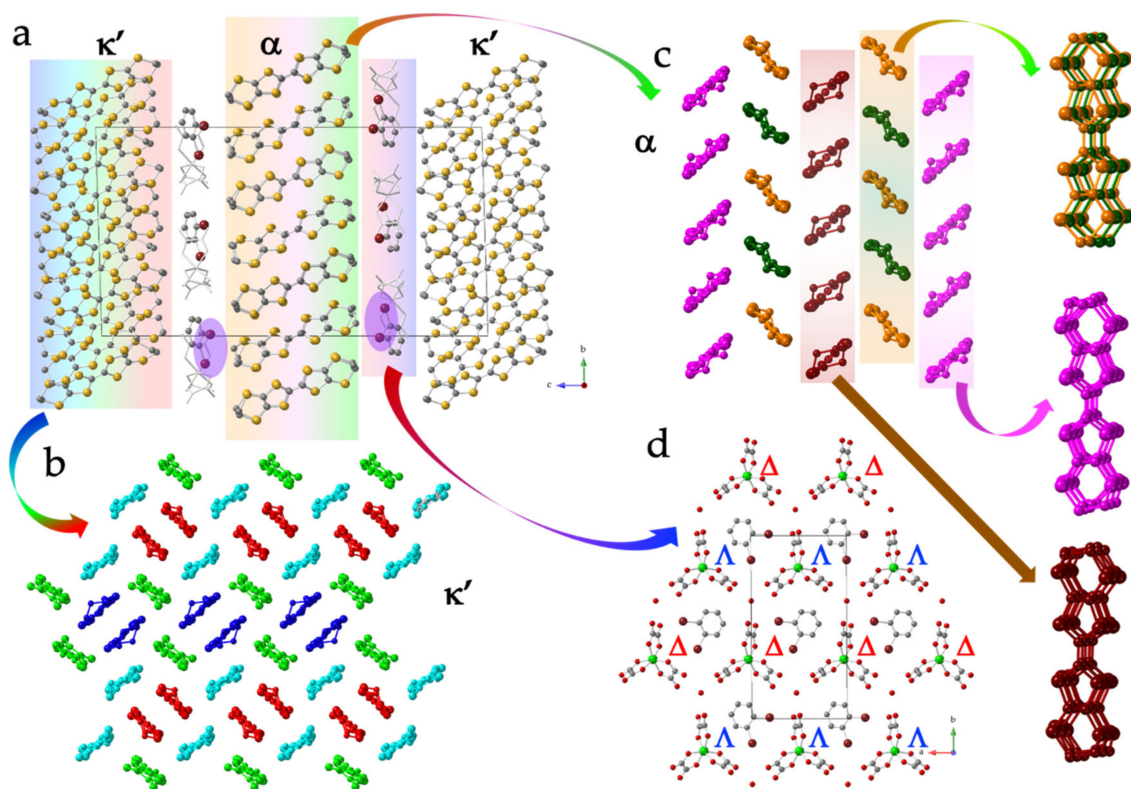


Figure 16. Structure of α, κ' -(ET)₄[(H₃O)Fe(C₂O₄)₃]·1,2-PhBr₂ (78): (a) View of the alternating cationic and anionic layers following the sequence $\kappa' \otimes / \Delta - \alpha - \otimes / \Delta - \kappa'$. The purple circles mark the position of the two Br atoms of the solvent molecules pointing to the α layer. (b) View of the κ' layer showing the four independent BEDT-TTF molecules in red, blue, green and light blue. (c) View of the α layer showing the four independent BEDT-TTF molecules in pink, orange, brown and dark green and the three eclipsed stacks. (d) View of the anionic layer with parallel rows of \otimes and Δ enantiomers. Color code in (a,d): Fe = green, C = gray, O = red, Br = brown and S = yellow. H atoms are omitted for clarity.

Table 5. Radical salts of BEDT-TTF with $[M(C_2O_4)_3]^{3-}$ anions with double-layer phases (72–78).

#	CCDC	Formula ^a	SG ^b	Elect. Prop.	A ⁺	M	G	Ref.
72	AQUZUH	α, β'' - (ET) ₄ [(NH ₄)Ga(ox) ₃] ·PhN(CH ₃)CHO	<i>P</i> -1	$\sigma = 0.26\text{--}0.60$ S/cm	NH ₄ ⁺	Ga	PhN(CH ₃)CHO	[40]
73	ARABAW	α, β'' - (ET) ₄ [(NH ₄)Ga(ox) ₃] ·PhCH ₂ CN	<i>P</i> -1	$\sigma = 0.24\text{--}1.34$ S/cm	NH ₄ ⁺	Ga	PhCH ₂ CN	[40]
74	ARABEA	α, β'' - (ET) ₄ [(NH ₄)Fe(ox) ₃]·PhCOCH ₃	<i>P</i> -1	-	NH ₄ ⁺	Fe	PhCOCH ₃	[40]
75	CILDIL	α, β'' -(ET) ₄ [(NH ₄)Fe(ox) ₃] ·(S)-PhC(OH)HCH ₃	<i>P</i> 1	$\sigma = 5.3$ S/cm T _{MI} = 170 K	NH ₄ ⁺	Fe	(S)- PhC(OH)OCH ₃	[41]
76	HOBTRIB	α, κ' - (ET) ₄ K _{0.45} (H ₃ O) _{0.55} [Ga(ox) ₃] ·1,2-PhBr ₂	<i>P</i> -1	Metal	K ⁺ /H ₃ O ⁺	Ga	1,2-PhBr ₂	[30]
77	NIPTM	α, β'' -(ET) ₄ [(NH ₄)Fe(ox) ₃] ·(R/S)-PhC(OH)HCH ₃	<i>P</i> -1	$\sigma = 10.4$ S/cm T _{MI} = 150 K	NH ₄ ⁺	Fe	(R/S)- PhC(OH)HCH ₃	[41]
78	TANDIX	α, κ' - (ET) ₄ [(H ₃ O)Fe(ox) ₃]·1,2- PhBr ₂	<i>P</i> -1	M > 1.5 K	H ₃ O ⁺	Fe	PhBr ₂	[42]

^a ox = oxalate = C₂O₄²⁻; ^b SG = space group.

4.3. BEDT-TTF:[M(C₂O₄)₃]³⁻ Phases with 3:1 Stoichiometry

Although most of the prepared radical salts of BEDT-TTF with [M(C₂O₄)₃]³⁻ anions present a 4:1 stoichiometry, as observed in the β'', κ', α,β'' and α,κ' phases and even in some salts with 18-crown-6, there are also radical salts with a 3:1 stoichiometry and the general formula (ET)₃[AM(C₂O₄)₃]·G with A⁺ = Na⁺ and NH₄⁺; M = Cr and Al and small solvent molecules in all cases (G = CH₃NO₂, CH₂Cl₂, CH₃CN, EtOH and dmf, Table 6). Interestingly, all these salts have been prepared with chiral solvents or mixtures of chiral and non-chiral solvents.

By using the chiral solvent (R)-(-)-carvone with small solvent molecules such as CH₃CN and CH₃NO₂, P. Day and L. Martin obtained a series of three isostructural chiral salts formulated as (BEDT-TTF)₃[NaM(C₂O₄)₃]·G with M/G = Al/CH₃NO₂ (**79**) [43], Cr/CH₃CN (**84**) [44] and Cr/CH₃NO₂ (**86**) [45] that crystallize in the monoclinic chiral P₂₁ space group (Table 6). The structure of this 3:1 phase also consists of alternating BEDT-TTF and anionic layers (Figure 17b). The BEDT-TTF layers contain three independent BEDT-TTF molecules arranged in rows containing BC dimers alternating with A monomers tilted ca. 45° with respect to the dimers (Figure 17a). This disposition resembles the κ' phase, but now each dimer is surrounded by four monomers and four dimers (compared to six monomers in the κ' phase). The anionic layer contains Na⁺ cations and a single enantiomer of the [M(C₂O₄)₃]³⁻ anions, forming a hexagonal honeycomb lattice (Figure 17c). The small solvent molecules (CH₃CN or CH₃NO₂) are located in the center of the hexagons. It is to be noted that now the hexagons are smaller and, accordingly, the organic layers contain only three BEDT-TTF molecules per hexagonal cavity. The inhomogeneous charge distribution with (BEDT-TTF)₂²⁺ dimers and neutral monomers and the lack of short intermolecular contacts explain the semiconductor behavior observed in these salts [43–45].

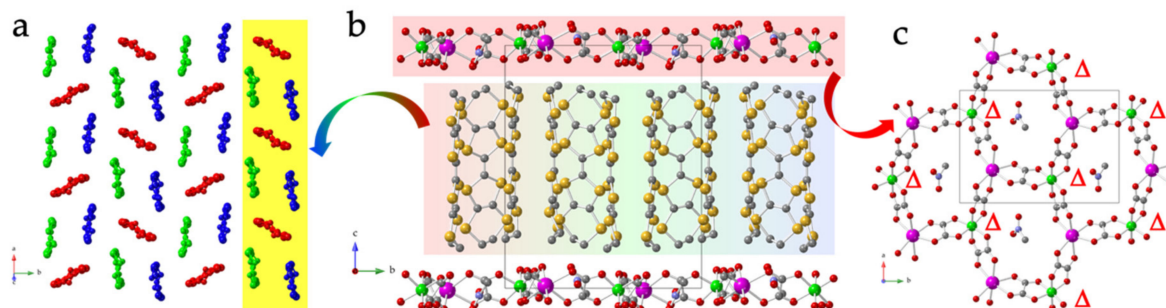


Figure 17. Structure of (ET)₃[NaAl(C₂O₄)₃]·CH₃NO₂ (**79**): (a) View of the BEDT-TTF layer showing the rows with alternating dimers and monomers. The three independent BEDT-TTF molecules are depicted in red, blue and green. (b) View of the alternating cationic and anionic layers. (c) View of the homochiral anionic layer. Color code in (b,c): Al = green, Na = pink, C = gray, O = red, N = blue and S = yellow. H atoms are omitted for clarity.

A very similar structure was found by L. Martin et al. in compounds (BEDT-TTF)₃[Li-M(C₂O₄)₃]·EtOH with M = Cr (**81**) and Fe (**82**) [46]. Although these compounds were also prepared with a chiral solvent (Λ-carvone), there is a disorder between the Li⁺ and M^{III} centers that leads to a non-chiral P₂₁/c space group. The BEDT-TTF and the anionic layers show the same structure as compounds **79**, **84** and **86** (Figure 17), although they are not, strictly speaking, isostructural since compounds **81** and **82** are not chiral.

L. Martin et al., using the same chiral solvent (R)-(-)-carvone, also obtained two isostructural chiral salts formulated as (BEDT-TTF)₃[Na{⊗-Cr(C₂O₄)₃}_{0.64}{Λ-Cr(C₂O₄)₃}_{0.36}]·CH₃NO₂ (**85**) [45] and (BEDT-TTF)₃[(NH₄)_{0.83}Cr_{1.17}(C₂O₄)₃]·CH₃NO₂ (**80**) [43] that crystallize in the orthorhombic P₂₁2₁2₁ chiral space group. The structure of these two salts also consists of alternating anionic and cationic layers, but now the organic layers present a different packing with double rows of face-to-face BEDT-TTF dimers (A-B) alternating with single rows of isolated BEDT-TTF molecules (C) tilted ca. 90° with respect to the dimers (Figure 18a). The charge distribution, determined from the bond distances in the BEDT-TTF

molecules, indicates an inhomogeneous charge distribution with charges of 0.33, 0.63 and 0.88 for the three independent molecules. The anionic layer is similar to that observed in the $P2_1$ salts with the same stoichiometry (Figure 17c) and also contains a single enantiomer of the $[\text{Cr}(\text{C}_2\text{O}_4)_3]^{3-}$ anion. In compound **80**, there is an excess of the $[\text{Cr}(\text{C}_2\text{O}_4)_3]^{3-}$ anion that results in a different charge distribution in the BEDT-TTF molecules, although no electrical properties are reported. The isostructural NaCr derivative (**85**) [45] presents an excess of the \otimes enantiomer, due to a disorder of the Cr and Na positions, and a slightly different charge distribution in the BEDT-TTF molecules since, now, the anionic layers have a charge of -2 per formula unit.

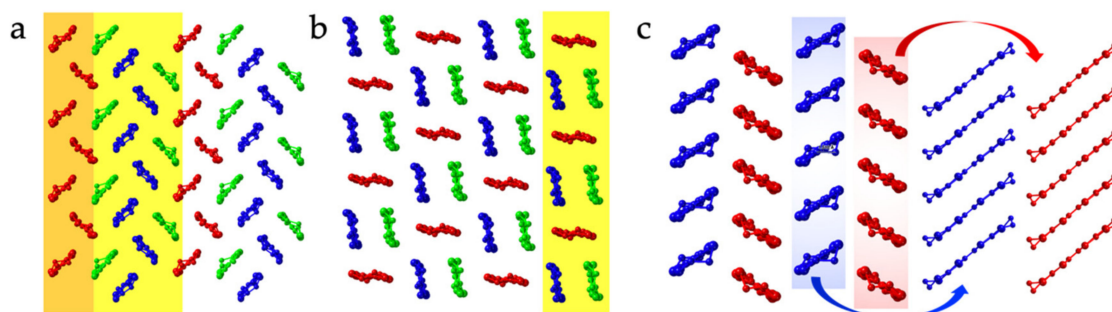


Figure 18. (a) Structure of the organic layer in $(\text{BEDT-TTF})_3[(\text{NH}_4)_{0.83}\text{Cr}_{1.17}(\text{C}_2\text{O}_4)_3]\cdot\text{CH}_3\text{NO}_2$ (**80**) showing the double stacks with dimers (in green and blue) and monomers (in red). (b) Structure of the organic layer in $(\text{BEDT-TTF})_3[\text{NaCr}(\text{C}_2\text{O}_4)_3]\cdot\text{EtOH}$ (**87**) showing the stacks with dimers (in green and blue) and monomers (in red). (c) Structure of the organic layer in $\theta\text{-(BEDT-TTF)}_3[\text{NaCr}(\text{C}_2\text{O}_4)_3]\cdot\text{dmf}$ (**88**) showing the alternating stacks (in red and blue). H atoms are omitted for clarity.

L. Martin et al. also used the chiral solvent R(-)-carvone with small solvent molecules such as CH_2Cl_2 and EtOH to prepare the isostructural salts $(\text{ET})_3[\text{Na}(\otimes\text{-Cr}(\text{C}_2\text{O}_4)_3)_{0.56}(\Lambda\text{-Cr}(\text{C}_2\text{O}_4)_3)_{0.44}]\cdot\text{CH}_2\text{Cl}_2$ (**83**) [47] and $(\text{ET})_3[\text{NaCr}(\text{C}_2\text{O}_4)_3]\cdot\text{EtOH}$ (**87**) [44] that crystallize in the triclinic $P1$ chiral space group. Salt **83** was the first chiral BEDT-TTF salt with $[\text{M}(\text{C}_2\text{O}_4)_3]^{3-}$ anions and also the first radical salt in this series with Na^+ ions in the anionic layer [47]. The structure of these two salts also consists of alternating anionic and cationic layers, but now the organic layers present a very slightly different packing to those of the $P2_1$ salts with similar compositions but different solvent molecules (**79**, **84** and **86**). In the $P1$ salts (**83** and **87**), the organic layers are also formed by rows containing alternating BEDT-TTF dimers and monomers, but now the monomers are tilted ca. 80° with respect to the dimers (compared to ca. 45° in the $P2_1$ salts, Figure 17b), and the offset inside the dimers is smaller in the $P1$ salts. Consecutive stacks are shifted to form a chessboard of monomers and dimers (Figure 18b).

Finally, when using dmf and the chiral solvent R(-)-carvone, L. Martin et al. also obtained a 3:1 salt formulated as $\theta\text{-(BEDT-TTF)}_3[\text{NaCr}(\text{C}_2\text{O}_4)_3]\cdot\text{dmf}$ (**88**) [44] that also crystallizes in the triclinic $P1$ chiral space group (as the CH_2Cl_2 and EtOH derivatives) but shows a completely different packing in the BEDT-TTF layer. Thus, salt **88** has only two independent BEDT-TTF molecules that pack in segregated parallel stacks with a tilt angle close to 116° between molecules of different stacks, giving rise to the so-called θ phase (Figure 18c). The two stacks show a similar shift of the BEDT-TTF molecules of half-rings along the stack. The anionic layer contains a single enantiomer of the $[\text{Cr}(\text{C}_2\text{O}_4)_3]^{3-}$ anions and Na^+ cations with the classical honeycomb structure [44].

Table 6. Radical salts of BEDT-TTF with $[\text{M}(\text{C}_2\text{O}_4)_3]^{3-}$ anions with 3:1 stoichiometry (79–88).

#	CCDC	Formula ^a	SG ^b	Elect. Prop.	A ⁺	M	G	Ref.
79	BOYTIU	$(\text{ET})_3[\text{NaAl}(\text{ox})_3] \cdot \text{CH}_3\text{NO}_2$	$P2_1$	$E_a = 140 \text{ meV}$	Na^+	Al	CH_3NO_2	[43]
80	BOYTOA	$(\text{ET})_3[(\text{NH}_4)_{0.83}\text{Cr}_{1.17}(\text{ox})_3] \cdot \text{CH}_3\text{NO}_2$	$P2_12_12_1$	$E_a = 140 \text{ meV}$	Na^+	Cr	CH_3NO_2	[43]
81	DUDWUW	$(\text{ET})_3[\text{LiCr}(\text{ox})_3] \cdot \text{EtOH}$	$P2_1/c$	$E_a = 179 \text{ meV}$	Li^+	Cr	EtOH	[46]
82	DUDXAD	$(\text{ET})_3[\text{LiFe}(\text{ox})_3] \cdot \text{EtOH}$	$P2_1/c$	$E_a = 126 \text{ meV}$	Li^+	Fe	EtOH	[46]
83	DUXNOA	$(\text{ET})_3[\text{Na}(\Delta\text{-Cr}(\text{ox})_3)_{0.56}(\Lambda\text{-Cr}(\text{ox})_3)_{0.44}] \cdot \text{CH}_2\text{Cl}_2$	$P1$	$E_a = 69 \text{ meV}$	Na^+	Cr	CH_2Cl_2	[47]
84	KOGMUQ01	$(\text{ET})_3[\text{NaCr}(\text{ox})_3] \cdot \text{CH}_3\text{CN}$	$P2_1$	$\sigma = 0.038 \text{ S/cm}$ $E_a = 172 \text{ meV}$	Na^+	Cr	CH_3CN	[44]
85	XUNXOU	$(\text{ET})_3\{\text{Na}[\otimes\text{-Cr}(\text{ox})_3]_{0.64}[\Lambda\text{-Cr}(\text{ox})_3]_{0.36}\} \cdot \text{CH}_3\text{NO}_2$	$P2_12_12_1$	$\sigma = 0.5 \text{ S/cm}$ $E_a = 80 \text{ meV}$	Na^+	Cr	CH_3NO_2	[45]
86	XUNXOU01	$(\text{ET})_3[\text{NaCr}(\text{ox})_3] \cdot \text{CH}_3\text{NO}_2$	$P2_1$	$\sigma = 0.045 \text{ S/cm}$ $E_a = 79 \text{ meV}$	Na^+	Cr	CH_3NO_2	[45]
87	YUCLOZ	$(\text{ET})_3[\text{NaCr}(\text{ox})_3] \cdot \text{EtOH}$	$P1$	Semi	Na^+	Cr	EtOH	[44]
88	YUCLUF	$\theta\text{-}(\text{ET})_3[\text{NaCr}(\text{ox})_3] \cdot \text{dmf}$	$P1$	Semi	Na^+	Cr	dmf	[44]

^a ox = oxalate = $\text{C}_2\text{O}_4^{2-}$; ^b SG = space group.

The lack of a homogeneous charge distribution on the BEDT-TTF molecules and the absence of short intermolecular contacts in all these chiral salts preclude the existence of an electron delocalization, and, accordingly, all these 3:1 salts obtained with chiral solvents are semiconductors or insulators (Table 6).

4.4. Other Phases of BEDT-TTF Salts with $[M(C_2O_4)_3]^{3-}$ Anions

Besides all the above-described phases, the combination of BEDT-TTF donors with $[M(C_2O_4)_3]^{3-}$ anions has also led to other crystal phases with unusual stoichiometries and/or packings in the cationic and anionic layers (Table 7).

The first of these salts is α''' -(ET)₉Na₁₈[Fe(C₂O₄)₃]₈·24H₂O (**95**) [39], also obtained with the $[Cr(C_2O_4)_3]^{3-}$ anion in α''' -(ET)₉Na₁₈[Cr(C₂O₄)₃]₈·24H₂O (**91**) [47]. These salts present a very original structure with four different layers following the sequence ... ABCD ... alternating along the *c* direction (Figure 19b). A-type layers contain BEDT-TTF molecules with a very unusual α''' packing (Figure 19a), B and D layers contain Na⁺ cations and $[Fe(C_2O_4)_3]^{3-}$ anions with one single enantiomer in each layer (Figure 19c) and C layers contain Na⁺ cations and H₂O molecules in rows parallel to the *b* axis (Figure 19d) [39]. In the very unusual α''' packing, the BEDT-TTF molecules form parallel columns as in the α and β'' packings, but in one of every three columns, the BEDT-TTF molecules are tilted in the opposite direction (Figure 19a). There are, thus, two columns with one orientation (++) formed by three independent BEDT-TTF molecules (A–C) with the sequence ... ABC ... , and one with the opposite orientation (-) formed by two independent BEDT-TTF molecules (D and E) with the sequence ... DDE In both stacks (+ and -), the BEDT-TTF molecules are eclipsed. The α''' packing is, therefore, described as parallel columns following the sequence ... /+ /+ /- /+ /+ /- / The anionic layer is also original since, now, the vertices of the hexagons contain alternating Fe(III) ions and (Na⁺)₂ dimers and there is an additional $[Fe(C_2O_4)_3]^{3-}$ anion in the center of the hexagon with its oxalate ligands pointing towards the Na⁺ dimers (Figure 19c). Interestingly, this unusual disposition has recently been found in a salt with the $[Fe(NA)_3]^{3-}$ anion (NA = nitranilato ligand = C₆O₄(NO₂)₂)²⁻ [48], which is topologically identical to the oxalate ligand and also forms tris-chelato anionic complexes $[M^{III}(L)_3]^{3-}$ (L = anilato-type ligand) [49] and even $[A^+M^{III}(L_3)]^{2-}$ honeycomb layers [50], such as the ones here described for oxalate in previous sections. This original salt, **95**, has an inhomogeneous charge distribution in the five independent BEDT-TTF molecules, and, therefore, it is a semiconductor.

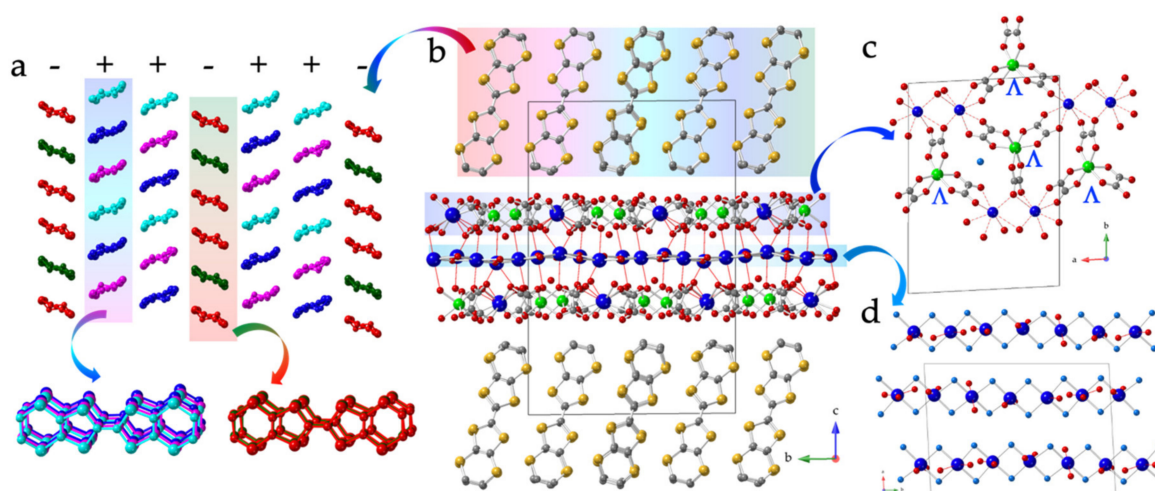


Figure 19. Structure of α''' -(ET)₉Na₁₈[Fe(C₂O₄)₃]₈·24H₂O (**95**): (a) View of the BEDT-TTF layer showing the two rows (++) with one orientation of the BEDT-TTF molecules (blue, pink and light blue molecules) and the row (-) with the opposite orientation (green and red molecules) and their eclipsed overlap. (b) View of the alternating cationic and anionic/Na⁺/anionic layers. (c) View of one of the two layers containing the $[Fe(C_2O_4)_3]^{3-}$ anions and the Na⁺ cations. (d) View of the layer with the Na⁺ ions and the water molecules. Color code: Fe = green, Na = blue, C = gray, O = red, O_{water} = light blue and S = yellow. H atoms are omitted for clarity.

Salts α -(BEDT-TTF)₁₂[Fe(C₂O₄)₃]₂·15H₂O (**93**) and α -(BEDT-TTF)₁₂[Fe(C₂O₄)₃]₂·16H₂O (**94**) are two solvates that, despite differing only in one water molecule, show different unit cell parameters and, therefore, are not isostructural [51]. The structure of both salts consists of cationic and anionic layers alternating along the *c* axis. Both salts show the α packing mode in the BEDT-TTF layer, formed by parallel stacks with an alternating orientation of the BEDT-TTF molecules. The only difference between both salts is that there are twelve independent BEDT-TTF molecules in **93**, compared to only three in salt **94**. The anionic layers in both compounds are formed by isolated [Fe(C₂O₄)₃]³⁻ anions surrounded by water molecules connected through H bonds in a 2D lattice (Figure 20a). The only difference is the presence of an extra water molecule in **94** and a slight twist in one oxalato ligand. Although the average charge per BEDT-TTF molecule is +0.5, there is an inhomogeneous charge distribution that results in a semiconducting behavior in both salts [51].

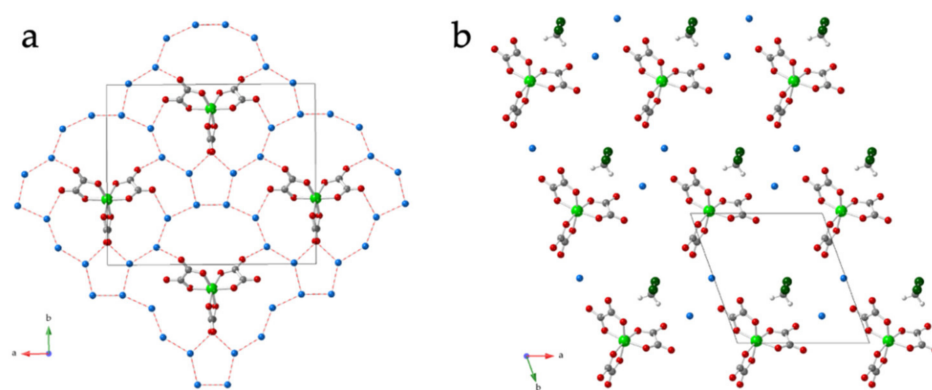


Figure 20. (a) View of the anionic layer in salt α -(BEDT-TTF)₁₂[Fe(C₂O₄)₃]₂·15H₂O (**93**) showing the [Fe(C₂O₄)₃]³⁻ anions and the water molecules around them. Red dotted lines represent the H bonds between the water molecules. (b) View of the anionic layers in β'' -(BEDT-TTF)₅[Fe(C₂O₄)₃]₁·2H₂O·CH₂Cl₂ (**96**). Color code: Fe = green, C = gray, O = red, O_{water} = light blue and Cl = dark green.

When using (NEt₄)₃[Fe(C₂O₄)₃] as a precursor salt and CH₂Cl₂ as a solvent, the lack of small cations in the medium such as H₃O⁺, Na⁺, K⁺ or NH₄⁺ results in an original salt with no other cations in the structure. This salt, formulated as β'' -(BEDT-TTF)₅[Fe(C₂O₄)₃]₁·2H₂O·CH₂Cl₂ (**96**) [52], shows cationic and anionic layers alternating along the *c* direction. The cationic layers of this 5:1 salt contain five independent BEDT-TTF molecules with the β'' packing mode, as in the superconducting 4:1 phase. The anionic layer is quite original since it contains isolated [Fe(C₂O₄)₃]³⁻ anions packed in parallel rows, surrounded by the H₂O and CH₂Cl₂ molecules (Figure 20b). There are two different anionic layers with only one enantiomer each. The analysis of the bond distances shows an inhomogeneous charge distribution with four BEDT-TTF molecules with a charge of +0.5 and one BEDT-TTF with a charge of +1. This inhomogeneous charge distribution explains the semiconducting behavior of this salt [52].

Another original salt is α -(BEDT-TTF)₆[Fe(C₂O₄)₃] (**92**) [17], which shows a 6:1 stoichiometry with an α packing type in the BEDT-TTF layer. Unfortunately, the crystals are not stable, precluding the determination of the anionic layer. The use of a large solvent such as 1,2,4-trichlorobenzene may be at the origin of the unusual structure of this salt [17].

The use of Li₃[Fe(C₂O₄)₃] as a precursor salt, besides the above-mentioned 3:1 phases (ET)₃[LiM(C₂O₄)₃]·EtOH (**81** and **82**) obtained with a chiral solvent, also gave crystals of a 4:1 phase: η -(ET)₄[(H₂O)LiFe(C₂O₄)₃] (**90**), when no chiral solvent was used [46]. The structure of this salt consists of cationic and anionic layers alternating along the *b* axis. In this salt, the BEDT-TTF layer shows an original η packing mode (Figure 21a) formed by parallel stacks of eclipsed BEDT-TTF molecules (Figure 21b) tilted with respect to the stack direction (as in the β'' phase), but now the orientation of the molecules changes every two stacks, following the sequence: ... /+ /+ /- /- / ... (Figure 21a). This original

packing can be considered as a mixture of the β'' phase, where all the stacks have the same orientation: (+/+/+/+), and the α phase, where the stacks show alternating orientations: (+/-/+/-). The two stacks with a given orientation are equivalent and are formed by two independent BEDT-TTF molecules following the sequence ... AB ... (or ... CD ... in the stacks with the opposite orientation, Figure 21a). The BEDT-TTF molecules are eclipsed in both types of stacks (Figure 21b). The anionic layer is also very original: it shows a distorted hexagonal packing of the $[\text{Fe}(\text{C}_2\text{O}_4)_3]^{3-}$ anions and the Li^+ cations. This distortion is due to the presence of a water molecule in the layer connected to the Li^+ ions, resulting in elongated $\text{Li}(\text{H}_2\text{O})^+$ entities that occupy alternating vertices of the hexagons (Figure 21c). The elongated hexagonal cavities are occupied by disordered CH_2Cl_2 solvent molecules. The BEDT-TTF molecules show an inhomogeneous charge distribution, and, accordingly, this original salt is a semiconductor (Table 7) [46].

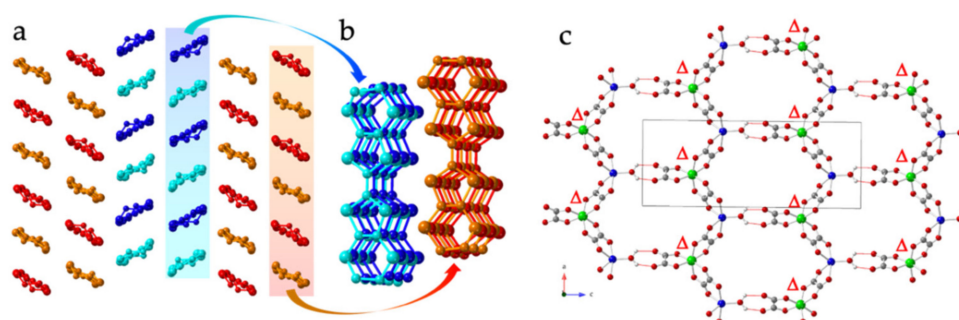


Figure 21. Structure of $\eta\text{-(ET)}_4[(\text{H}_2\text{O})\text{LiFe}(\text{C}_2\text{O}_4)_3]$ (**90**). (a) View of the cationic layer showing the four independent BEDT-TTF molecules (as light blue, dark blue, red and orange). (b) View of the eclipsed packing of the BEDT-TTF molecules. (c) View of the anionic layer showing the elongated hexagonal cavities. Thin red lines represent the H bonds between the water molecule coordinated to the Li^+ ions and the terminal oxalate oxygen atoms. Color code in (c): Fe = green, Li = blue, C = gray and O = red. H atoms in (a) are omitted for clarity.

A final example of a radical salt with an unusual structure is a 5:1 phase formulated as $\alpha''\text{-(BEDT-TTF)}_5[\text{Ga}(\text{C}_2\text{O}_4)_3]\cdot 3.4\text{H}_2\text{O}\cdot 0.6\text{EtOH}$ (**89**) [27]. This salt is the first orthorhombic *Pbca* BEDT-TTF salt with an oxalate complex. The structure consists of cationic and anionic layers alternating along the *c* axis (Figure 22c). The cationic layers show an α'' or η packing mode (Figure 22a), previously observed in $\eta\text{-(BEDT-TTF)}_4[(\text{H}_2\text{O})\text{LiFe}(\text{C}_2\text{O}_4)_3]$ (**90**) [46], although in salt **89**, each BEDT-TTF stack contains five independent molecules with the sequence ... ABCDE ..., showing a dislocation every five molecules along the stack (Figure 22b), whereas in compound **90**, there are four BEDT-TTF independent molecules in two different stacks with the sequences ... AB ... and ... CD ... The anionic layers are formed by rows along the *a* direction with alternating \otimes and Δ enantiomers of the $[\text{Ga}(\text{C}_2\text{O}_4)_3]^{3-}$ anions (Figure 22d).

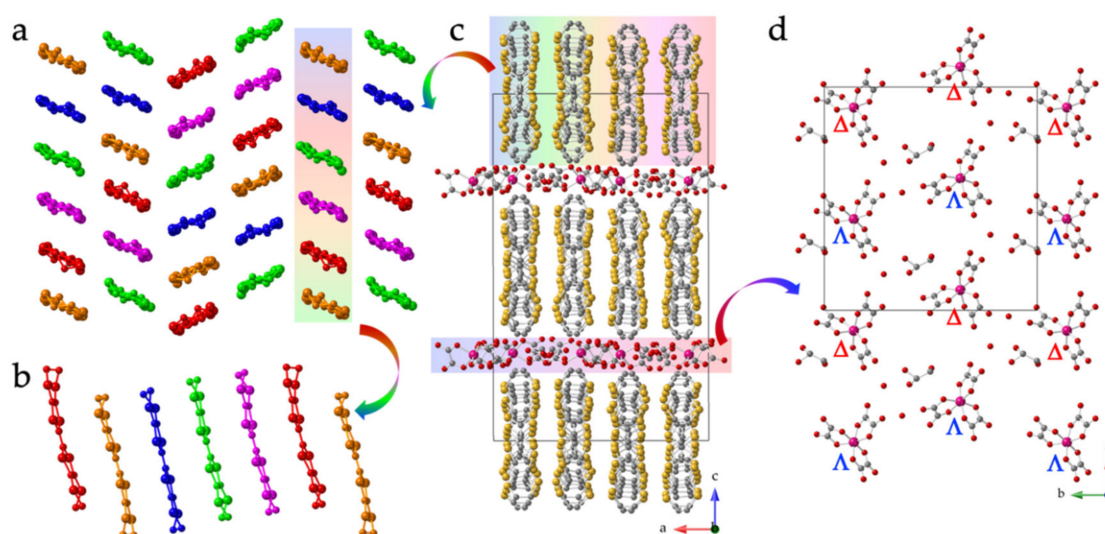


Figure 22. Structure of α'' -(BEDT-TTF)₅[Ga(C₂O₄)₃]·3.4H₂O·0.6EtOH (89). (a) View of the cationic layer showing the five independent BEDT-TTF molecules (as blue, red, orange, green and pink). (b) Side view of the BEDT-TTF stack showing the pentameric repeating unit. (c) View of the alternating cationic and anionic layers along the *c* direction. (d) View of the anionic layer showing the rows along the *a* axis with alternating \otimes and Δ [Ga(C₂O₄)₃]^{3−} anions. Color code in (b): Ga = pink, C = gray and O = red. H atoms are omitted for clarity.

Table 7. Radical salts of BEDT-TTF with [M(C₂O₄)₃]^{3−} anions showing other α and β phases (89–96).

#	CCDC	Formula ^a	SG ^b	Elect. Prop.	A ⁺	M	G	Ref.
89	CIWNAA	α'' - (ET) ₅ [Ga(ox) ₃]·3.4H ₂ O·0.6EtOH	<i>Pbca</i>	<i>E</i> _a = 71 meV	-	Ga	EtOH/H ₂ O	[27]
90	DUDWOQ	η -(ET) ₄ [(H ₂ O)LiFe(ox) ₃]	<i>P2₁/c</i>	σ = 0.41 S/cm <i>E</i> _a = 80 meV	Li ⁺ /H ₂ O	Fe	-	[46]
91	DUXNUG	α''' - (ET) ₉ Na ₁₈ [Cr(ox) ₃] ₈ ·24H ₂ O	<i>P</i> -1	<i>E</i> _a = 66 meV	Na ⁺	Cr	H ₂ O	[47]
92	IPEKAQ	α -(ET) ₆ [Fe(ox) ₃]	<i>P2₁</i>	-	-	Fe	H ₂ O/EtOH?	[17]
93	KIVKAC	α -(ET) ₁₂ [Fe(ox) ₃] ₂ ·15H ₂ O	<i>C2/c</i>	σ = 0.055 S/cm	H ₃ O ⁺	Fe	H ₂ O	[51]
94	KIVKEG	α -(ET) ₁₂ [Fe(ox) ₃] ₂ ·16H ₂ O	<i>C2/c</i>	σ = 0.111 S/cm	H ₃ O ⁺	Fe	H ₂ O	[51]
95	NIHPAW	α''' - (ET) ₉ Na ₁₈ [Fe(ox) ₃] ₈ ·24H ₂ O	<i>P</i> -1	<i>E</i> _a = 77 meV	Na ⁺	Fe	H ₂ O	[39]
96	OGUPAI	β'' - (ET) ₅ [Fe(ox) ₃](H ₂ O) ₂ CH ₂ Cl ₂	<i>P</i> -1	σ = 4 S/cm <i>E</i> _a = 30 meV	-	Fe	CH ₂ Cl ₂ /H ₂ O	[52]

^a ox = oxalate = C₂O₄^{2−}; ^b SG = space group.

4.5. BEDT-TTF Salts with [Ge(C₂O₄)₃]^{2−} and [Cu(C₂O₄)₂]^{2−} Dianions

Interestingly, besides all the above-mentioned M(III)-based [M(C₂O₄)₃]^{3−} anions, there are also two oxalate-based dianions that have been combined with BEDT-TTF (Table 8): (i) the Ge(IV)-based [Ge(C₂O₄)₃]^{2−} anion, which presents the same 3:1 stoichiometry and octahedral geometry as the previously used [M(C₂O₄)₃]^{3−} anions, although with a −2 charge, and (ii) the Cu(II)-based [Cu(C₂O₄)₂]^{2−} anion, also with a −2 charge, but with a 2:1 stoichiometry and a square planar geometry (Figure 1b). As we will show here, the change in the charge in the [Ge(C₂O₄)₃]^{2−} anion leads to very important changes in the structure and properties of these radical salts.

The first salt with the dianion [Ge(C₂O₄)₃]^{2−} was reported by P. Day's group and shows a 2:1 stoichiometry: (BEDT-TTF)₂[Ge(C₂O₄)₃]·PhCN (97) [53]. Surprisingly, this salt does not show alternating cationic and anionic layers but a chessboard arrangement of BEDT-TTF face-to-face dimers and [Ge(C₂O₄)₃]^{2−} dianions interspersed with layers of

PhCN solvent molecules (Figure 23a,b). The presence of isolated $(\text{BEDT-TTF})_2^{2+}$ dimers is at the origin of the semiconducting behavior shown by this salt [53].

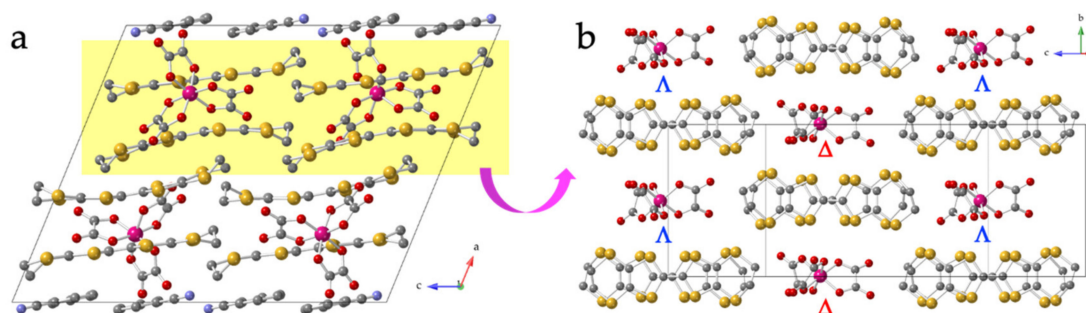


Figure 23. Structure of $(\text{BEDT-TTF})_2[\text{Ge}(\text{C}_2\text{O}_4)_3]\cdot\text{PhCN}$ (**97**). (a) View of the ac plane. (b) Projection perpendicular to the bc plane showing the chessboard arrangement of the BEDT-TTF dimers and the $[\text{Ge}(\text{C}_2\text{O}_4)_3]^{2-}$ anions. Color code: Ge = pink, C = gray, O = red, N = blue and S = yellow. H atoms are omitted for clarity.

Salts $(\text{BEDT-TTF})_5[\text{Ge}(\text{C}_2\text{O}_4)_3]_2$ (**98**) and $(\text{BEDT-TTF})_7[\text{Ge}(\text{C}_2\text{O}_4)_3]_2\cdot 0.87\text{CH}_2\text{Cl}_2\cdot 0.09\text{H}_2\text{O}$ (**99**) were prepared using the same conditions but changing the solvent (chiral R(-)-carvone for **98** and CH_2Cl_2 for **99**) [54]. The change in the solvent leads to two very different structures and stoichiometries. Salt $(\text{BEDT-TTF})_5[\text{Ge}(\text{C}_2\text{O}_4)_3]_2$ (**98**) contains mixed layers parallel to the ac plane with BEDT-TTF molecules and $[\text{Ge}(\text{C}_2\text{O}_4)_3]^{2-}$ anions (Figure 24a). In these layers, the BEDT-TTF molecules form diagonal stacks where the molecules are displaced along their long molecular axis. These stacks are separated by isolated $[\text{Ge}(\text{C}_2\text{O}_4)_3]^{2-}$ anions (Figure 24b) [54].

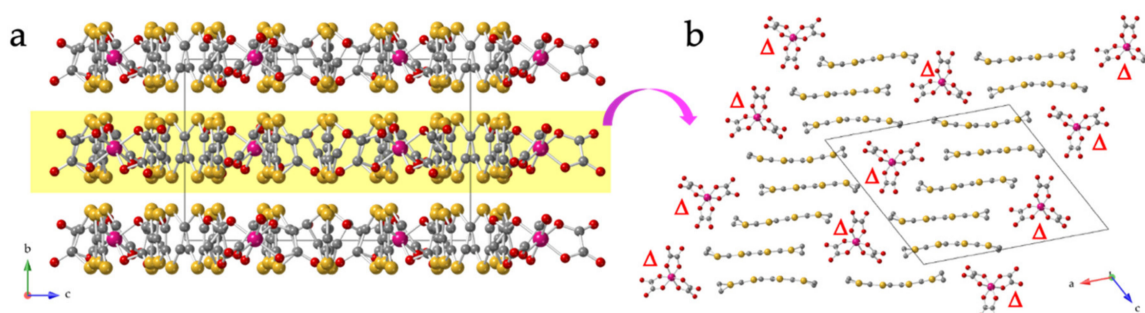


Figure 24. Structure of $(\text{BEDT-TTF})_5[\text{Ge}(\text{C}_2\text{O}_4)_3]_2$ (**98**). (a) View of the mixed layers parallel to the ac plane. (b) Projection of the ac plane showing the stacks of BEDT-TTF molecules separated by rows of isolated $[\text{Ge}(\text{C}_2\text{O}_4)_3]^{2-}$ anions. Color code: Ge = pink, C = gray, O = red and S = yellow. H atoms are omitted for clarity.

In contrast, salt $(\text{BEDT-TTF})_7[\text{Ge}(\text{C}_2\text{O}_4)_3]_2\cdot 0.87\text{CH}_2\text{Cl}_2\cdot 0.09\text{H}_2\text{O}$ (**99**) shows alternating cationic and anionic layers parallel to the bc plane (Figure 25c), with the BEDT-TTF molecules packed with the α packing mode (Figure 25a) [54]. There are four independent BEDT-TTF molecules packed following the sequence ... ABCDCBA ..., with a dislocation in the stacks every seven molecules (Figure 25b). The anionic layer is very original since it shows $[\text{Ge}(\text{C}_2\text{O}_4)_3]^{2-}$ anions grouped in homochiral dimers with a water molecule in between them forming H bonds with both monomers (Figure 25c). Dimers with different chirality alternate along the c axis. Disordered CH_2Cl_2 molecules are located between the $[\text{Ge}(\text{C}_2\text{O}_4)_3]^{2-}$ dimers.

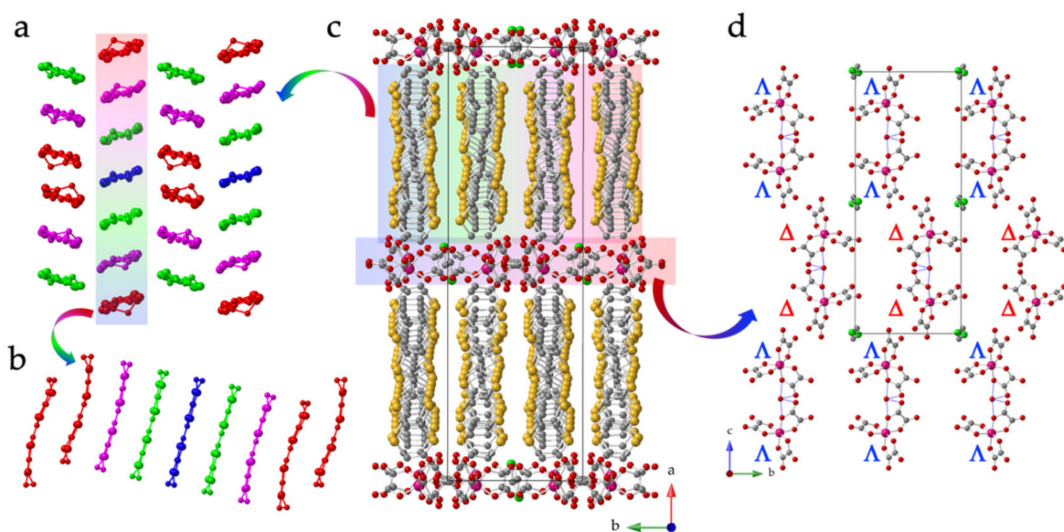


Figure 25. Structure of $(\text{BEDT-TTF})_7[\text{Ge}(\text{C}_2\text{O}_4)_3]_2 \cdot 0.87\text{CH}_2\text{Cl}_2 \cdot 0.09\text{H}_2\text{O}$ (**99**). (a) View of the cationic layer showing the four independent BEDT-TTF molecules (A–D, as red, pink, green and blue, respectively). (b) Side view of the chain. (c) View of the alternating cationic and anionic layers. (d) View of the anionic layer showing the $[\text{Ge}(\text{C}_2\text{O}_4)_3]^{2-}$ dimers H bonded to a water molecule (H bonds as thin blue lines). Color code in (b,c): Ge = pink, C = gray, O = red, Cl = green and S = yellow. H atoms are omitted for clarity.

Although salts **97–99** were prepared with the NH_4^+ salt of the $[\text{Ge}(\text{C}_2\text{O}_4)_3]^{2-}$ dianion, the NH_4^+ cation did not enter in the structure of the salts. Attempts to change the cation, using the Cs^+ salt, led to a new and original salt, although without the Cs^+ cation: $(\text{BEDT-TTF})_4[\text{Ge}(\text{C}_2\text{O}_4)_3] \cdot 0.5\text{CH}_2\text{Cl}_2$ (**100**) [55]. This salt also presents alternating cationic and anionic layers (Figure 26b), both layers being original. There are four independent BEDT-TTF molecules (A–D) packed in parallel stacks following the sequence ... ABCD ... (Figure 26a), with a dislocation every four molecules (Figure 26b). Within each group of the four BEDT-TTF molecules, the two central ones (B and C) are completely ionized, whereas the external ones (A and D) are neutral, resulting in $(\text{BEDT-TTF})_2^{2+}$ dimers surrounded by neutral monomers from the electronic point of view. This charge distribution results in a semiconducting behavior, as observed experimentally (Table 8) [55]. The anionic layer is also original. It contains dimers of $[\text{Ge}(\text{C}_2\text{O}_4)_3]^{2-}$ anions (with \otimes and Δ chirality) with a CH_2Cl_2 molecule connecting both anions (Figure 26c).

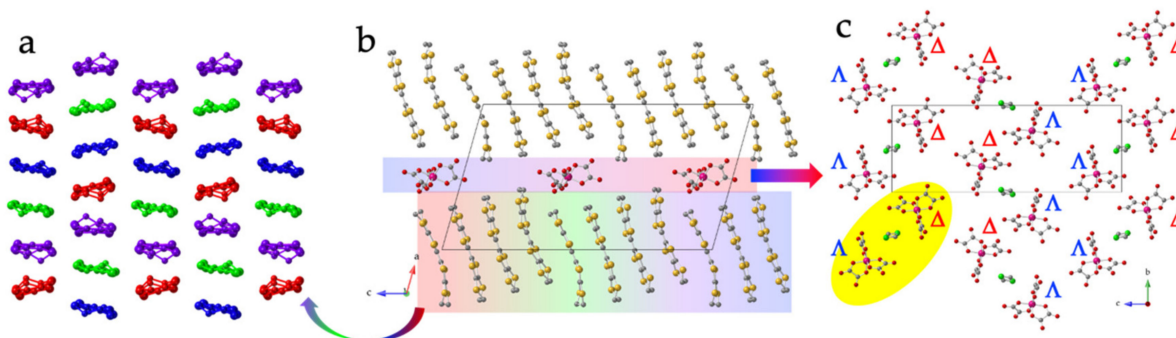


Figure 26. Structure of $(\text{BEDT-TTF})_4[\text{Ge}(\text{C}_2\text{O}_4)_3] \cdot 0.5\text{CH}_2\text{Cl}_2$ (**100**). (a) View of the cationic layer showing the four independent BEDT-TTF molecules (as blue, green, purple and red). (b) View of the alternating cationic and anionic layers showing the dislocation in the BEDT-TTF stacks every four molecules. (c) View of the anionic layer showing the $[\text{Ge}(\text{C}_2\text{O}_4)_3]^{2-}$ dimers (highlighted in yellow) with a disordered CH_2Cl_2 molecule located between them. Color code in (b,c): Ge = pink, C = gray, O = red and S = yellow. H atoms are omitted for clarity.

The only salt reported with the $[\text{Cu}(\text{C}_2\text{O}_4)_2]^{2-}$ dianion: $(\text{BEDT-TTF})_4[\text{Cu}(\text{C}_2\text{O}_4)_2]$ (**101**), is also the first radical salt prepared with any metal-oxalate complex. It shows alternating cationic and anionic layers parallel to the ac plane (Figure 27b). The BEDT-TTF layers are formed by two independent molecules with the β packing mode (Figure 27a). The $[\text{Cu}(\text{C}_2\text{O}_4)_2]^{2-}$ dianions are isolated and show a square planar geometry (Figure 27c). The salt is metallic down to 65 K, where it shows a metal–semiconductor transition with a low activation energy of 15 meV below 65 K (Table 8) [56,57].

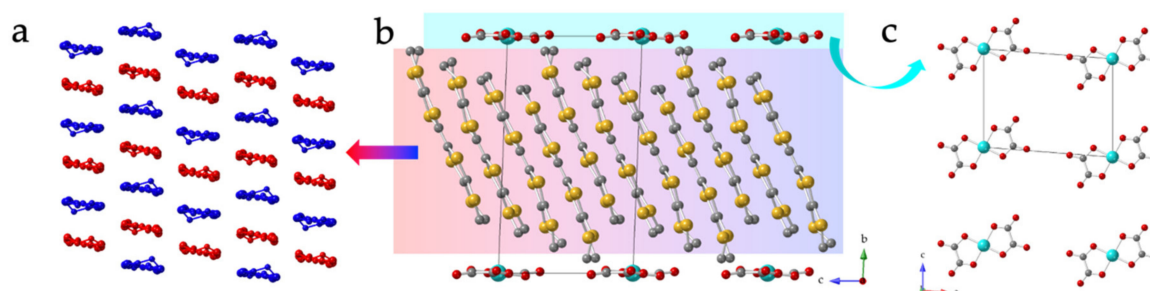


Figure 27. Structure of $(\text{BEDT-TTF})_4[\text{Cu}(\text{C}_2\text{O}_4)_2]$ (**101**). (a) View of the cationic layer showing the β packing mode of the two independent BEDT-TTF molecules (red and blue). (b) View of the alternating cationic and anionic layers. (c) View of the anionic layer showing the isolated square planar $[\text{Cu}(\text{C}_2\text{O}_4)_2]^{2-}$ anions. Color code in (b,c): Cu = blue, C = gray, O = red and S = yellow. H atoms are omitted for clarity.

Table 8. Radical salts of BEDT-TTF with the $[\text{Ge}(\text{C}_2\text{O}_4)_3]^{2-}$ and $[\text{Cu}(\text{C}_2\text{O}_4)_2]^{2-}$ dianions (**97–101**).

#	CCDC	Formula ^a	SG ^b	Elect. Prop.	G	Anion	Ref.
97	MAJYUR	$(\text{ET})_2[\text{Ge}(\text{ox})_3] \cdot \text{PhCN}$	$P2_1/c$	$E_a = 127 \text{ meV}$	PhCN	$[\text{Ge}(\text{ox})_3]^{2-}$	[53]
98	MUVFUF	$(\text{ET})_5[\text{Ge}(\text{ox})_3]_2$	C2	$\sigma = 10^{-3} \text{ S/cm}$ $E_a = 225 \text{ meV}$	-	$[\text{Ge}(\text{ox})_3]^{2-}$	[54]
99	MUVGAM	$(\text{ET})_7[\text{Ge}(\text{ox})_3]_2 \cdot 0.87\text{CH}_2\text{Cl}_2 \cdot 0.09\text{H}_2\text{O}$	$C2/c$	$\sigma = 1.75 \text{ S/cm}$ $E_a = 117\text{--}172 \text{ meV}$	$\text{CH}_2\text{Cl}_2/\text{H}_2\text{O}$	$[\text{Ge}(\text{ox})_3]^{2-}$	[54]
100	PADDOQ	$(\text{ET})_4[\text{Ge}(\text{ox})_3] \cdot 0.5\text{CH}_2\text{Cl}_2$	$P2_1/c$	$\sigma = 4.7 \times 10^{-3} \text{ S/cm}$ $E_a = 224 \text{ meV}$	CH_2Cl_2	$[\text{Ge}(\text{ox})_3]^{2-}$	[55]
101	SOJLUY	$(\text{ET})_4[\text{Cu}(\text{ox})_2]$	$P-1$	$T_{M-I} = 65 \text{ K}$ $E_a = 15 \text{ meV}$	-	$[\text{Cu}(\text{ox})_2]^{2-}$	[56,57]

^a ox = oxalate = $\text{C}_2\text{O}_4^{2-}$; ^b SG = space group.

5. BEDT-TTF Salts with Oxalate Dimers and 2D Lattices

Besides monomeric tri-anions such as $[\text{M}(\text{C}_2\text{O}_4)_3]^{3-}$ (M = Fe, Cr, Co, Al, Ga, Mn, Ru, Rh, Ir, etc.) and dianions such as $[\text{Ge}(\text{C}_2\text{O}_4)_3]^{2-}$ and $[\text{Cu}(\text{C}_2\text{O}_4)_2]^{2-}$, there are a few reported radical salts of BEDT-TTF with the dimer $[\text{Fe}_2(\text{C}_2\text{O}_4)_5]^{4-}$ and even with extended homo- and heterometallic hexagonal honeycomb lattices such as $[\text{MnCr}(\text{C}_2\text{O}_4)_3]^-$, $[\text{MnRh}(\text{C}_2\text{O}_4)_3]^-$ and $[\text{Cu}_2(\text{C}_2\text{O}_4)_3]^{2-}$ (Table 9).

The only known salt with BEDT-TTF and a dimeric anion is: $(\text{BEDT-TTF})_4[\text{Fe}_2(\text{C}_2\text{O}_4)_5]$ (**105**), also reported by P. Day's group [58]. In this radical salt, the dimeric anion $[\text{Fe}_2(\text{C}_2\text{O}_4)_5]^{4-}$ is formed in situ from the precursor $[\text{Fe}(\text{C}_2\text{O}_4)_3]^{3-}$ monomer in the electrochemical cell. The structure of this unusual salt consists of mixed layers parallel to the ac plane (Figure 28a) containing the $[\text{Fe}_2(\text{C}_2\text{O}_4)_5]^{4-}$ dimers interspersed with BEDT-TTF molecules that form stacks running parallel to the a direction (Figure 28b). The $[\text{Fe}_2(\text{C}_2\text{O}_4)_5]^{4-}$ dimers are formed by two $[\text{Fe}(\text{C}_2\text{O}_4)_3]^{3-}$ monomers with different chirality sharing an oxalate bridge (Figure 1c). There are two independent BEDT-TTF molecules, both with a +1 charge, in agreement with the 4:1 stoichiometry and the -4 charge of the anion, resulting in a semiconducting salt with a high activation energy and a low room temperature conductivity (Table 9) [58]. The oxalate-bridged Fe(III) dimer in this salt shows, as expected, a weak antiferromagnetic interaction with

$J = -3.44 \text{ cm}^{-1}$, similar to that found in the TTF and TM-TTF salts with the same dimer that will be described in the next section [59,60].

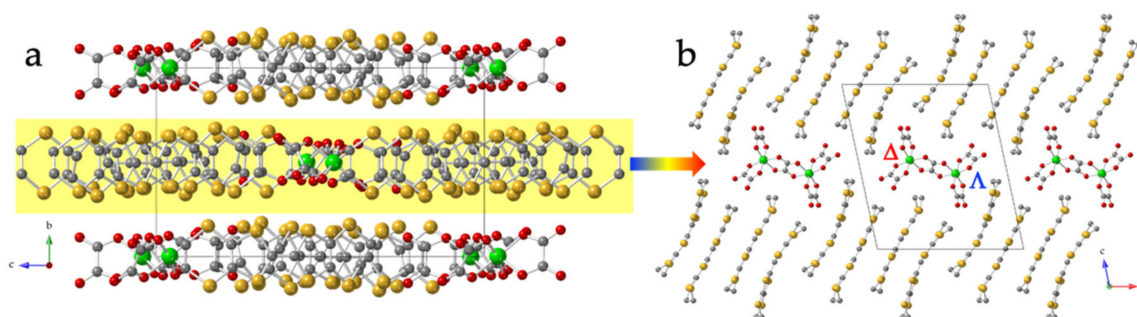


Figure 28. (a) View of the structure of $(\text{BEDT-TTF})_4[\text{Fe}_2(\text{C}_2\text{O}_4)_5]$ (**105**) showing the mixed layers parallel to the ac plane. (b) Top view of one mixed layer showing the stacks of the BEDT-TTF molecules and the $[\text{Fe}_2(\text{C}_2\text{O}_4)_5]^{4-}$ dimeric anion in between the stacks of BEDT-TTF molecules. Color code: Fe = green, C = gray, O = red and S = yellow. H atoms are omitted for clarity.

There are three closely related BEDT-TTF salts prepared with a heterometallic honeycomb oxalate-based layer: $(\text{ET})_{2.53}[\text{MnCr}(\text{C}_2\text{O}_4)_3] \cdot \text{CH}_2\text{Cl}_2$ (**103**), $(\text{ET})_{2.53}[\text{MnRh}(\text{C}_2\text{O}_4)_3] \cdot \text{CH}_2\text{Cl}_2$ (**104**) and $(\text{ET})_3[\text{MnCr}(\text{C}_2\text{O}_4)_3]$ (**106**) [7,8]. These three salts are isostructural and show alternating layers of BEDT-TTF molecules and anionic honeycomb layers (Figure 29b). The BEDT-TTF molecules are tilted around 45° with respect to the anionic layer and show a β packing mode (Figure 29a). The anionic layers show the classical honeycomb structure and contain Mn(II) and Cr(III) ions (or Rh(III) in **104**) with alternating chirality connected by oxalate bridges (Figure 29c).

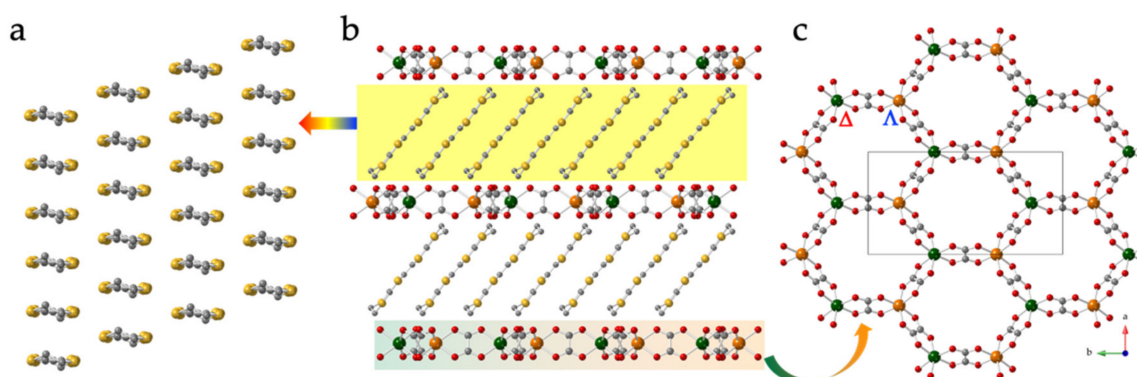


Figure 29. Structure of $(\text{BEDT-TTF})_3[\text{MnCr}(\text{C}_2\text{O}_4)_3]$ (**106**). (a) View of the BEDT-TTF layer showing the β packing mode. (b) View of the alternating cationic and anionic layers. (c) View of the honeycomb $[\text{MnCr}(\text{C}_2\text{O}_4)_3]^-$ anionic layer. Color code: Cr = dark green, Mn = orange, C = gray, O = red and S = yellow. H atoms are omitted for clarity.

Salt $(\text{BEDT-TTF})_3[\text{MnCr}(\text{C}_2\text{O}_4)_3]$ (**106**) was the first molecular compound showing metallic conductivity and a ferromagnetic long-range ordering, with an ordering temperature T_{curie} of ca. 5.5 K (Figure 30a) [7]. This salt presents magnetoresistance below ca. 10 K (Figure 30b), indicating that both sublattices are *quasi*-independent from the electronic point of view. Attempts to change the metal ions and the donor molecules and the use of other solvents led to different radical salts [61], including isostructural compounds $(\text{ET})_{2.53}[\text{MnCr}(\text{C}_2\text{O}_4)_3] \cdot \text{CH}_2\text{Cl}_2$ (**103**) and $(\text{ET})_{2.53}[\text{MnRh}(\text{C}_2\text{O}_4)_3] \cdot \text{CH}_2\text{Cl}_2$ (**104**) that are also metallic and show long-range magnetic ordering, although in compound **104**, there is a broad metal to semiconducting transition at around 100 K [8]. The use of this honeycomb layer with other TTF-type donors will be revised in the next section.

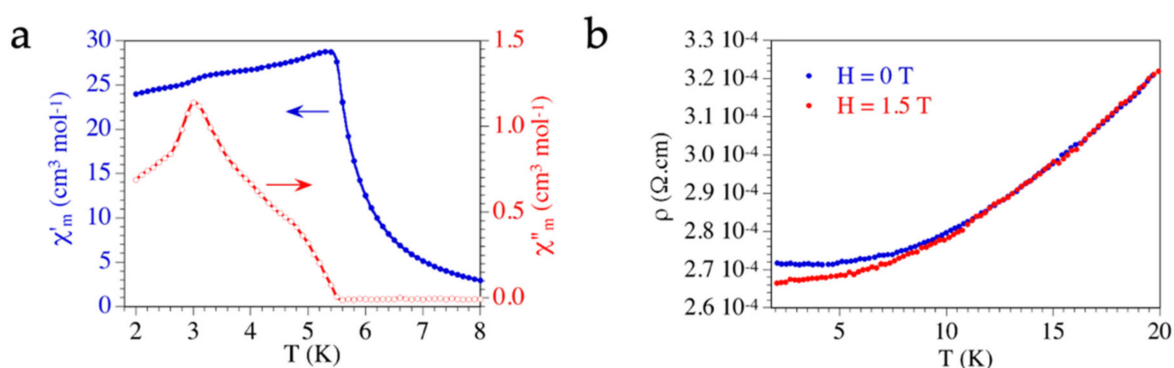


Figure 30. (a) Temperature dependencies of the in-phase (χ'_m) and the out-of-phase (χ''_m) AC susceptibility of (BEDT-TTF)₃[MnCr(C₂O₄)₃] (**106**) showing the long-range ordering at ca. 5.5 K. (b) Electrical conductivity of a single crystal of (BEDT-TTF)₃[MnCr(C₂O₄)₃] (**106**) with and without applied DC magnetic field.

A last example of extended lattices is provided by the series of salts formulated as (BEDT-TTF)₃[Cu₂(C₂O₄)₃]-G, with G = H₂O (**108**), CH₂Cl₂ (**102**) and CH₃OH (**107**) [62]. The structure of these isostructural salts shows alternating cationic and anionic layers parallel to the *ab* plane (Figure 31b). The BEDT-TTF layers show a θ^{21} packing mode, similar to that observed in α''' -(ET)₉Na₁₈[Fe(C₂O₄)₃]₈·24H₂O (**95**), formed by two stacks of BEDT-TTF tilted in one direction (+/+) and one stack tilted in the opposite direction (-), following the sequence (... /+ /+ /- /+ /+ /- / ...) (Figure 31a). The anionic layer is also a honeycomb hexagonal lattice formed by Cu(II) ions in the vertices of the hexagons and oxalate bridges as the sides of the hexagons. The crystallization solvent molecules are located in the hexagonal cavities. As a result of the expected Jahn–Teller distortions in the Cu(II) ions, the hexagons are quite distorted (Figure 31c). The properties of the CH₃OH derivative (the only one reported to date) show that this radical salt is a semiconductor with an activation energy of 50 meV and presents a moderate antiferromagnetic Cu–Cu interaction through the oxalate bridge [62].

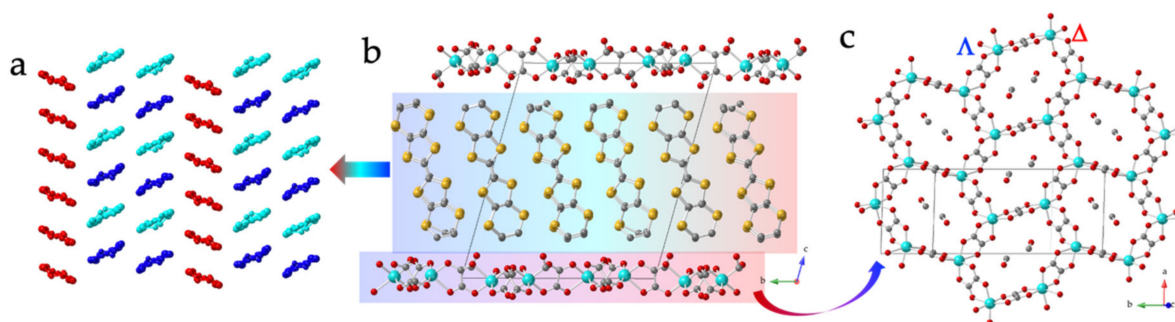


Figure 31. Structure of (BEDT-TTF)₃[Cu₂(C₂O₄)₃]₂·2CH₃OH (**107**). (a) View of the BEDT-TTF layer showing the θ^{21} packing mode with the three independent BEDT-TTF molecules (in red, blue and light blue). (b) View of the alternating cationic and anionic layers. (c) View of the distorted honeycomb [Cu₂(C₂O₄)₃]²⁻ anionic layer with the CH₃OH molecules in the hexagonal cavities. Color code in (b,c): Cu = light blue, C = gray, O = red and S = yellow. H atoms are omitted for clarity.

The tuneability of these metallic magnets was evidenced by the synthesis of different derivatives of the metallic ferromagnet (BEDT-TTF)₃[MnCr(C₂O₄)₃] (**106**). One of these derivatives is the salt (BEDT-TTF)₃[CoCr(C₂O₄)₃]₂·CH₂Cl₂, which showed an ordering temperature of 9.2 K and a high electrical conductivity of 1 S/cm at room temperature, although no metallic behavior was observed, maybe because the measurements were performed on a pressed pellet as no big single crystals could be obtained [63]. The other derivatives, prepared with different TTF-type donors, will be revised in the next section.

Table 9. Radical salts of BEDT-TTF with metal-oxalate dimers and 2D lattices (102–108).

#	CCDC	Formula ^a	SG ^b	Elect. Prop.	Anion	G	Ref.
102	CEMMUF	(ET) ₃ [Cu ₂ (ox) ₃]·CH ₂ Cl ₂	<i>P</i> -1	-	[Cu ₂ (ox) ₃] ²⁻	CH ₂ Cl ₂	^c
103	IPOZIY	(ET) _{2.53} [MnCr(ox) ₃]·CH ₂ Cl ₂	<i>P</i> -1	$\sigma = 10$ S/cm metal > 0.4 K	[MnCr(ox) ₃] ⁻	CH ₂ Cl ₂	[8]
104	IPOZOE	(ET) _{2.53} [MnRh(ox) ₃]·CH ₂ Cl ₂	<i>P</i> -1	$\sigma = 13$ S/cm metal > 100 K	[MnRh(ox) ₃] ⁻	CH ₂ Cl ₂	[8]
105	LOHWIO	(ET) ₄ [Fe ₂ (ox) ₅]	<i>P</i> _{21/n}	$\sigma = 2 \times 10^{-3}$ S/cm E _a = 1200 meV	[Fe ₂ (ox) ₅] ⁴⁻	-	[58]
106	NALVIG	(ET) ₃ [MnCr(ox) ₃]	<i>P</i> -1	$\sigma = 250$ S/cm metal > 0.3 K	[MnCr(ox) ₃] ²⁻	-	[7]
107	SAMMEA	(ET) ₃ [Cu ₂ (ox) ₃]·2CH ₃ OH	<i>P</i> -1	$\sigma = 4$ S/cm E _a = 50 meV	[Cu ₂ (ox) ₃] ²⁻	CH ₃ OH	[62]
108	WUXWET	(ET) ₃ [Cu ₂ (ox) ₃]·2H ₂ O	<i>P</i> -1	-	[Cu ₂ (ox) ₃] ²⁻	H ₂ O	^c

^a ox = oxalate = C₂O₄²⁻; ^b SG = space group. ^c Unpublished results.

6. Radical Salts of Metal-Oxalate Anions with Other TTF-Type Donor Molecules

Although BEDT-TTF is, by far, the most used donor molecule with metal-oxalato complexes, with more than one hundred reported salts (see Tables 1–9), other TTF-type donors have been combined with metal-oxalato complexes and lattices (Scheme 1). Here, we will revise all these salts, prepared with donors such as tetrathiafulvalene (TTF), tetramethyl-tetrathiafulvalene (TM-TTF), bis(ethylenediseleno)tetrathiafulvalene (BEDS-TTF = BEST), bis(ethylenedithio)tetraselenafulvalene (BEDT-TSF = BETS) and 4,5-bis((2S)-2-hydroxypropylthio)-4',5'-(ethylenedithio)tetrathiafulvalene (DMPET).

6.1. TTF and TM-TTF Salts with Oxalate Complexes

There are only two radical salts with [M(C₂O₄)₃]³⁻ anions and the donor TTF: (TTF)₇-[Fe(C₂O₄)₃]₂·4H₂O (**114**) [59,60] and (TTF)₃[Ru(C₂O₄)₃]₁·0.5EtOH·4H₂O (**118**) [64]. Salt **114** is an unusual 7:2 salt that shows corrugated mixed layers containing TTF molecules and the [Fe(C₂O₄)₃]³⁻ anions with the water molecules located between the layers (Figure 32a) [60]. The top view of these layers shows chains of TTF molecules, running parallel to the *a* axis (perpendicular to the layer), surrounded by TTF dimers and [Fe(C₂O₄)₃]³⁻ anions (Figure 32b). The TTF dimers contain two independent TTF molecules (C and D), and the TTF chains are formed by two different independent TTF molecules (A and B) following the sequence ... ABB ... (Figure 32c). The [Fe(C₂O₄)₃]³⁻ anions form homochiral rows running along the *b* axis, with opposite chirality in alternating rows, meaning that two of the four [Fe(C₂O₄)₃]³⁻ anions surrounding the TTF chains are ⊗ enantiomers and the other two are Λ (Figure 32b).

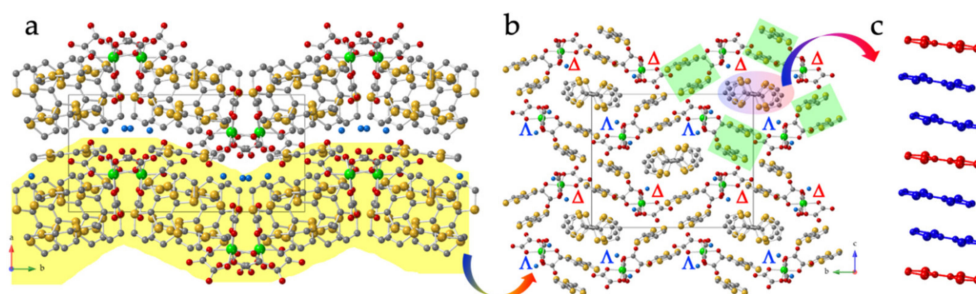


Figure 32. Structure of (TTF)₇[Fe(C₂O₄)₃]₂·4H₂O (**114**): (a) View of the corrugated mixed layers. (b) Top view (down the *a* direction) of the mixed layers showing the TTF dimers (green rectangles) and the TTF chains. (c) Side view of the TTF chains showing the ... ABB ... sequence. Color code in (a,b): Fe = green, C = gray, O = red, O_{water} = blue and S = yellow. H atoms are omitted for clarity.

The other salt with TTF and a monomeric $[M(C_2O_4)_3]^{3-}$ anion, $(TTF)_3[Ru(C_2O_4)_3] \cdot 0.5EtOH \cdot 4H_2O$ (**118**), was the first radical salt prepared with a 4d $[M(C_2O_4)_3]^{3-}$ anion and shows a very original structure in both sublattices [64]. Its structure consists of alternating cationic and anionic layers parallel to the ab plane (Figure 33a). There are two different anionic layers each containing a single enantiomer. The anionic layers contain the $[M(C_2O_4)_3]^{3-}$ anions and the solvent molecules with a hexagonal arrangement (Figure 33b), although different to the one observed in the BEDT-TTF salts of previous sections since, now, there is no extra A^+ cation orienting the terminal O atoms of the oxalate ligands. The TTF layers are also original: they contain three independent TTF molecules (A–C) arranged in AA dimers and chains following the sequence ... BBCC ... (Figure 33c). The TTF molecules of consecutive layers run in opposite directions (Figure 33d). This salt shows a paramagnetic behavior with contributions from the $[Ru(C_2O_4)_3]^{3-}$ $S = \frac{1}{2}$ anions and from the TTF molecules that show a charge localization, in agreement with the semiconducting behavior observed in this salt [64].

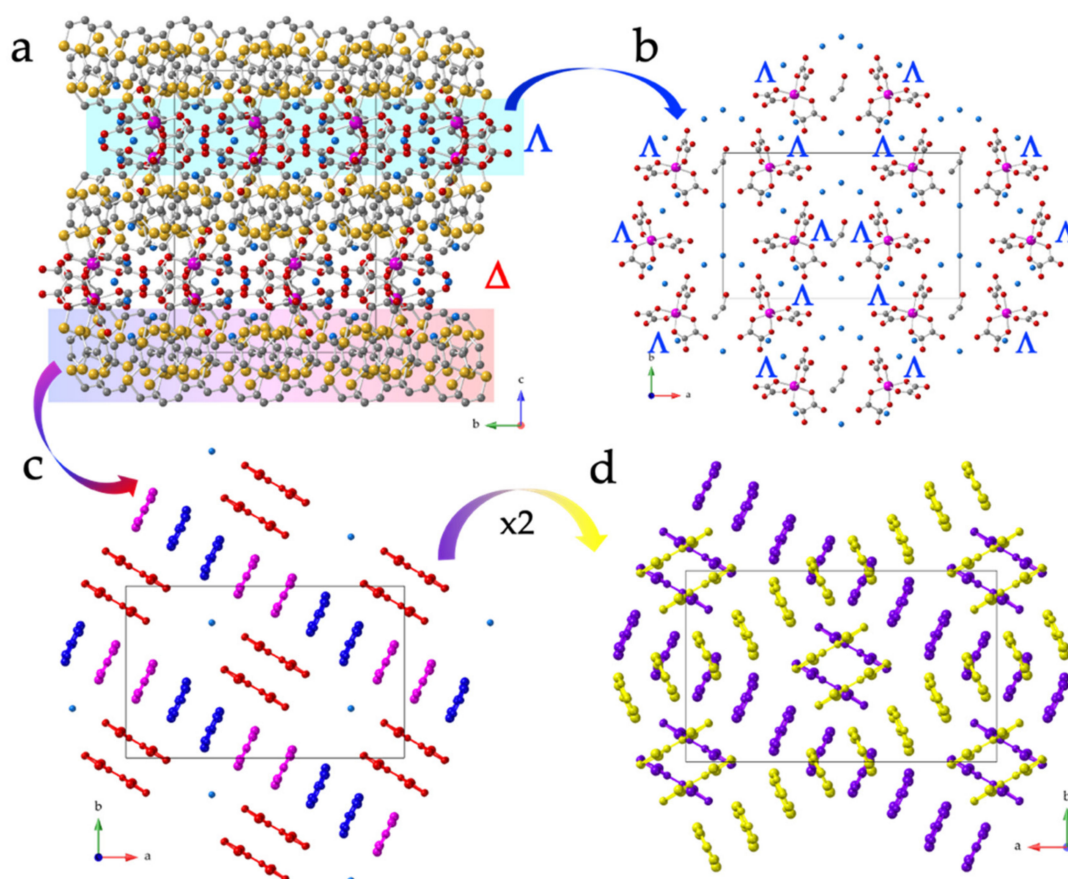


Figure 33. Structure of $(TTF)_3[Ru(C_2O_4)_3] \cdot 0.5EtOH \cdot 4H_2O$ (**118**): (a) View of the alternating cationic and anionic layers parallel to the ab plane. (b) View of the Λ anionic layer. (c) View of the cationic layer showing the AA dimers (in red) and the ... BBCC ... chains (in blue and pink). (d) View of two consecutive TTF layers (in yellow and purple) showing the opposite orientations of the chains and the dimers. Color code in (a,b): Ru = pink, C = gray, O = red, O_{water} = blue and S = yellow. H atoms are omitted for clarity.

There are two other salts with oxalate complexes and TTF, although they do not contain monomeric $[M(C_2O_4)_3]^{3-}$ anions but an $[Fe_2(C_2O_4)_5]^{4-}$ dimer in $(TTF)_5[Fe_2(C_2O_4)_5] \cdot 2PhCH_3 \cdot 2H_2O$ (**115**) [59,60], or a $[Mn(H_2O)_2[Cr(C_2O_4)_3]_2]^{4-}$ trimer in $(TTF)_4\{Mn(H_2O)_2[Cr(C_2O_4)_3]_2\} \cdot 14H_2O$ (**120**) [65,66]. Interestingly, salts **115** and **120** are the first examples of any salt with the previously unknown $[Fe_2(C_2O_4)_5]^{4-}$ dimer and $\{Mn(H_2O)_2[Cr(C_2O_4)_3]_2\}^{4-}$ trimer, respectively. In both cases, the anions are assembled during the electrochemical

synthesis of the radical salts from the corresponding $[M(C_2O_4)_3]^{3-}$ anions (and Mn^{2+} cations in salt **120**).

Salt **115** shows alternating cationic and anionic layers parallel to the ab plane (Figure 34b). The cationic layers contain two independent TTF molecules (A and B). A-type TTF molecules form chains running parallel to the b axis, whereas B-type molecules are monomers located between the chains. The packing of the TTF molecules is unique because not only the planes of the A- and B-type molecules are orthogonal but also their long molecular axis (Figure 34a,b). The $[Fe_2(C_2O_4)_5]^{4-}$ dimer is formed by the fusion of one \otimes and one Λ monomer through a bis-bidentate oxalate ligand (Figure 1c). These dimers are packed in rows along the b axis with $PhCH_3$ molecules located between the rows (Figure 34c). The electrical properties show that this salt is a semiconductor (Table 10), in agreement with the presence of neutral isolated TTF molecules. The magnetic properties show that the $[Fe_2(C_2O_4)_5]^{4-}$ dimer presents a weak antiferromagnetic Fe–Fe coupling with $J = -3.57 \text{ cm}^{-1}$, through the oxalate bridge, as observed in the other salts prepared with this dimer [58,60].

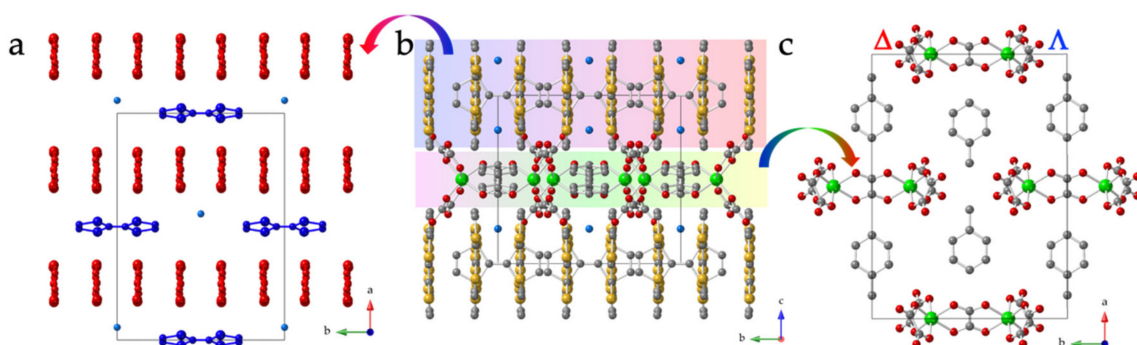


Figure 34. Structure of $(TTF)_4[Fe_2(C_2O_4)_5] \cdot 2PhCH_3 \cdot 2H_2O$ (**115**): (a) View of the cationic layer showing the chains along the b axis containing the A-type molecules (in red) and the isolated orthogonal monomers (in blue). (b) View of the alternating cationic and anionic layers parallel to the ab plane. (c) View of the anionic layer. Color code in (b,c): Fe = green, C = gray, O = red, O_{water} = blue and S = yellow. H atoms are omitted for clarity.

The last salt with TTF and an oxalate complex is $(TTF)_4\{Mn(H_2O)_2[Cr(C_2O_4)_3]_2\} \cdot 14H_2O$ (**120**) [65,66]. This salt was the first one prepared with TTF and any oxalate complex and contains the then-unknown $\{Mn(H_2O)_2[Cr(C_2O_4)_3]_2\}^{4-}$ trimer. The structure shows alternating cationic and anionic layers parallel to the ab plane (Figure 35b). There are three independent TTF molecules forming orthogonal AA and BC dimers (similar to the κ -phase in BEDT-TTF) [67], although now the dimers form stacks separated by water molecules (Figure 35a). The anionic layer contains linear trimeric $\{Mn(H_2O)_2[Cr(C_2O_4)_3]_2\}^{4-}$ anions formed by the fusion of two $[Cr(C_2O_4)_3]^{3-}$ monomers with different chirality with a Mn(II) ion coordinated by two equatorial bidentate oxalato ligands and two axial H_2O molecules (Figure 1d). These trimers are packed in a rhombic disposition with strong H bonds between the two coordinated water molecules and the terminal O atoms of the oxalato ligands of neighboring trimers (Figure 35c).

The magnetic properties show the presence of a weak ferromagnetic Cr–Mn coupling with $J = 1.08 \text{ cm}^{-1}$, although the salt is a semiconductor since the TTF molecules are completely oxidized and there are no short intermolecular contacts (Table 10) [65,66]. An additional interest of this salt is the possibility to change the anion by simply changing Cr(III) to Fe(III) and Mn(II) to other metal ions such as Fe(II), Co(II), Ni(II), Cu(II) and Zn(II). In this way, it was possible to prepare the series of salts $(TTF)_4\{M^{II}(H_2O)_2[M^{III}(C_2O_4)_3]_2\} \cdot nH_2O$ with $M^{III}/M^{II} = Cr/Mn, Cr/Fe, Cr/Co, Cr/Ni, Cr/Cu, Cr/Zn, Fe/Mn, Fe/Fe, Fe/Co, Fe/Ni$ and Fe/Zn [66]. The use of different metal ions in these series allowed a modulation of the magnetic coupling that is weak ferromagnetic for the Cr(III) derivatives and weak antiferromagnetic for the Fe(III) ones [66].

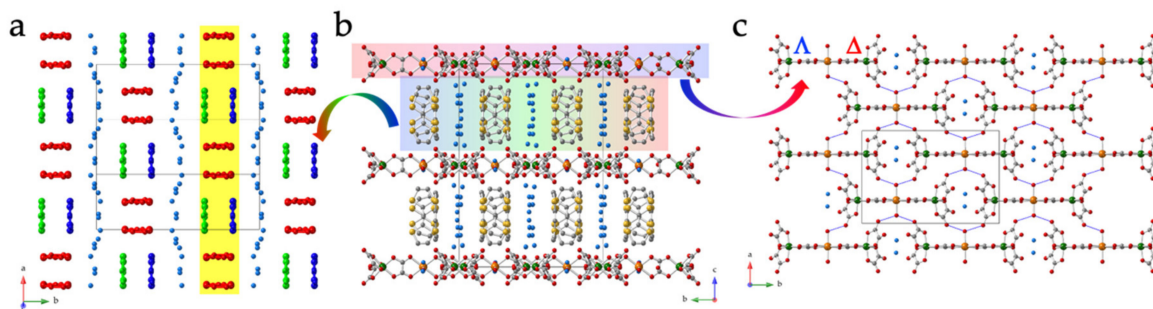


Figure 35. Structure of $(\text{TTF})_4[\text{Mn}(\text{H}_2\text{O})_2[\text{Cr}(\text{C}_2\text{O}_4)_3]_2] \cdot 14\text{H}_2\text{O}$ (**120**): (a) View of the cationic layer showing the orthogonal AA (in red) and BC (green and blue) dimers arranged in chains separated by water molecules. (b) View of the alternating cationic and anionic layers parallel to the ab plane. (c) View of the anionic layer. Thin blue lines are the H bonds between the anions. Color code in (a,c): Cr = dark green, Mn = orange, C = gray, O = red, O_{water} = blue and S = yellow. H atoms are omitted for clarity.

The then-unknown $[\text{Fe}_2(\text{C}_2\text{O}_4)_5]^{4-}$ dimer was also obtained with the donor tetramethyl-tetrathiafulvalene (TM-TTF) and published with the TTF salt described above [60]. This salt, formulated as $(\text{TM-TTF})_4[\text{Fe}_2(\text{C}_2\text{O}_4)_5] \cdot \text{PhCN} \cdot 4\text{H}_2\text{O}$ (**116**), shows mixed layers of TM-TTF molecules and $[\text{Fe}_2(\text{C}_2\text{O}_4)_5]^{4-}$ anions with crystallization PhCN and water molecules (Figure 36a). The layers contain stacks of TM-TTF separated by rows with the $[\text{Fe}_2(\text{C}_2\text{O}_4)_5]^{4-}$ anions and crystallization solvent molecules (Figure 36b). The TM-TTF stacks are formed by two independent TM-TTF molecules following the sequence ... AABB ... Although the molecular planes of the donor molecules are parallel, the long axis of the molecules is slightly tilted (Figure 36c). As the TM-TTF molecules are completely oxidized, the salt is a semiconductor with a high activation energy (Table 10). As observed in the TTF and BEDT-TTF salts of the same $[\text{Fe}_2(\text{C}_2\text{O}_4)_5]^{4-}$ anion, in compound **116**, this anion shows a weak antiferromagnetic Fe–Fe coupling with $J = -3.69 \text{ cm}^{-1}$, through the oxalate bridge, similar to those of the other salts with this dimer [58,60].

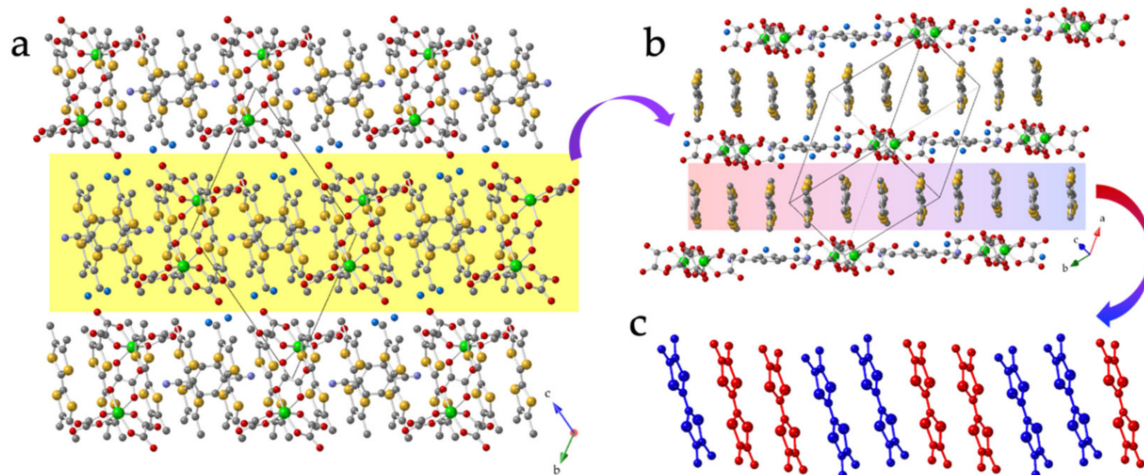


Figure 36. Structure of $(\text{TM-TTF})_4[\text{Fe}(\text{C}_2\text{O}_4)_3]_2 \cdot \text{PhCN} \cdot 4\text{H}_2\text{O}$ (**116**): (a) Side view of the mixed cationic and anionic layers. (b) Top view of the mixed layer showing the TM-TTF chains separated by $[\text{Fe}(\text{C}_2\text{O}_4)_5]^{4-}$ anions and water molecules. (c) View of the TM-TTF chains formed by A (red) and B (blue) TM-TTF molecules. Color code in (a,b): Fe = green, C = gray, O = red, O_{water} = blue and S = yellow. H atoms are omitted for clarity.

6.2. Salts with Se-Containing Donors (BEST and BETS)

There are two selenium-containing derivatives of BEDT-TTF that have also been used with oxalate complexes: bis(ethylenediseleno)tetrathiafulvalene (BEDS-TTF = BEST), which contains four Se atoms in the outer rings, and bis(ethylenedithio)tetraselenafulvalene

(BEDT-TSF = BETS), which contains four Se atoms in the inner rings (Scheme 1). With the donor BEST, a total of five salts have been reported [68]. There are two isostructural salts with benzoic acid and water as crystallization solvents: $(\text{BEST})_4[\text{M}(\text{C}_2\text{O}_4)_3] \cdot \text{PhCOOH} \cdot \text{H}_2\text{O}$, with $\text{M} = \text{Cr}$ (**109**) and Fe (**110**), and a couple of isostructural salts with the same stoichiometry but different solvents formulated as $(\text{BEST})_4[\text{M}(\text{C}_2\text{O}_4)_3] \cdot 1.5\text{H}_2\text{O}$, with $\text{M} = \text{Cr}$ (**111**) and Fe (**113**). The fifth salt is a 9:2 salt formulated as $(\text{BEST})_9[\text{Fe}(\text{C}_2\text{O}_4)_3]_2 \cdot 7\text{H}_2\text{O}$ (**112**) [68].

The structure of salts $(\text{BEST})_4[\text{M}(\text{C}_2\text{O}_4)_3] \cdot \text{PhCOOH} \cdot \text{H}_2\text{O}$, with $\text{M} = \text{Cr}$ (**109**) and Fe (**110**) consists of alternating cationic and anionic layers parallel to the ab plane (Figure 37b). The cationic layer is formed by four independent BEST molecules (A–D) packed with the β packing mode (Figure 37a) in parallel stacks, with a step every four BEST molecules (Figure 37b), following the sequence ... ABCDDCBA ... (Figure 37a). The anionic layers show an original arrangement with pairs of anions with different chirality separated by PhCOOH molecules, also arranged in pairs, and water molecules forming moderate H bonds (Figure 37c). A- and C-type BEST molecules are completely ionized, whereas B and D molecules bear a charge of +1/2. The presence of totally ionized BEST molecules is responsible of the semiconducting behavior of these two salts (Table 10) [68]. The magnetic properties show that there is no noticeable contribution from the organic layers, and the salts behave as isolated $S = 3/2$ or $S = 5/2$ ions for **109** and **110**, respectively.

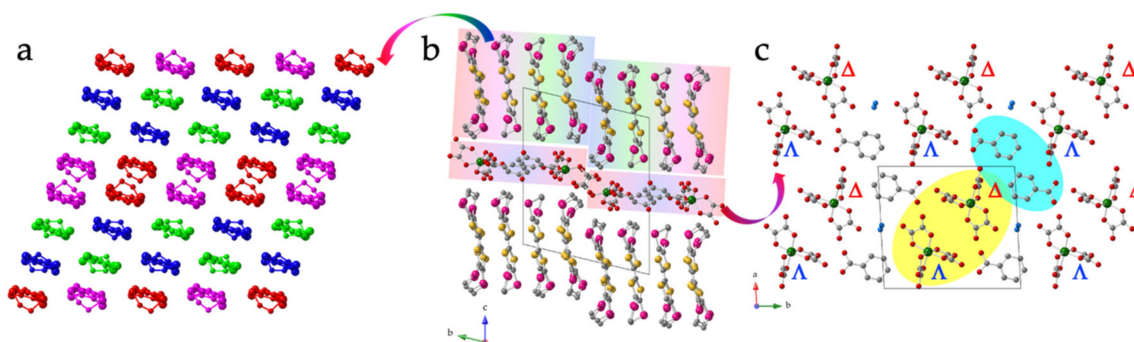


Figure 37. Structure of $(\text{BEST})_4[\text{Cr}(\text{C}_2\text{O}_4)_3] \cdot \text{PhCOOH} \cdot \text{H}_2\text{O}$ (**109**): (a) View of the cationic layer showing the β packing formed by four independent BEST molecules (in red, blue, green and pink). (b) View of the alternating cationic and anionic layers parallel to the ab plane. (c) View of the anionic layer. Color code in (b,c): Cr = dark green, C = gray, O = red, O_{water} = blue, Se = pink and S = yellow. H atoms are omitted for clarity.

Salts $(\text{BEST})_4[\text{M}(\text{C}_2\text{O}_4)_3] \cdot 1.5\text{H}_2\text{O}$, with $\text{M} = \text{Cr}$ (**111**) and Fe (**113**), are isostructural and represent a pair of solvates of **109** and **110**, respectively, since they show the same stoichiometry and composition and only differ in the crystallization solvent molecules (PhCOOH and H_2O in **109** and **110**, compared to only H_2O in **111** and **113**) [68]. The structure of salts **111** and **113** also consists of alternating cationic and anionic layers parallel to the ab plane (Figure 38b). The cationic layer contains two independent BEST molecules (A and B) packed in parallel stacks following the sequence ... ABAB ..., also with the β packing mode (Figure 38a). The anions appear with a disorder since they are located close to an inversion center. When only one of the two possible locations is considered, the anions show zigzag chains with alternating chirality along the c axis (Figure 38c). The A-type BEST molecules are completely ionized, whereas B molecules bear a charge of +1/2, in agreement with the stoichiometry and the anionic charge. The presence of alternating totally ionized BEST molecules results in a semiconducting behavior for these two salts (Table 10). The magnetic properties are, as expected, similar to those of salts **109** and **110** since the Cr(III) $S = 3/2$ and Fe(III) $S = 5/2$ ions are isolated from the magnetic point of view and there is no noticeable contribution from the organic layers [68].

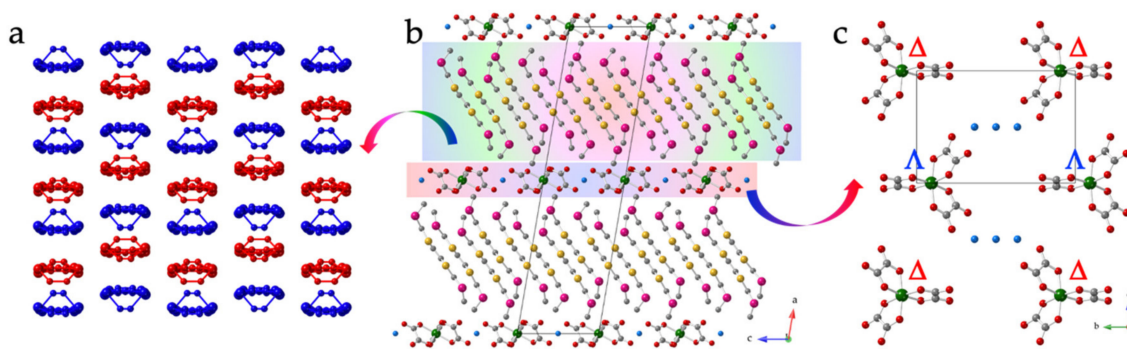


Figure 38. Structure of $(\text{BEST})_4[\text{Cr}(\text{C}_2\text{O}_4)_3] \cdot 1.5\text{H}_2\text{O}$ (**111**): (a) View of the cationic layer showing the β packing formed by two independent BEST molecules (in red and blue). (b) View of the alternating cationic and anionic layers parallel to the ac plane. (c) View of the anionic layer showing only one of the two orientations of the $[\text{Cr}(\text{C}_2\text{O}_4)_3]^{3-}$ anions. Color code in (b,c): Cr = dark green, C = gray, O = red, O_{water} = blue, Se = pink and S = yellow. H atoms are omitted for clarity.

The last salt containing the donor BEST is a very original 9:2 phase, formulated as $(\text{BEST})_9[\text{Fe}(\text{C}_2\text{O}_4)_3]_2 \cdot 7\text{H}_2\text{O}$ (**112**) [68]. This salt also presents alternating cationic and anionic layers parallel to the ab plane (Figure 39b), and the cationic layer also shows the β packing mode (Figure 39a). The main difference with the other BEST layers is the presence of five independent BEST molecules (A–E) that form two different chains (I and II) with steps every three BEST molecules (Figure 39b). Chains of type I are formed by D and E molecules packed following the sequence ... DED ..., whereas chains of type II contain three independent molecules (A–C) packed following the sequence ... ABC ... There are two chains of type II and one of type I alternating in the direction perpendicular to the stacks following the sequence ... /I/II/II/ ... (Figure 39a). The $[\text{Fe}(\text{C}_2\text{O}_4)_3]^{3-}$ anions are located to form dimers with the opposite chirality, and the crystallization water molecules are located in between the anions forming several H bonds with the anions and with the water molecules (Figure 39c). The inhomogeneous charge distribution of the five BEST-TTF molecules is at the origin of the semiconducting behavior observed in this salt (Table 10). As in the previous BEST salts, the magnetic properties correspond to isolated $[\text{Fe}(\text{C}_2\text{O}_4)_3]^{3-}$ anions with no noticeable contribution from the organic layers [68].

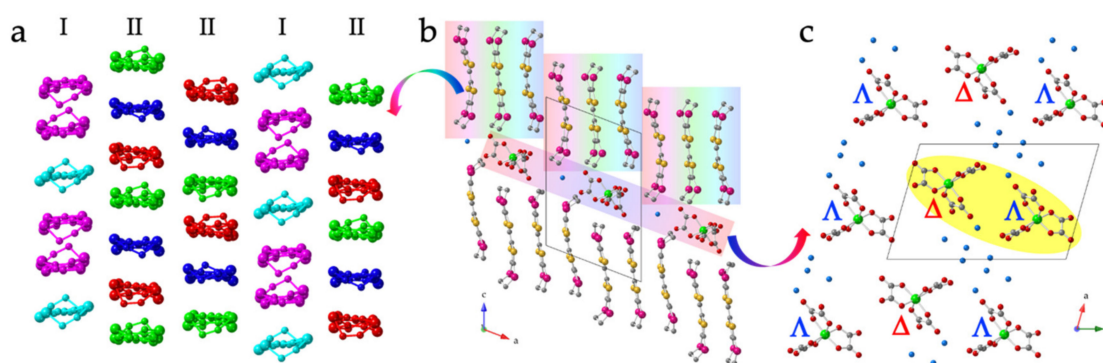


Figure 39. Structure of $(\text{BEST})_9[\text{Fe}(\text{C}_2\text{O}_4)_3]_2 \cdot 7\text{H}_2\text{O}$ (**112**): (a) View of the cationic layer showing the β packing and the two different stacks (I and II) with the five independent BEST molecules (A–E in red, dark blue, green, pink and light blue, respectively). (b) View of the alternating cationic and anionic layers parallel to the ab plane. (c) View of the anionic layer showing the $[\text{Fe}(\text{C}_2\text{O}_4)_3]^{3-}$ anions and the crystallization water molecules. Color code in (b,c): Fe = green, C = gray, O = red, O_{water} = blue, Se = pink and S = yellow. H atoms are omitted for clarity.

The other Se-containing donor, bis(ethylenedithio)tetraselenafulvalene (BETS), has never been combined with monomeric $[\text{M}(\text{C}_2\text{O}_4)_3]^{3-}$ anions but only with two extended honeycomb lattices, in compounds $(\text{BETS})_3[\text{Cu}_2(\text{C}_2\text{O}_4)_3] \cdot 2\text{CH}_3\text{OH}$ (**117**) [69] and $(\text{BETS})_3[\text{MnCr}(\text{C}_2\text{O}_4)_3] \cdot \text{CH}_2\text{Cl}_2$ (**119**) [70].

Compound $(\text{BETS})_3[\text{Cu}_2(\text{C}_2\text{O}_4)_3]\cdot 2\text{CH}_3\text{OH}$ (**117**) contains alternating cationic and anionic layers parallel to the ab plane (Figure 40b) [69]. The organic layer presents the θ^{21} phase with two stacks tilted in one direction and one stack in the opposite direction (Figure 40a), also observed in the BEDT-TTF derivatives with the same $[\text{Cu}_2(\text{C}_2\text{O}_4)_3]^{2-}$ layer (compound **107**, see above). The anionic sublattice in **117** is a hexagonal honeycomb layer that shows important distortion due to the Jahn–Teller effect on the Cu(II) ions (Figure 40c). The electrical properties show that the BETS salt is a much better electrical conductor than the BEDT-TTF one with a higher room temperature conductivity and a metallic behavior down to 180 K (the BEDT-TTF salt is semiconducting). The improved electrical properties are attributed to the enhanced intermolecular interactions when S is substituted by Se. The Cu···Cu interaction is also antiferromagnetic, as in the BEDT-TTF derivative [69].

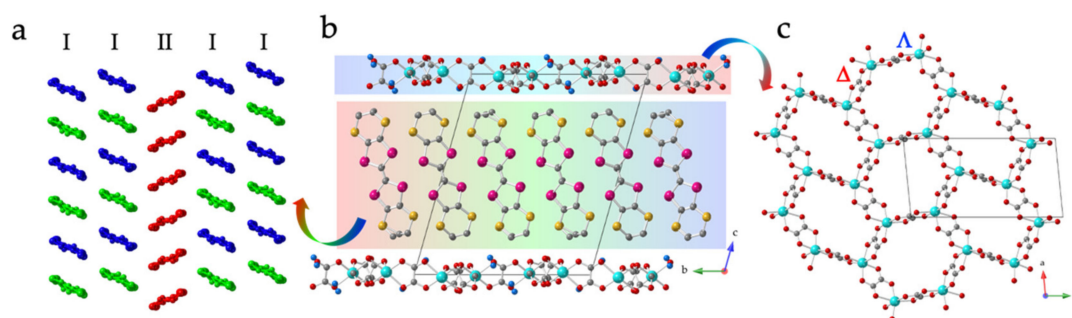


Figure 40. Structure of $(\text{BETS})_3[\text{Cu}_2(\text{C}_2\text{O}_4)_3]\cdot 2\text{CH}_3\text{OH}$ (**117**): (a) View of the cationic layer showing the θ^{21} packing and the two different stacks (I and II) with the three independent BEST molecules (A–C in red, dark blue and green, respectively). (b) View of the alternating cationic and anionic layers parallel to the ab plane. (c) View of the anionic layer showing the $[\text{Cu}_2(\text{C}_2\text{O}_4)_3]^{3-}$ honeycomb lattice. Color code in (b,c): Cu = light blue, C = gray, O = red, O_{water} = blue, Se = pink and S = yellow. H atoms are omitted for clarity.

The other salt prepared with BETS is $(\text{BETS})_3[\text{MnCr}(\text{C}_2\text{O}_4)_3]\cdot \text{CH}_2\text{Cl}_2$ (**119**) [70]. This salt is the first one prepared with the BETS donor and an oxalate complex and also shows alternating cationic and anionic layers parallel to the ab plane. The cationic layer shows the α packing mode, where consecutive stacks are tilted in opposite directions (Figure 41a). The anionic layer is identical to the one observed in the BEDT-TTF derivative: it shows the classical honeycomb structure with alternating Mn(II) and Cr(III) centers connected through oxalato bridges. This salt is metallic down to 150 K (Figure 41b) and shows the expected ferromagnetic long-range order below 5.3 K (Figure 41c). In this case, the change of S to Se in the donor molecule did not improve the electrical properties [70].

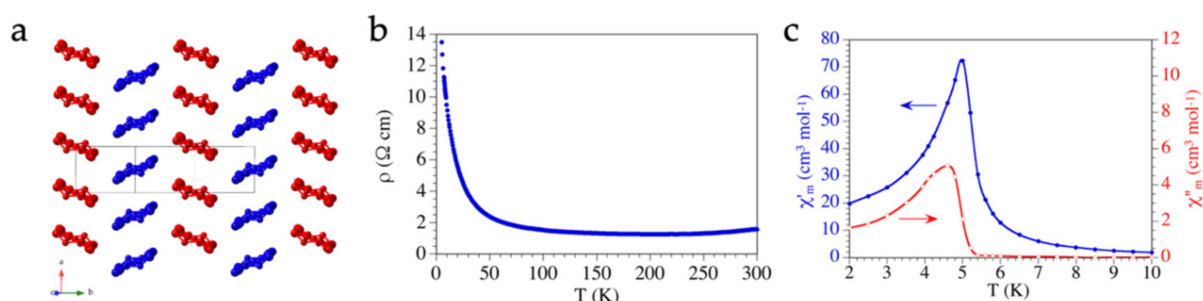


Figure 41. (a) View of the cationic layer in $(\text{BETS})_3[\text{MnCr}(\text{C}_2\text{O}_4)_3]\cdot \text{CH}_2\text{Cl}_2$ (**119**) showing the α packing with the two different stacks formed by the A- (in red) and B-type (in blue) BETS molecules. H atoms are omitted for clarity. (b) Thermal variation in the electrical resistivity of compound **119**. (c) Thermal variation in the in-phase (χ'_m) and out-of-phase (χ''_m) susceptibilities in compound **119**.

Finally, although its structure could not be determined, the $[\text{MnCr}(\text{C}_2\text{O}_4)_3]^-$ lattice has also been combined with BEST to obtain a radical salt with a formula of $(\text{BEST})_3[\text{MnCr}(\text{C}_2\text{O}_4)_3]$ that shows a low room temperature conductivity of 10^{-6} S/cm and a ferromagnetic order at $T_c = 5.6$ K [61]. The change of Mn(II) to Co(II) in this honeycomb lattice leads to the isostructural lattice $[\text{CoCr}(\text{C}_2\text{O}_4)_3]^-$ with a higher ordering temperature that has also been combined with the donors BEST and BETS to prepare salts $(\text{BEST})_3[\text{CoCr}(\text{C}_2\text{O}_4)_3]$ and $(\text{BETS})_3[\text{CoCr}(\text{C}_2\text{O}_4)_3]$. These two salts show ferromagnetic ordering temperatures of 10.8 and 9.2 K, respectively, and show room temperature conductivities of 10^{-6} S/cm for the BEST salt and 2.3 S/cm for the BETS one [61].

6.3. Salts with Other Donors

Finally, there is one reported salt with the $[\text{Fe}_2(\text{C}_2\text{O}_4)_5]^{4-}$ dimeric anion and the chiral donor 4,5-bis((2S)-2-hydroxypropylthio)-4',5'-(ethylenedithio)tetrathiafulvalene (DMPET-TTF, Scheme 1): $(\text{DMPET})_4[\text{Fe}_2(\text{C}_2\text{O}_4)_5]$ (**121**) [71]. The structure of this compound shows alternating cationic and anionic layers parallel to the *ac* plane (Figure 42b), although the large size of the two 2-hydroxypropylthio groups precludes the formation of parallel donor stacks. Thus, the cationic layers are formed by single stacks of the DMPET-TTF molecules running along the *c* axis (Figure 42a). The anionic layers contain well-isolated $[\text{Fe}_2(\text{C}_2\text{O}_4)_5]^{4-}$ anions as a result of the large size of the DMPET molecules (Figure 42c). No physical properties are reported for this salt [71].

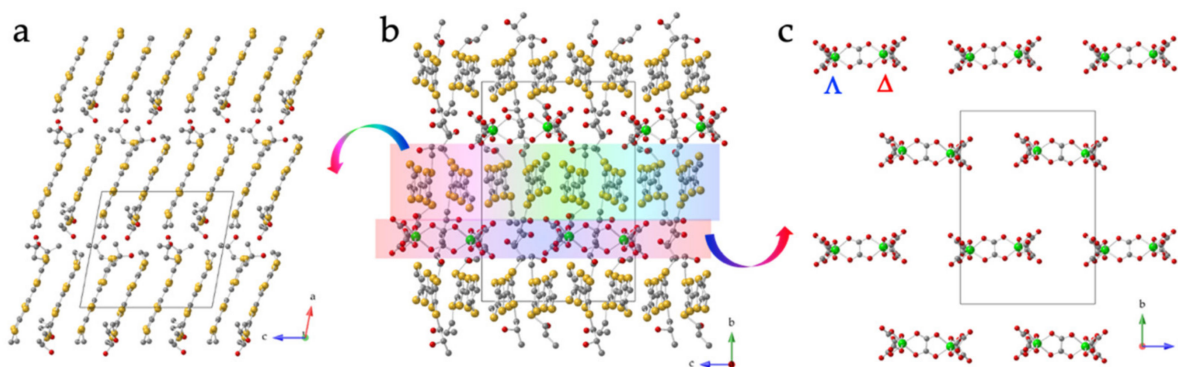


Figure 42. Structure of $(\text{DMPET-TTF})_4[\text{Fe}_2(\text{C}_2\text{O}_4)_5]$ (**121**): (a) View of the cationic layer showing the individual chains of DMPET-TTF molecules along the *c* direction. (b) View of the alternating cationic and anionic layers parallel to the *ac* plane. (c) View of the anionic layer showing the $[\text{Fe}_2(\text{C}_2\text{O}_4)_5]^{4-}$ anions. Color code: Fe = green, C = gray, O = red and S = yellow. H atoms are omitted for clarity.

Finally, although there is no structural report, the honeycomb lattice $[\text{MnCr}(\text{C}_2\text{O}_4)_3]^-$ has also been combined with other donors such as bis(ethylenedithio)tetrathiafulvalene (BET), bis(methylenedithio)tetrathiafulvalene (BMDT-TTF), bis(ethylenedioxo)tetrathiafulvalene (BEDO-TTF) and bis(ethylenedithio)trithiaselenafulvalene (ET-1Se), whereas the isostructural $[\text{CoCr}(\text{C}_2\text{O}_4)_3]^-$ lattice was combined with the donor BET. The ferromagnetic ordering temperatures are in the range 5.0–5.6 K for the MnCr lattices and 13.0 K for the CoCr one. The room temperature conductivities, measured on pressed pellets, are quite high, in the range 0.1–21 S/cm [61].

Table 10. Radical salts of metal-oxalate anions with other TTF-type donor molecules (109–121).

#	CCDC	Formula ^a	SG ^b	Elect. Prop.	Donor ^c	G	Ref
109	CEWMEX	(BEST) ₄ [Cr(ox) ₃]·PhCOOH·H ₂ O	<i>P</i> -1	$\sigma = 1.5 \text{ S/cm}$ $E_a = 49 \text{ meV}$	BEST	PhCOOHH ₂ O	[68]
110	CEWMIB	(BEST) ₄ [Fe(ox) ₃]·PhCOOH·H ₂ O	<i>P</i> -1	$\sigma = 6.4 \text{ S/cm}$ $E_a = 54 \text{ meV}$	BEST	PhCOOHH ₂ O	[68]
111	CEWMOH	(BEST) ₄ [Cr(ox) ₃]·1.5H ₂ O	<i>C</i> 2/ <i>m</i>	$\sigma = 8.5 \text{ S/cm}$ $E_a = 62 \text{ meV}$	BEST	H ₂ O	[68]
112	CEWMUN	(BEST) ₉ [Fe(ox) ₃] ₂ ·7H ₂ O	<i>P</i> -1	$\sigma = 2.4 \text{ S/cm}$ $E_a = 44 \text{ meV}$	BEST	H ₂ O	[68]
113	CEWNAU	(BEST) ₄ [Fe(ox) ₃]·1.5H ₂ O	<i>C</i> 2/ <i>m</i>	$\sigma = 14.0 \text{ S/cm}$ $E_a = 60 \text{ meV}$	BEST	H ₂ O	[68]
114	DIQFOY	(TTF) ₇ [Fe(ox) ₃] ₂ ·4H ₂ O	<i>P</i> 2 ₁ / <i>c</i>	$\sigma = 10^{-4} \text{ S/cm}$ $E_a = 279 \text{ meV}$	TTF	H ₂ O	[59,60]
115	DIQFUE	(TTF) ₅ [Fe ₂ (ox) ₅]·2PhCH ₃ ·2H ₂ O	<i>C</i> 2/ <i>m</i>	$\sigma = 1.8 \times 10^{-6} \text{ S/cm}$	TTF	PhCH ₃ H ₂ O	[59,60]
116	DIQGAL	(TMTTF) ₄ [Fe ₂ (ox) ₅]·PhCN·4H ₂ O	<i>P</i> -1	$\sigma = 2.2 \times 10^{-3} \text{ S/cm}$ $E_a = 290 \text{ meV}$	TMTTF	PhCNH ₂ O	[59,60]
117	NIDDIP	(BETS) ₃ [Cu ₂ (ox) ₃]·2CH ₃ OH	<i>P</i> -1	$M > 180 \text{ K}$	BETS	CH ₃ OH	[69]
118	OLABAE	(TTF) ₃ [Ru(ox) ₃]·0.5EtOH·4H ₂ O	<i>C</i> 2/ <i>c</i>	$\sigma = 1.5 \times 10^{-4} \text{ S/cm}$ $E_a = 61 \text{ meV}$	TTF	EtOHH ₂ O	[64]
119	RUDNOT02	(BETS) ₃ [MnCr(ox) ₃]·CH ₂ Cl ₂	<i>P</i> -1	$M > 150 \text{ K}$	BETS	CH ₂ Cl ₂	[70]
120	TUHDOP	(TTF) ₄ [Mn(H ₂ O) ₂ [Cr(ox) ₃] ₂]·14H ₂ O	<i>C</i> 2/ <i>c</i>	$\sigma = 2 \times 10^{-4} \text{ S/cm}$ $E_a = 200 \text{ meV}$	TTF	H ₂ O	[65,66]
121	VIPYUQ	(DMPET) ₄ [Fe ₂ (ox) ₅]	<i>P</i> 2 ₁	-	DMPET	-	[71]

^a ox = oxalate = C₂O₄²⁻; ^b SG = space group; ^c BEST = bis(ethylenediseleno)tetrathiafulvalene; TTF = tetrathiafulvalene; TMTTF = tetramethyl-tetrathiafulvalene; BETS = bis(ethylenedithio)tetraselenafulvalene; DMPET = 4,5-bis((2S)-2-hydroxypropylthio)-4',5'-(ethylenedithio)tetrathiafulvalene.

7. Conclusions

The seminal work of Peter Day's group in 1995 [2,3] with the synthesis of the first paramagnetic superconductors in the family of salts β'' -(BEDT-TTF)₄[AM(C₂O₄)₃]·G (A = monocation, M = trivalent metal ion and G = solvent) is at the origin of the largest series of molecular metals and superconductors prepared to date. This series constitutes a paradigmatic example of the tuneability of molecular materials, as shown by the large number of related compounds prepared by changing: (i) the A⁺ cation with other monocations (H₃O⁺, NH₄⁺, K⁺, Na⁺ and Li⁺) or even with dications (Mn²⁺, Co²⁺ and Cu²⁺); (ii) the TTF-type donors (TTF, TM-TTF, BEST, BETS, BET, BEDO, BMDT-TTF, etc.); (iii) the M(III) ion (Fe, Cr, Ga, Mn, Rh, Ru, Al, Co and Ir), or even M(IV) as Ge(IV) and M(II) as Cu(II); and (iv) the solvent molecule (PhCN, PhNO₂, PhF, PhCl, PhBr, PhI, PhCOOH, H₂O, CH₂Cl₂, CH₃OH, py, dmf, Cl-Py, Br-py, etc.). These relatively easy-to-perform modifications have led to the synthesis of more than one hundred and twenty radical salts with oxalate complexes combining electrical properties (semiconductors, metals and superconductors) with magnetic properties (paramagnetism, ferro-, ferri- and antiferromagnetic couplings and even long-range magnetic ordering). These series constitute, by far, the largest family of multifunctional molecular materials prepared to date.

No doubt, the research on this type of salt was boosted by the preparation by P. Day's group of the first molecular paramagnetic superconductor in 1995 [2,3]. Since then, several groups have prepared and characterized many different salts to try to understand the key aspects of these magnetic superconductors and to improve the magnetic and/or the electrical properties. Furthermore, this search has allowed the synthesis of magnetic conductors with other properties such as chirality or proton conductivity.

As a homage to the legacy of the late Peter Day, we have shown, here, the so-called Day series of radical salts formulated as β'' -(BEDT-TTF)₄[AM(C₂O₄)₃]·G, with more than fifty reported structures to date, and of the closely related series prepared with other oxalate complexes and different donors. Many of these related series were also initiated by Peter Day's group, and still, twenty-five years later, most of the most active researchers in this field were part of his group in the past.

Author Contributions: Both authors contributed equally to the manuscript. Both authors have read and agreed to the published version of the manuscript.

Funding: This research was funded by the Spanish MINECO (project CTQ2017-87201-P AEI/FEDER, UE) and the Generalidad Valenciana (project PrometeoIII/2019/076).

Acknowledgments: This research was funded by the Spanish MINECO (project CTQ2017-87201-P AEI/FEDER, UE) and the Generalidad Valenciana (project PrometeoIII/2019/076), who we thank for the financial support. We also thank all the co-authors that appear in our contributions in this field.

Conflicts of Interest: The authors declare no conflict of interest.

References

1. Robin, M.B.; Day, P. Mixed Valence Chemistry-A Survey and Classification. *Adv. Inorg. Chem. Radiochem.* **1968**, *10*, 247–422.
2. Kurmoo, M.; Graham, A.W.; Day, P.; Coles, S.J.; Hursthouse, M.B.; Caulfield, J.L.; Singleton, J.; Pratt, F.L.; Hayes, W. Superconducting and Semiconducting Magnetic Charge Transfer Salts: (BEDT-TTF)₄AFe(C₂O₄)₃·C₆H₅CN (A = H₂O, K, NH₄). *J. Am. Chem. Soc.* **1995**, *117*, 12209–12217. [[CrossRef](#)]
3. Graham, A.W.; Kurmoo, M.; Day, P. β'' -(BEDT-TTF)₄[(H₂O)Fe(C₂O₄)₃]·PhCN: The First Molecular Superconductor Containing Paramagnetic Metal Ions. *J. Chem. Soc. Chem. Commun.* **1995**, 2061–2062. [[CrossRef](#)]
4. Martin, L.; Turner, S.S.; Day, P.; Guionneau, P.; Howard, J.A.K.; Hibbs, D.E.; Light, M.E.; Hursthouse, M.B.; Uruichi, M.; Yakushi, K. Crystal Chemistry and Physical Properties of Superconducting and Semiconducting Charge Transfer Salts of the Type (BEDT-TTF)₄[A^IM^{III}(C₂O₄)₃]·PhCN (A^I = H₃O, NH₄, K.; M^{III} = Cr, Fe, Co, Al; BEDT-TTF = Bis(Ethylenedithio)Tetrathiafulvalene). *Inorg. Chem.* **2001**, *40*, 1363–1371. [[CrossRef](#)]
5. Ojima, E.; Fujiwara, H.; Kato, K.; Kobayashi, H.; Tanaka, H.; Kobayashi, A.; Tokumoto, M.; Cassoux, P. Antiferromagnetic Organic Metal Exhibiting Superconducting Transition, κ -(BETS)₂FeBr₄ [BETS = Bis(Ethylenedithio)Tetraselenafulvalene]. *J. Am. Chem. Soc.* **1999**, *121*, 5581–5582. [[CrossRef](#)]
6. Kobayashi, H.; Fujiwara, E.; Fujiwara, H.; Tanaka, H.; Otsuka, T.; Kobayashi, A.; Tokumoto, M.; Cassoux, P. Antiferromagnetic Organic Superconductors, BETS₂FeX₄ (X = Br, Cl). *Mol. Cryst. Liq. Cryst.* **2002**, *380*, 139–144. [[CrossRef](#)]

7. Coronado, E.; Galán-Mascarós, J.R.; Gómez-García, C.J.; Laukhin, V. Coexistence of Ferromagnetism and Metallic Conductivity in a Molecule-Based Layered Compound. *Nature* **2000**, *408*, 447–449. [[CrossRef](#)]
8. Coronado, E.; Galán-Mascarós, J.R.; Gómez-García, C.J.; Martínez-Ferrero, E.; van Smaalen, S. Incommensurate Nature of the Multilayered Molecular Ferromagnetic Metals Based on Bis(Ethylenedithio)Tetrathiafulvalene and Bimetallic Oxalate Complexes. *Inorg. Chem.* **2004**, *43*, 4808–4810. [[CrossRef](#)]
9. Uji, S.; Shinagawa, H.; Terashima, T.; Yakabe, T.; Terai, Y.; Tokumoto, M.; Kobayashi, A.; Tanaka, H.; Kobayashi, H. Magnetic-Field-Induced Superconductivity in a Two-Dimensional Organic Conductor. *Nature* **2001**, *410*, 908–910. [[CrossRef](#)]
10. Coronado, E.; Day, P. Magnetic Molecular Conductors. *Chem. Rev.* **2004**, *104*, 5419–5448. [[CrossRef](#)]
11. Mori, T. Structural Genealogy of BEDT-TTF-Based Organic Conductors I. Parallel Molecules: Beta and Beta Phases. *Bull. Chem. Soc. Jpn.* **1998**, *71*, 2509–2526. [[CrossRef](#)]
12. Guionneau, P.; Kepert, C.J.; Bravic, G.; Chasseau, D.; Truter, M.R.; Kurmoo, M.; Day, P. Determining the Charge Distribution in BEDT-TTF Salts. *Synth. Met.* **1997**, *86*, 1973–1974. [[CrossRef](#)]
13. Prokhorova, T.G.; Khasanov, S.S.; Zorina, L.V.; Buravov, L.I.; Tkacheva, V.A.; Baskakov, A.A.; Morgunov, R.B.; Gener, M.; Canadell, E.; Shibaeva, R.P.; et al. Molecular Metals Based on BEDT-TTF Radical Cation Salts with Magnetic Metal Oxalates as Counterions: $B''-(BEDT-TTF)_4[A[M(C_2O_4)_3] \cdot DMF$ ($A = NH_4^+$, K^+ ; $M = Cr^{III}$, Fe^{III}). *Adv. Funct. Mater.* **2003**, *13*, 403–411. [[CrossRef](#)]
14. Rashid, S.; Turner, S.S.; Day, P.; Howard, J.A.K.; Guionneau, P.; McInnes, E.J.L.; Mabbs, F.E.; Clark, R.J.H.; Firth, S.; Biggs, T. New Superconducting Charge-Transfer Salts $(BEDT-TTF)_4[A \cdot M(C_2O_4)_3] \cdot C_6H_5NO_2$ ($A = H_3O$ Or NH_4 , $M = Cr$ Or Fe , $BEDT-TTF = Bis(Ethylenedithio)Tetrathiafulvalene$). *J. Mater. Chem.* **2001**, *11*, 2095–2101. [[CrossRef](#)]
15. Turner, S.S.; Day, P.; Malik, K.M.A.; Hursthouse, M.B.; Teat, S.J.; MacLean, E.J.; Martin, L.; French, S.A. Effect of Included Solvent Molecules on the Physical Properties of the Paramagnetic Charge Transfer Salts $\beta''-(BEDT-TTF)_4[(H_3O)Fe(C_2O_4)_3] \cdot solvent$ ($BEDT-TTF = Bis(Ethylenedithio)Tetrathiafulvalene$). *Inorg. Chem.* **1999**, *38*, 3543–3549. [[CrossRef](#)]
16. Akutsu-Sato, A.; Akutsu, H.; Yamada, J.; Nakatsuji, S.; Turner, S.S.; Day, P. Suppression of Superconductivity in a Molecular Charge Transfer Salt by Changing Guest Molecule: $\beta''-(BEDT-TTF)_4[(H_3O)Fe(C_2O_4)_3](C_6H_5CN)_x(C_5H_5N)_{1-x}$. *J. Mater. Chem.* **2007**, *17*, 2497–2499. [[CrossRef](#)]
17. Prokhorova, T.G.; Buravov, L.I.; Yagubskii, E.B.; Zorina, L.V.; Khasanov, S.S.; Simonov, S.V.; Shibaeva, R.P.; Korobenko, A.V.; Zverev, V.N. Effect of Electrocrystallization Medium on Quality, Structural Features, and Conducting Properties of Single Crystals of the $(BEDT-TTF)_4A^+[Fe^{III}(C_2O_4)_3] \cdot G$. *CrystEngComm* **2011**, *13*, 537–545. [[CrossRef](#)]
18. Zorina, L.V.; Khasanov, S.S.; Simonov, S.V.; Shibaeva, R.P.; Bulanchuk, P.O.; Zverev, V.N.; Canadell, E.; Prokhorova, T.G.; Yagubskii, E.B. Structural Phase Transition in the $\beta''-(BEDT-TTF)_4H_3O[Fe(C_2O_4)_3] \cdot G$ Crystals (Where G is a Guest Solvent Molecule). *CrystEngComm* **2012**, *14*, 460–465. [[CrossRef](#)]
19. Prokhorova, T.G.; Buravov, L.I.; Yagubskii, E.B.; Zorina, L.V.; Simonov, S.V.; Zverev, V.N.; Shibaeva, R.P.; Canadell, E. Effect of Halopyridine Guest Molecules on the Structure and Superconducting Properties of $\beta''-[Bis(Ethylenedithio)tetra thiafulvalene]_4(H_3O)[Fe(C_2O_4)_3] \cdot Guest$ Crystals. *Eur. J. Inorg. Chem.* **2015**, *2015*, 5611–5620. [[CrossRef](#)]
20. Coronado, E.; Curreli, S.; Giménez-Saiz, C.; Gómez-García, C.J. The Series of Molecular Conductors and Superconductors $ET_4[AFe(C_2O_4)_3] \cdot PhX$ ($ET = Bis(Ethylenedithio)Tetrathiafulvalene$; $(C_2O_4)^{2-} = Oxalate$; $A^+ = H_3O^+$, K^+ ; $X = F$, Cl , Br , and I): Influence of the Halobenzene Guest Molecules on the Crystal Structure and Superconducting Properties. *Inorg. Chem.* **2012**, *51*, 1111–1126.
21. Coronado, E.; Curreli, S.; Giménez-Saiz, C.; Gómez-García, C.J. A Novel Paramagnetic Molecular Superconductor Formed by Bis(Ethylenedithio)Tetrathiafulvalene, Tris(Oxalato) Ferrate(III) Anions and Bromobenzene as Guest Molecule: $ET_4[(H_3O)Fe(C_2O_4)_3] \cdot C_6H_5Br$. *J. Mater. Chem.* **2005**, *15*, 1429–1436. [[CrossRef](#)]
22. Sun, S.Q.; Wu, P.J.; Zhang, Q.C.; Zhu, D.B. The New Semiconducting Magnetic Charge Transfer Salt $(BEDT-TTF)_4 \cdot H_2O \cdot Fe(C_2O_4)_3 \cdot C_6H_5NO_2$: Crystal Structure and Physical Properties. *Mol. Cryst. Liq. Cryst.* **1998**, *319*, 259–269. [[CrossRef](#)]
23. Zorina, L.; Prokhorova, T.; Simonov, S.; Khasanov, S.; Shibaeva, R.; Manakov, A.; Zverev, V.; Buravov, L.; Yagubskii, E. Structure and Magnetotransport Properties of the New Quasi-Two-Dimensional Molecular Metal $\beta''-(BEDT-TTF)_4H_3O[Fe(C_2O_4)_3] \cdot C_6H_4Cl_2$. *J. Exp. Theor. Phys.* **2008**, *106*, 347–354. [[CrossRef](#)]
24. Martin, L.; Turner, S.S.; Day, P.; Mabbs, F.E.; McInnes, E.J.L. New Molecular Superconductor Containing Paramagnetic Chromium(III) Ions. *Chem. Commun.* **1997**, 1367–1368. [[CrossRef](#)]
25. Martin, L.; Turner, S.S.; Day, P.; Malik, K.M.A.; Coles, S.J.; Hursthouse, M.B. Polymorphism Based on Molecular Stereoisomerism in Tris(Oxalato) Cr(III) Salts of BEDT-TTF [Bis(Ethylenedithio)Tetrathiafulvalene]. *Chem. Commun.* **1999**, 513–514. [[CrossRef](#)]
26. Coronado, E.; Curreli, S.; Giménez-Saiz, C.; Gómez-García, C.J. New Magnetic Conductors and Superconductors Based on BEDT-TTF and BEDS-TTF. *Synth. Met.* **2005**, *154*, 245–248. [[CrossRef](#)]
27. Prokhorova, T.G.; Yagubskii, E.B.; Zorina, L.V.; Simonov, S.V.; Zverev, V.N.; Shibaeva, R.P.; Buravov, L.I. Specific Structural Disorder in an Anion Layer and its Influence on Conducting Properties of New Crystals of the $(BEDT-TTF)_4A^+[M^{3+}(Ox)_3]G$ Family, Where G is 2-Halopyridine; M is Cr, Ga; A^+ is $[K_{0.8}(H_3O)_{0.2}]^+$. *Crystals* **2018**, *8*, 92. [[CrossRef](#)]
28. Rashid, S.; Turner, S.S.; Le Pevelen, D.; Day, P.; Light, M.E.; Hursthouse, M.B.; Firth, S.; Clark, R.J.H. $\beta''-(BEDT-TTF)_4[(H_3O)Cr(C_2O_4)_3]CH_2Cl_2$: Effect of Included Solvent on the Structure and Properties of a Conducting Molecular Charge-Transfer Salt. *Inorg. Chem.* **2001**, *40*, 5304–5306. [[CrossRef](#)]

29. Akutsu, H.; Akutsu-Sato, A.; Turner, S.S.; Le Pevelen, D.; Day, P.; Laukhin, V.; Klehe, A.; Singleton, J.; Tocher, D.A.; Probert, M.R.; et al. Effect of Included Guest Molecules on the Normal State Conductivity and Superconductivity of β' -(ET)₄[(H_3O)Ga(C_2O_4)₃]-G (G = Pyridine, Nitrobenzene). *J. Am. Chem. Soc.* **2002**, *124*, 12430–12431. [[CrossRef](#)]
30. Prokhorova, T.G.; Buravov, L.I.; Yagubskii, E.B.; Zorina, L.V.; Simonov, S.V.; Shibaeva, R.P.; Zverev, V.N. Metallic Bi- and Monolayered Radical Cation Salts Based on Bis(Ethylenedithio) tetrathiafulvalene (BEDT-TTF) with the Tris(Oxalato)Gallate Anion. *Eur. J. Inorg. Chem.* **2014**, 3933–3940. [[CrossRef](#)]
31. Prokhorova, T.G.; Zorina, L.V.; Simonov, S.V.; Zverev, V.N.; Canadell, E.; Shibaeva, R.P.; Yagubskii, E.B. The First Molecular Superconductor Based on BEDT-TTF Radical Cation Salt with Paramagnetic Tris(Oxalato)Ruthenate Anion. *CrystEngComm* **2013**, *15*, 7048–7055. [[CrossRef](#)]
32. Martin, L.; Morritt, A.L.; Lopez, J.R.; Nakazawa, Y.; Akutsu, H.; Imajo, S.; Ihara, Y.; Zhang, B.; Zhang, Y.; Guo, Y. Molecular Conductors from Bis(Ethylenedithio)Tetrathiafulvalene with Tris(Oxalato)Rhodate. *Dalton Trans.* **2017**, *46*, 9542–9548. [[CrossRef](#)] [[PubMed](#)]
33. Benmansour, S.; Sánchez-Mañez, Y.; Gómez-García, C.J. Mn-Containing Paramagnetic Conductors with Bis(Ethylenedithio)Tetrathiafulvalene (BEDT-TTF). *Magnetochemistry* **2017**, *3*, 7. [[CrossRef](#)]
34. Rashid, S.; Turner, S.S.; Day, P.; Light, M.E.; Hursthouse, M.B.; Firth, S.; Clark, R.J.H. The First Molecular Charge Transfer Salt Containing Proton Channels. *Chem. Commun.* **2001**, 1462–1463. [[CrossRef](#)]
35. Akutsu-Sato, A.; Akutsu, H.; Turner, S.S.; Day, P.; Probert, M.R.; Howard, J.A.K.; Akutagawa, T.; Takeda, S.; Nakamura, T.; Mori, T. The First Proton-Conducting Metallic Ion-Radical Salts. *Angew. Chem. Int. Ed.* **2005**, *44*, 292–295. [[CrossRef](#)]
36. Morritt, A.L.; Lopez, J.R.; Blundell, T.J.; Canadell, E.; Akutsu, H.; Nakazawa, Y.; Imajo, S.; Martin, L. 2D Molecular Superconductor to Insulator Transition in the β'' -(BEDT-TTF)₂[(H_2O)(NH_4)₂M(C_2O_4)₃] · 18-Crown-6 Series (M = Rh, Cr, Ru, Ir). *Inorg. Chem.* **2019**, *58*, 10656–10664. [[CrossRef](#)]
37. Martin, L.; Lopez, J.R.; Akutsu, H.; Nakazawa, Y.; Imajo, S. Bulk Kosterlitz–Thouless Type Molecular Superconductor β'' -(BEDT-TTF)₂[(H_2O)(NH_4)₂Cr(C_2O_4)₃] · 18-Crown-6. *Inorg. Chem.* **2017**, *56*, 14045–14052. [[CrossRef](#)]
38. Martin, L.; Morritt, A.L.; Lopez, J.R.; Akutsu, H.; Nakazawa, Y.; Imajo, S.; Ihara, Y. Ambient-Pressure Molecular Superconductor with a Superlattice Containing Layers of Tris(Oxalato)Rhodate Enantiomers and 18-Crown-6. *Inorg. Chem.* **2017**, *56*, 717–720. [[CrossRef](#)]
39. Martin, L.; Day, P.; Clegg, W.; Harrington, R.W.; Horton, P.N.; Bingham, A.; Hursthouse, M.B.; McMillan, P.; Firth, S. Multi-Layered Molecular Charge-Transfer Salts Containing Alkali Metal Ions. *J. Mater. Chem.* **2007**, *17*, 3324–3329. [[CrossRef](#)]
40. Akutsu, H.; Akutsu-Sato, A.; Turner, S.S.; Day, P.; Canadell, E.; Firth, S.; Clark, R.J.H.; Yamada, J.; Nakatsuji, S. Superstructures of Donor Packing Arrangements in a Series of Molecular Charge Transfer Salts. *Chem. Commun.* **2004**, *10*, 18–19. [[CrossRef](#)]
41. Martin, L.; Day, P.; Akutsu, H.; Yamada, J.; Nakatsuji, S.; Clegg, W.; Harrington, R.W.; Horton, P.N.; Hursthouse, M.B.; McMillan, P.; et al. Metallic Molecular Crystals Containing Chiral or Racemic Guest Molecules. *CrystEngComm* **2007**, *9*, 865–867. [[CrossRef](#)]
42. Zorina, L.V.; Khasanov, S.S.; Simonov, S.V.; Shibaeva, R.P.; Zverev, V.N.; Canadell, E.; Prokhorova, T.G.; Yagubskii, E.B. Coexistence of Two Donor Packing Motifs in the Stable Molecular Metal α -Pseudo- κ -(BEDT-TTF)₄(H_3O)[Fe(C_2O_4)₃] · C₆H₄Br₂. *CrystEngComm* **2011**, *13*, 2430–2438. [[CrossRef](#)]
43. Martin, L.; Akutsu, H.; Horton, P.N.; Hursthouse, M.B.; Harrington, R.W.; Clegg, W. Chiral Radical-Cation Salts of BEDT-TTF Containing a Single Enantiomer of Tris(Oxalato)Aluminate(III) and -chromate(III). *Eur. J. Inorg. Chem.* **2015**, 1865–1870. [[CrossRef](#)]
44. Martin, L.; Akutsu, H.; Horton, P.N.; Hursthouse, M.B. Chirality in Charge-Transfer Salts of BEDT-TTF of Tris(Oxalato)Chromate(III). *CrystEngComm* **2015**, *17*, 2783–2790. [[CrossRef](#)]
45. Martin, L.; Day, P.; Horton, P.; Nakatsuji, S.; Yamada, J.; Akutsu, H. Chiral Conducting Salts of BEDT-TTF Containing a Single Enantiomer of Tris(Oxalato)Chromate(III) Crystallised from a Chiral Solvent. *J. Mater. Chem.* **2010**, *20*, 2738–2742. [[CrossRef](#)]
46. Martin, L.; Engelkamp, H.; Akutsu, H.; Nakatsuji, S.; Yamada, J.; Horton, P.; Hursthouse, M.B. Radical-Cation Salts of BEDT-TTF with Lithium Tris(Oxalato)Metallate(III). *Dalton Trans.* **2015**, *44*, 6219–6223. [[CrossRef](#)]
47. Martin, L.; Day, P.; Nakatsuji, S.; Yamada, J.; Akutsu, H.; Horton, P. A Molecular Charge Transfer Salt of BEDT-TTF Containing a Single Enantiomer of Tris(Oxalato)Chromate(III) Crystallised from a Chiral Solvent. *CrystEngComm* **2010**, *12*, 1369–1372. [[CrossRef](#)]
48. Benmansour, S.; Gómez-García, C.J. A Heterobimetallic Anionic 3,6-Connected 2D Coordination Polymer Based on Nitranilate as Ligand. *Polymers* **2016**, *8*, 89. [[CrossRef](#)]
49. Benmansour, S.; Gómez-Claramunt, P.; Vallés-García, C.; Mínguez Espallargas, G.; Gómez García, C.J. Key Role of the Cation in the Crystallization of Chiral Tris(Anilato)Metalate Magnetic Anions. *Cryst. Growth Des.* **2016**, *16*, 518–526. [[CrossRef](#)]
50. Benmansour, S.; Vallés-García, C.; Gómez-Claramunt, P.; Mínguez Espallargas, G.; Gómez-García, C.J. 2D and 3D Anilato-Based Heterometallic M(I)M(III) Lattices: The Missing Link. *Inorg. Chem.* **2015**, *54*, 5410–5418. [[CrossRef](#)]
51. Martin, L.; Day, P.; Barnett, S.A.; Tocher, D.A.; Horton, P.N.; Hursthouse, M.B. Magnetic Molecular Charge-Transfer Salts Containing Layers of Water and Tris(Oxalato)Ferrate(III) Anions. *CrystEngComm* **2008**, *10*, 192–196. [[CrossRef](#)]
52. Zhang, B.; Zhang, Y.; Liu, F.; Guo, Y. Synthesis, Crystal Structure, and Characterization of Charge-Transfer Salt: (BEDT-TTF)₅[Fe(C_2O_4)₃] · (H_2O)₂ · CH₂Cl₂ (BEDT-TTF = Bis(Ethylenedithio) Tetrathiafulvalene). *CrystEngComm* **2009**, *11*, 2523–2528. [[CrossRef](#)]

53. Martin, L.; Turner, S.S.; Day, P.; Guionneau, P.; Howard, J.A.K.; Uruichi, M.; Yakushi, K. Synthesis, Crystal Structure and Properties of the Semiconducting Molecular Charge-Transfer Salt (BEDT-TTF)₂Ge(C₂O₄)₃·PhCN [BEDT-TTF = Bis(Ethylenedithio)Tetrathiafulvalene]. *J. Mater. Chem.* **1999**, *9*, 2731–2736. [[CrossRef](#)]
54. Martin, L.; Day, P.; Nakatsuji, S.; Yamada, J.; Akutsu, H.; Horton, P.N. BEDT-TTF Tris(Oxalato)Germanate(IV) Salts with Novel Donor Packing Motifs. *Bull. Chem. Soc. Jpn.* **2010**, *83*, 419–423. [[CrossRef](#)]
55. Lopez, J.R.; Akutsu, H.; Martin, L. Radical-Cation Salt with Novel BEDT-TTF Packing Motif Containing Tris(Oxalato)Germanate(IV). *Synth. Met.* **2015**, *209*, 188–191. [[CrossRef](#)]
56. Wang, P.; Bandow, S.; Maruyama, Y.; Wang, X.; Zhu, D. Physical and Structural Properties of a New Organic Conductor (BEDT-TTF)₄Cu(C₂O₄)₂. *Synth. Met.* **1991**, *44*, 147–157. [[CrossRef](#)]
57. Qian, M.; Rudert, R.; Luger, P.; Ge, C.; Wang, X. Structure of the 1:4 Complex of Bis[1,2-Oxalato(2-)] Copper(II) and Bis(Ethylenedithio)Tetrathiafulvalene (BEDT-TTF). *Acta Cryst. C* **1991**, *47*, 2358–2362. [[CrossRef](#)]
58. Rashid, S.; Turner, S.S.; Day, P.; Light, M.E.; Hursthouse, M.B. Molecular Charge-Transfer Salt of BEDT-TTF [Bis(Ethylenedithio)Tetrathiafulvalene] with the Oxalate-Bridged Dimeric Anion [Fe₂(C₂O₄)₅]⁴⁻. *Inorg. Chem.* **2000**, *39*, 2426–2428. [[CrossRef](#)]
59. Clemente-Leon, M.; Coronado, E.; Galán-Mascarós, J.R.; Giménez-Saiz, C.; Gómez-García, C.J.; Fabre, J.M. Molecular Conductors Based upon TTF-Type Donors and Octahedral Magnetic Complexes. *Synth. Met.* **1999**, *103*, 2279–2282. [[CrossRef](#)]
60. Coronado, E.; Galán-Mascarós, J.R.; Gómez-García, C.J. Charge Transfer Salts of Tetrathiafulvalene Derivatives with Magnetic Iron(III) Oxalate Complexes: [TTF]₇[Fe(Ox)₃]₂·4H₂O, [TTF]₅[Fe₂(Ox)₅]·2PhMe·2H₂O and [TMTTF]₄[Fe₂(Ox)₅]·PhCN·4H₂O (TMTTF = Tetramethyltetrathiafulvalene). *J. Chem. Soc. Dalton Trans.* **2000**, 205–210. [[CrossRef](#)]
61. Alberola, A.; Coronado, E.; Galán-Mascarós, J.R.; Giménez-Saiz, C.; Gómez-García, C.J.; Martínez-Ferrero, E.; Murcia-Martínez, A. Multifunctionality in Hybrid Molecular Materials: Design of Ferromagnetic Molecular Metals. *Synth. Met.* **2003**, *135*, 687–689. [[CrossRef](#)]
62. Zhang, B.; Zhang, Y.; Zhu, D. (BEDT-TTF)₃Cu₂(C₂O₄)₃(CH₃OH)₂: An Organic-Inorganic Hybrid Antiferromagnetic Semiconductor. *Chem. Commun.* **2012**, *48*, 197–199. [[CrossRef](#)] [[PubMed](#)]
63. Alberola, A.; Coronado, E.; Galán-Mascarós, J.R.; Giménez-Saiz, C.; Gómez-García, C.J.; Romero, F.M. Multifunctionality in Hybrid Molecular Materials: Design of Ferromagnetic Molecular Metals and Hybrid Magnets. *Synth. Met.* **2003**, *133*, 509–513. [[CrossRef](#)]
64. Coronado, E.; Galán-Mascarós, J.R.; Giménez-Saiz, C.; Gómez-García, C.J.; Martínez-Agudo, J.M.; Martínez-Ferrero, E. Magnetic Properties of Hybrid Molecular Materials Based on Oxalato Complexes. *Polyhedron* **2003**, *22*, 2381–2386. [[CrossRef](#)]
65. Coronado, E.; Galán-Mascarós, J.R.; Giménez-Saiz, C.; Gómez-García, C.J.; Ruiz-Pérez, C.; Triki, S. Hybrid Molecular Materials Formed by Alternating Layers of Bimetallic Oxalato Complexes and Tetrathiafulvalene Molecules: Synthesis, Structure, and Magnetic Properties of TTF₄{Mn(H₂O)₂[Cr(Ox)₃]₂}·14H₂O. *Adv. Mater.* **1996**, *8*, 737–740. [[CrossRef](#)]
66. Coronado, E.; Galán-Mascarós, J.R.; Giménez-Saiz, C.; Gómez-García, C.J.; Ruiz-Pérez, C. Hybrid organic/inorganic Molecular Materials Formed by Tetrathiafulvalene Radicals and Magnetic Trimeric Clusters of Dimetallic Oxalate-Bridged Complexes: The Series (TTF)₄[M^{II}(H₂O)₂[M^{III}(Ox)₃]₂]·nH₂O (M^{II} = Mn, Fe, Co, Ni, Cu and Zn; M^{III} = Cr and Fe; Ox = C₂O₄²⁻). *Eur. J. Inorg. Chem.* **2003**, 2290–2298. [[CrossRef](#)]
67. Mori, T.; Mori, H.; Tanaka, S. Structural Genealogy of BEDT-TTF-Based Organic Conductors—II. Inclined Molecules: Theta, Alpha, and Chi Phases. *Bull. Chem. Soc. Jpn.* **1999**, *72*, 179–197. [[CrossRef](#)]
68. Coronado, E.; Curreli, S.; Giménez-Saiz, C.; Gómez-García, C.J.; Alberola, A. Radical Salts of Bis(Ethylenediseleno)Tetrathiafulvalene with Paramagnetic Tris(Oxalato)Metalate Anions. *Inorg. Chem.* **2006**, *45*, 10815–10824. [[CrossRef](#)]
69. Zhang, B.; Zhang, Y.; Wang, Z.; Gao, S.; Guo, Y.; Liu, F.; Zhu, D. BETS₃[Cu₂(C₂O₄)₃](CH₃OH)₂: An Organic-Inorganic Hybrid Antiferromagnetic Metal (BETS = Bisethylene(Tetraselenfulvalene)). *CrystEngComm* **2013**, *15*, 3529–3535. [[CrossRef](#)]
70. Alberola, A.; Coronado, E.; Galán-Mascarós, J.R.; Giménez-Saiz, C.; Gómez-García, C.J. A Molecular Metal Ferromagnet from the Organic Donor Bis(Ethylenedithio)Tetraselenfulvalene and Bimetallic Oxalato Complexes. *J. Am. Chem. Soc.* **2003**, *125*, 10774–10775. [[CrossRef](#)]
71. Awheda, I.; Krivickas, S.J.; Yang, S.; Martin, L.; Guziak, M.A.; Brooks, A.C.; Pelletier, F.; Le Kerneau, M.; Day, P.; Horton, P.N.; et al. Synthesis of New Chiral Organosulfur Donors with Hydrogen Bonding Functionality and their First Charge Transfer Salts. *Tetrahedron* **2013**, *69*, 8738–8750. [[CrossRef](#)]